RESPIRABLE COAL MINE DUST RESEARCH: CHARACTERIZATION AND TOXICITY

by

Vanessa Paola Salinas Torres

Submitted in Partial Fulfillment
of the Requirements for the Degree of
Master of Science in Mineral Engineering with
Specialization in Geotechnical and Geomechanical Engineering

New Mexico Institute of Mining and Technology
Socorro, New Mexico
December, 2022

This thesis is dedicated to my mother, who made this dream possible since the very first day, to my father, who always encouraged me to pursue excellence, and to my lovely sisters for always believing in me. I love you immensely and always will…

Vanessa Paola Salinas Torres
New Mexico Institute of Mining and Technology
December, 2022

ABSTRACT

Coal mine workers are continuously exposed to respirable coal mine dust (RCMD) in workplaces. RCMD is released into the mine air during cutting, drilling, blasting, and transportation. Exposure to RCMD is a severe health hazard that affects thousands of miners in the United States. When dust particles are inhaled, the respirable fraction can be deposited in the lungs' deeper region, deteriorating their gas exchange capacity. Continued exposure over the years to RCMD can lead to progressive pulmonary diseases, such as coal worker's pneumoconiosis (CWP), silicosis, mixed dust pneumoconiosis, dust-related diffuse fibrosis (DDF), and progressive massive fibrosis (PMF). RCMD characteristics and their relations with dust toxicity need further research to understand the adverse exposure effects of RCMD. Different variables may be involved in RCMD toxicity, such as geographic location and dust sources. The map of the coal workers' pneumoconiosis death rates from 2001-2010 in the U.S. shows a noticeable area with higher rates in the eastern side of the country. This region is well known as the Appalachian Mountains. The geographic clustering of coal workers' pneumoconiosis (CWP) suggests that RCMD in the Appalachian region may exhibit more toxicity than in other geographic regions like the Rocky Mountains. Additionally, dust particles in the mine coming from different sources might have different compositions, which may make the dust particles display different toxicity when exposed to the lungs. RCMD generated by cutting host rock may be more toxic than the dust from cutting coal seam. This study investigates the RCMD characteristics and toxicity based on geographic locations and sources. Dissolution experiments in simulated lung fluids (SLFs) and in-vitro response were conducted to determine the toxicity level of samples collected from 5 mines in the Rocky Mountains and Appalachian regions. Dust characteristics were investigated using Fourier-transform infrared spectroscopy, scanning electron microscope, BET method, total microwave digestion, X-ray diffraction, and X-ray photoelectron spectroscopy. Inductively coupled plasma mass spectrometry (ICP-MS) was conducted to determine the concentration of metals dissolved in the SLFs. Finer particle sizes and higher mineral and elemental contents were found in samples from the Appalachian regions. Host rock also showed significantly higher elemental and mineral content than coal. Si, Al, Fe, Cu, Ba, Sr, and Pb were found in dissolution experiments. No trends indicated higher dissolutions in the Appalachian region, but higher elemental bio-accessibility in samples from the host rock was found when dust was exposed to artificial lysosomal fluid (ALF). In-vitro studies indicated a pro-inflammatory response, especially in macrophage cells. The toxicity of the samples based on the metal dissolutions in SLFs and the in-vitro inflammatory response could not be related to the geographic location but to the source. Therefore, the higher incidence of lung diseases in the Appalachian region may be related to other factors like exposure to RCMD, the particle size distribution of the actual RCMD in each mine, and the mineral contributions from the different sources in the mine. Still, the inflammatory response obtained in the studied cells suggests their possible participation in pneumoconiosis and lung diseases-development.

Keywords: RCMD; respirable dust characteristics; simulated lung fluids; in vitro toxicity studies

ACKNOWLEDGMENTS

This study was funded by the National Institute for Occupational Safety and Health (NIOSH) under contracts #75D30119C06390 and #75D30121C12182. I would like to acknowledge NIOSH first for funding this research and giving me the opportunity to be part of this research.

I would like to express my deepest gratitude to my research advisor, Dr. Pedram Roghanchi, who generously provided knowledge and expertise. His support and guidance during this journey were invaluable. I could not have undertaken this journey without him.

Special thanks to my academic advisor and committee member, Dr. Navid Mojtabai, for his constant advisory and support during these years.

I would like to express my thanks to my committee members, Dr. Gayan Rubasinghege, for providing precise comments and support on the experimental phase, and to Dr. Mohammad Rezaee, who agreed to serve on my thesis committee.

I am also thankful to all the people who helped me with training and conducting the experiments, the sample preparation, and providing data for this research. Milton Das in the Department of Chemistry for providing training in dissolution experiments, BET, and FTIR, and his support in conducting these experiments and analyzing the SEM images. Virgil Lueth, Bonnie Frey, and Kelsey McNamara at the New Mexico Bureau of Geology for providing training to perform XRD and total microwave digestion experiments. Dr. Katherine Zychowski from the College of Nursing, University of New Mexico-Health Sciences Center for providing the data for the in-vitro analysis and providing feedback on the analysis. Dr. Jonas Baltrusaitis from the Department of Chemical and Biomolecular Engineering, Lehigh University, for providing the data of the XPS experiment. Maria Pineda, Alexander Medina, Carlha Barreto, Luis Tejada, James Hogan, and Maria Lozano for helping with the sample preparation. Mark Hovingh from the Pennsylvania State University for supporting the sample collection and conducting the DLS experiment.

Finally, my sincere thanks to Alexander Medina for reviewing and giving accurate corrections to my thesis writing, and in general, for his unconditional support during this journey.

.

CONTENTS

Page

LIST OF TABLES

Table Page

LIST OF FIGURES

Figure Page

LIST OF ABBREVIATIONS AND SYMBOLS

NMT	New Mexico Tech
RCMD	Respirable Coal Mine Dust
CWP	Coal Worker's Pneumoconiosis
DDF	Dust-Related Diffuse Fibrosis
PMF	Progressive Massive Fibrosis
SLFs	Simulated Lung Fluids
ALF	Artificial Lysosomal Fluid
GS	Gambles' Solution
NIOSH	National Institute for Occupational Safety and Health
SEM	Scanning Electron Microscope
XRD	X-Ray Diffraction
BET	Brunauer-Emmett-Teller Method
XPS	X-Ray Photoelectron Spectroscopy
FTIR	Fourier-Transform Infrared Spectroscopy
ICP-MS	Inductively Coupled Plasma Mass Spectrometry
RCS	Respirable Crystalline Silica
COPD	Chronic Obstructive Pulmonary Diseases
CWHSP	Coal Workers' Health Surveillance Program
MSHA	Mine Safety and Health Administration
AFM	Atomic Force Microscopy
APS	Aerodynamic Particle Sizer
TEM	Transmission Electron Microscopy
IR	Infrared Spectroscopy
ICP-AES	Inductively-Coupled Plasma Atomic-Emission Spectrometry
EDS/EDX	Energy-Dispersive X-Ray Spectroscopy
DPM	Diesel Particulate Matter
IARC	International Agency for Research on Cancer
PEL	Permissible Exposure Limit
ROS	Reactive Oxygen Species
OP	Oxidative Potential
DLS	Dynamic Light Scattering
PSD	Particle Size Distributions
CINT	Center For Integrated Nanotechnologies
SRM	Standard Reference Material
QSDFT	Quenched Solid Density Functional Theory
UHV	Ultra-High Vacuum
IPA	Isopropyl Alcohol
RO	Reverse Osmosis
RDA	Recommended Dietary Allowance
UL	Tolerable Upper Intake Levels
AI	Average Intake
PRRs	Pattern Recognition Receptors

The dissertation is accepted on behalf of the faculty Institute by the following committee:

Navid Mojtabai

Academic Advisor

Pedram Roghanchi

Research Advisor

Gayan Rubasinghege

Committee Member

Mohammad Rezaee

Committee Member

I release this document to the New Mexico Institute of Mining and Technology.

Vanessa Paola Salinas Torres December 2, 2022

CHAPTER 1

INTRODUCTION[1]

Respirable coal mine dust (RCMD) refers to the mixture of airborne particles present in the air of surface and underground coal mines coming from different sources such as rock breakage, intake air, rock dusting, diesel equipment, and any activity involving abrasion [1]–[3]. These particles are small enough to reach the deepest region of the human lungs, causing damage to the lung tissues [1], [4]–[6].

Several researchers have described RCMD as those particles that are smaller than 10 μm and/or with a mean particle size of 4 μm (aerodynamic diameter) [1], [2], [4]–[8]. However, others restrict the respirable fraction only to the one smaller than 4 μm [2], [6].

Coal mine workers are frequently at-risk for RCMD inhalation. A portion of dust may be retained by the mask (if worn properly) and in the upper part of the respiratory system. Large particles may be eliminated via mucociliary clearance [9]. Smaller particles penetrate deep into the lungs and are deposited in the alveolar region. A portion of the inhaled particles stay in the alveoli since the body's defense mechanisms cannot expel them [8], [10].

Long-term exposure to RCMD can lead to pulmonary diseases such as coal workers' pneumoconiosis (CWP), mixed dust pneumoconiosis, dust-related diffuse fibrosis (DDF), progressive massive fibrosis (PMF), emphysema, chronic bronchitis, and silicosis. All these diseases are irreversible and may result in serious lung injuries and death [5].

[1] This chapter is based on large on the author's paper V. Salinas *et al.*, "Characterization and Toxicity Analysis of Lab-Created Respirable Coal Mine Dust from the Appalachians and Rocky Mountains Regions," *Minerals*, vol. 12, no. 7, p. 898, Jul. 2022, doi: 10.3390/min12070898.

During the last decades, tremendous efforts have been made to reduce miners' exposure to RCMD. However, lung diseases caused by RCMD remain a major concern in the coal mining industry.

Mineral coal continues nowadays to be important in industry and life because it still provides a significant percentage of the energy consumed in the U.S. [11]. RCMD toxicity gained considerable relevance in coal mining in the last 50 years after encountering thousands of coal mine workers suffering from lung diseases and even dying as a result of years of continued exposure to RCMD.

The toxicity of RCMD has been related to several factors, such as particle size, shape, composition, silica content, and mine practices, among others [1]. The higher rates of reported miners diagnosed with coal workers' pneumoconiosis in the eastern region of the U.S. have also suggested that the RCMD coming from this area may exhibit higher toxicity, but until now, the reason why has not been clarified [1], [12], [13]. Some studies have suggested that the seam thickness may influence due to the high silica in the air resulting from cutting the rock strata of the floor and roof in the production areas [14].

Silica has been pointed out as an enhancer of toxicity in RCMD [15]–[17]. It is classified as "Class I Human Carcinogen" by the International Agency for Research on Cancer and has been pointed out as the leading cause of silicosis [5], [13]. Long-term exposure to respirable crystalline silica (RCS) is also known to cause chronic obstructive pulmonary diseases (COPD) and lung cancer [18]. It is believed that higher silica content in the RCMD may make it more toxic [19]. Quartz is the most common crystalline silica polymorph and the second most abundant mineral in the continental crust. It is one of the most common minerals in forming rocks and soil and is often found in coal mines and as a component of RCMD [17], [20].

Also, several studies have tried to determine whether the content of Fe in RCMD can increase its toxicity, but until now, there have been findings indicating both that it is related and not [2], [21]–[24].

In the early 2000s, an increase in the prevalence and severity of CWP, especially in central Appalachia, was observed [5], [13], [14]. The data indicated that coal miners in the Appalachia and Interior regions are at a higher risk of CWP prevalence than in the Western region [25].

The numbers of CWP cases in the US by state and county (from 1986 to 2018) shows hot spot areas in the Appalachian region, with a higher number of cases in West Virginia, Kentucky, Virginia, and Pennsylvania [25]. Figure 1 shows the map of coal workers' pneumoconiosis death rates from 2001-2010 in the U.S. [26]. Additionally, an analysis of the chest radiographs of underground coal miners reported from 1996 to 2002 found CWP in 3% of the miners evaluated. From the miners that showed CWP, 35.4% presented rapidly progressive CWP, and 14.8% evidenced PMF. Also, a proportion between 61.5% - 80% of evaluated miners with rapidly progressive CWP was found in different counties in West Virginia, Kentucky, Virginia, and Pennsylvania, suggesting a cluster along the Appalachian region [27]. Similar observations that suggest a higher incidence of lung diseases in the Appalachian region have been obtained by NIOSH when examining chest radiographs from the Coal Workers' Health Surveillance Program (CWHSP) [5].

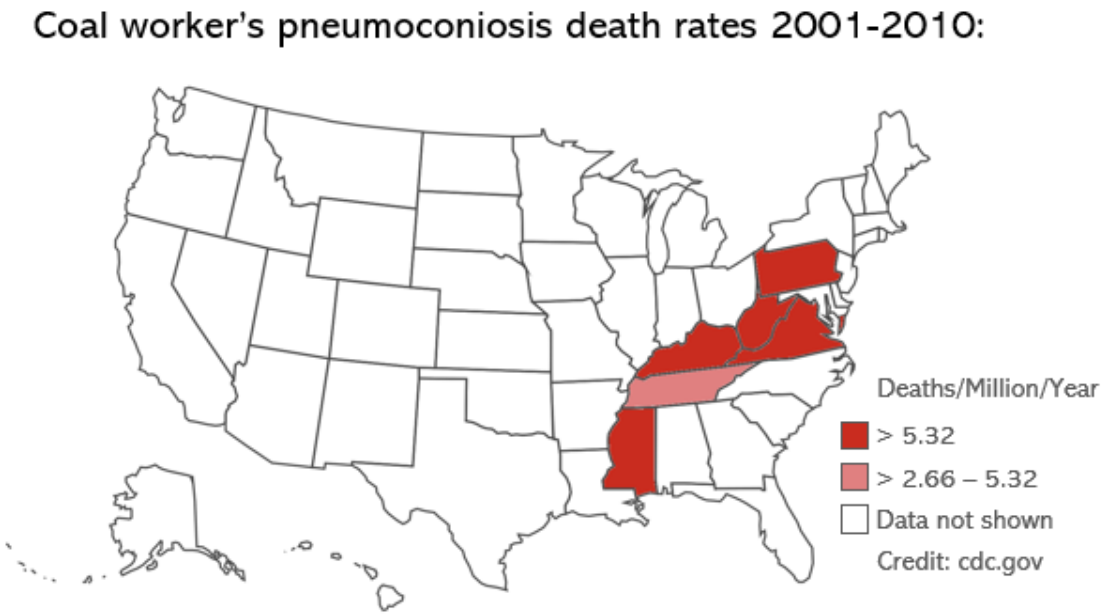

Figure 1. Map of coal workers' pneumoconiosis death rates from 2001 – 2010 [26][2].

The higher rates of CWP cases in the Appalachian region have been linked to the thinner seams usually found in the mines from this region [14], [25].

A study by Rahimi [15] investigated the geographic location of an underground mine as a contributing factor in RCMD and RCS concentrations. The study used the Mine Safety and Health Administration (MSHA) database between 1989-2018, dividing the data into Appalachia, Interior, and Western regions. This study determined that geographic location is a contributing factor for RCMD concentrations in underground mines (Interior vs. Western), and RCS concentration for surface and underground mines (Appalachia vs. Western). Further research into the key differences in coal dust characteristics from different regions was recommended [15].

Although efforts have been made to identify the characteristics and root causes of RCMD toxicity, they remain unclear and are a subject of investigation [15]. Several studies have focused on the RCMD characterization [8], [14], [28], [29], but investigation of the toxicity of RCMD based on the elements and their influence on the inflammatory response of the lungs remains scarce. However, investigation of RCMD characteristics and the level of toxicity will significantly help to understand better the actual reasons for the higher prevalence of lung diseases in the Appalachian region.

[2] The use of this material, including any links to the material on the CDC website, does not constitute its endorsement or recommendation by the U.S. Government, Department of Health and Human Services, or Centers for Disease Control and Prevention. The material is otherwise available on the agency website for no charge (https://wwwn.cdc.gov/eWorld/Data/763).

Considering that different factors may influence the toxicity of RCMD, this research focused on two variables to determine RCMD toxicity: geographic location and dust source.

This study aims to characterize and analyze the toxicity of dust particles from different regions in the US. The geographic clustering of coal workers' pneumoconiosis (CWP) suggests that RCMD in the Appalachian region may exhibit more toxicity than in other geographic regions like the Rocky Mountains.

Regarding the dust source influence, as mentioned before, the dust particles in the mine can come from different sources, such as the host rock, rock dust, the coal seam, diesel equipment, and inlet air, among others [1], [12], [14], [19], [30]. All these particles from different sources have different compositions, mineralogic and elemental wise. These differences may make the dust particles display different toxicity when exposed to the lungs. The hypothesis is that the RCMD generated by cutting host rock is more toxic than the dust coming from cutting coal seam.

The samples for this study were collected from five mines located in the Appalachian region and in the Rocky Mountains, covering two coal basins in the US; two regions for comparison. Also, samples from the host rock were taken from one of the five mines to conduct a preliminary analysis of the influence of dust sources on RCMD toxicity. The toxicity analysis of dust particles was conducted based on the elements that dissolve in simulated lung fluids (SLF) and the inflammatory response they produce. For this purpose, dissolution experiments in simulated lung fluids (SLF) and in-vitro responses were conducted.

Fourier transform infrared spectroscopy (FTIR), scanning electron microscope (SEM), BET method, microwave total digestion, X-ray diffraction (XRD), and X-ray photoelectron spectroscopy (XPS) to characterize the dust samples. The characterization consisted of the functional groups, particle size distribution, specific surface area, elemental content, mineral composition, and surface composition of the samples. The dissolution experiments exposed dust samples to two SLFs (gamble's solution and artificial lysosomal fluid). The concentrations of the metals dissolved after 24 hours were obtained using inductively coupled plasma mass spectrometry (ICP-MS). For in-vitro responses, HL-60, A549, and THP-1 cells were exposed to different concentrations of RCMD to evaluate the change in protein expression.

Results were analyzed to find trends related to the geographic location and dust sources to link dust samples' characteristics and toxicity to the higher incidence of lung diseases in the Appalachian region and to evaluate the influence of host rock in RCMD toxicity.

CHAPTER 2

LITERATURE REVIEW

2.1 RCMD Characterization

RCMD characterization comprehends the study of specific characteristics or properties of dust particles, such as size, shape, mineralogy, and chemical composition, with the primary purpose of evaluating how they may interact, with the human body and with dust control systems. It is essential to know the specific characteristics of RCMD because they may influence the toxicity level and the incidence of lung diseases in mine workers [8]. Studying dust particles characteristics can also help to improve the current monitoring and control techniques. Some of the characteristics that are important to study are described below.

2.1.1 Particle Size

The particle size is crucial because it defines whether the particles are respirable or not and also the main region of the respiratory system where the particles will be deposited [31]. The particle size also determines how long the particles can remain airborne, being available for inhalation (the smaller the particle, the more time will remain in the air). By knowing the particle size of the dust, more accurate mitigation and control techniques can be implemented, and a better understanding of the particle lung deposition can be led.

Particles can be classified by their size, and some of the most common particle matter classes are:

- Inhalable dust: This is the portion of dust that can enter the respiratory system through the mouth or nose. This dust is commonly deposited between the mouth, nasal cavity, and larix. The aerodynamic particle size is <100 µm [32].
- Thoracic dust: This is the portion of the dust that penetrates the head of the airways. These are the particles with an aerodynamic diameter of <30 µm and a mean diameter of 10 µm [4].
- Respirable dust: The respirable dust is the portion of the dust that can enter the lung region and may reach the alveoli, where gas exchange takes place [8]. The aerodynamic particle size for respirable dust has a wide range. Different authors set different sizes for respirable dust. The most common size used for respirable dust in mining is the particles with an aerodynamic diameter <10 µm and with a mean of 4 µm [1], [4], [32].

- Nuisance dust: This one is described as dust that may be uncomfortable but has a low hazard (<1% silica) and causes symptoms of irritation, cough, and reversible illnesses mostly [33].
- PM_1: Particulate matter with an aerodynamic diameter of <1 µm, generally used in environmental monitoring [34].
- $PM_{2.5}$: Particulate matter with an aerodynamic diameter of <2.5 µm, generally used in environmental monitoring [34].
- PM_{10}: Particulate matter with an aerodynamic diameter of <10 µm, generally used in environmental monitoring [34].
- DPM: Particulate matter exhausted by diesel engines with an aerodynamic diameter < 1 µm [35].

Particle size characterization includes methods that use image analysis, light diffraction, and time of flight [36]. Scanning electron microscopy (SEM), atomic force microscopy (AFM), and aerosol particle sizer (APS) spectrometer are used for 2D imaging, 3D imaging, and time of flight, respectively [37]. The last one provides particle size distribution and concentration but does not distinguish between mineral components [38]. Dynamic light scattering has also been widely used to obtain the particle size distribution of samples suspended in a solution [39]. Another technique that is less used is transmission electron microscopy (TEM), which can provide 3D imaging as well, among other characteristics, being this one a technique with higher resolution than SEM [40]–[42].

2.1.2 Shape

Microscopy imaging techniques such as SEM and AFM are used for shape characterization. These techniques allow obtaining images of the particles individually, making it easier to evaluate their surface roughness and structure and to count them. Figure 2 shows examples of shapes following the different 2D particle shape classifications provided by Sellaro et al. 2015 [8]. Rounded edges indicate a longer lifetime of the particle in the air [37], so it may help to identify the source of the silica dust. Angular edges may considerably influence the particles' interaction in lung tissue, increasing inflammation [37].

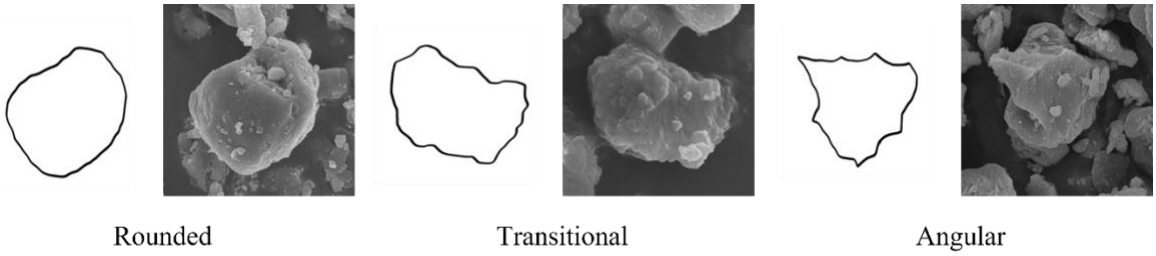

Figure 2. SEM images of dust particles and angularity classification categories based on the sharpness of particle edges [8]

2.1.3 Composition

The composition of dust particles is one of the most important characteristics and has been extensively studied. The composition of the samples can be studied to determine the minerals, elements, and functional groups in the whole samples, elements in the particles' surface, or the minerals of each particle. If the mineral composition is known, it is possible to determine the concentration of silica in the air and distinguish between the different phases of crystalline silica (quartz, cristobalite, and tridymite).

As cristobalite and tridymite have been categorized as more hazardous than quartz [43], it is crucial to measure the amount of these minerals in the air and assess the miners' exposure. The exposure limits of cristobalite or tridymite forms of silica in the industry used to be half that of quartz exposure limit [44]. In the current regulation, for general industry and construction, the limit is 50 $\mu g/m^3$ for all three polymorphs. In comparison, in underground coal mines, the permissible exposure limit is 100 $\mu g/m^3$ of crystalline silica (quartz) [45]–[47].

The most common techniques to measure the silica content in the samples are x-ray diffraction (XRD) and infrared (IR) spectroscopy due to their accuracy. However, other methods such as colorimetric spectrophotometry, are also used [17]. XRD is generally used for mineral phases identification, providing information about the crystallographic structure, chemical composition, and physical properties of a material [48].

Fourier transform infrared spectroscopy (FTIR) is a technique used to identify the different functional groups of organic and inorganic compounds in solid, liquid, or gaseous samples [49]–[51]. Inductively-coupled plasma atomic-emission spectrometry (ICP-AES) and inductively-coupled plasma mass spectrometry (ICP-MS) are used in conjunction with total microwave digestion to identify the elemental composition in samples [2], [12], [14]. X-ray photoelectron spectroscopy (XPS) is another technique that provides information about the surface sample composition [15]. TEM can also be used to identify the morphology, structure, chemistry, and even the nature of bonds in samples [52].

Another technique is energy-dispersive x-ray spectroscopy (EDX or EDS), which is used for the chemical characterization of samples and can identify and quantify the elemental compositions of samples [53], [54]. This technique is frequently used in conjunction with SEM or TEM to provide combined information of images and composition [55], [56] and recently started to be used in RCMD characterization [8].

2.1.4 Other Properties

Other properties of the particles that may play an essential role in RCMD characterization are the particles' hydrophobic properties and surface charges. A better understanding of these properties would help to improve and better target the dust control techniques to obtain higher efficiency in decreasing exposure.

2.2 RCMD Toxicity

It is well known that RCMD particles are toxic for humans since it has been demonstrated that continuous exposure to RCMD can lead to severe lung diseases such as coal workers' pneumoconiosis (CWP), silicosis, pulmonary massive fibrosis (PMF), among others [1], [12], [13], [15], [16], [19], [23], [30], [31], [57]–[60].

The toxicity of RCMD particles has been related to several factors, such as the size and shape of the particles, the mineral and chemical composition, solubility of the particles, surface area, coal rank, diesel particulate matter (DPM), the concentration in the air, silica content, iron or pyrite content, geology, sources, seam thickness, mine practices, among others [1], [12], [14], [19], [30], [58]

Inhalation of dust is widely known to be more toxic than other exposure pathways, such as ingestion or dermal contact [30], so RCMD toxicity assessments are focused on the effects of its inhalation. In general, particles below 10 µm and/or with a mean particle size of 4 µm have been described as the most toxic, and it is believed that the smaller the particle, the higher the hazard because have more chances to penetrate the lung gas-exchange regions [1], [30].

Some of the components of RCMD that are considered important regarding its toxicity are crystalline silica and diesel particulate matter (DPM), which are materials classified as Class I human carcinogens by the International Agency for Research on Cancer (IARC) [19].

Respirable crystalline silica (RCS) has been pointed out as one of the main responsible of RCMD toxicity and is associated with the development of silicosis, PMF, and lung cancer [2], [15], [16], [19], [61]. The current permissible exposure limit (PEL) allows up to 0.1 mg/m^3 of silica concentration in the RCMD in underground coal mines [13], [62]. Nevertheless, Porter et al. (2002) found in experiments in rats that silica concentration can be toxic even at very low concentrations, suggesting that diseases may develop below the PEL [16]. In 1995, NIOSH recommended limiting the silica concentration in RCMD to 0.05 mg/m^3, but until now, the PEL remains at 0.1 mg/m^3 [13].

Porter et al. (2002) found that freshly fractured silica caused more significant toxic effects than aged silica, i.e., fractured long time before. The shape of the particles is an influential variable in the RCMD toxicity [16], as described by Turci et al. (2016), where the crystal fragmentation played an important role in toxicity [63]. Aged particles have more rounded edges than fresh silica, decreasing the inflammatory and toxic effects produced by angular edges that can penetrate the lung tissue [1], [2]. Also, it has been reported that RCS toxicity is reduced when crystals are coated with clay minerals [2].

Several studies on the toxicity of RCMD particles have been conducted from different viewpoints. They have helped to understand better the effects of RCMD exposures and the factors that give them their toxicity. Usually, they look to analyze the inflammatory response of lung cells, as well as the location and amount of the particles deposition, production of carcinogen cells, fibrosis, epithelial cell proliferation [57], production of reactive oxygen species (ROS) [2], dissolution of elements in simulated lung fluids (SLF) [12], [14], [64], lung tissue damage [57], among others. These studies

include mostly analysis in-vitro [12], [23], in-vivo [57], in SLF [12], [14], [64], and post-mortem with the imaging of lung sections [57].

In-vivo experiments are carried out in living organisms [65], commonly rats and other rodents like mice and hamsters, and also in non-human primates like monkeys [66], [67]. Several studies in rats and rodents have been conducted evaluating the deposition, clearance of dust particles, and the induction of oxidative stress when they are exposed to different concentrations of dust materials, finding negative contributions to health [16], [57], [59], [60], [68]. Few others have been conducted in monkeys and lung tissue sections of post-mortem coal mine workers [57].

Warheit et al. (2016) conducted an extensive literature review and update about dust overload studies in different animal models, including coal dust. Usually, negative impacts on animals' health were found, such as retention of particles in the lungs, fibrosis, inflammation, and lung cancer risk. Several studies were conducted on rats with two years of exposure. However, when comparing the available data from previous studies on mice, hamsters, monkeys, and humans, significant differences in the inflammatory response and development of cancer between the rats and the other species were found. These studies determined that the pulmonary tumors reported in particle-overload studies with poorly soluble particles (such as coal) in rats are irrelevant for humans due to these differences. In general, rats showed to be more sensitive to cancer development than other species, while the responses in monkeys were found to be limited to normal. Additionally, different studies observed that the retention of particles in rats was mainly found in the alveolar region. However, in monkeys and diseased coal miners, the retained particles were found translocated to interstitial sites (interstitial compartments). Differences between rats and monkeys were attributed to their anatomical differences, suggesting that in-vivo analysis in rats is not appropriate for carrying out lung cancer risk assessments. Since monkeys are significantly bigger animals than rats, they may possess an enhanced clearance system compromising the results of 2 years of exposure studies. Similar to mine workers' exposure time, exposure in monkeys may take longer to show the same impacts rats showed in the pulmonary responses after two years of exposure [57].

On the other hand, in vitro studies involve experiments with cell cultures in controlled environments outside of living organisms. These studies have the advantage that they are cheaper than experiments in vivo with animals or in humans [69].

Commonly, in-vitro toxicologic studies of coal dust have focused on the proinflammatory response of macrophages and epithelial cells (lung cells), as well as in the study of fibroblast cells due to their relationship with the formation of fibrosis in lung tissue [24]. In-vitro studies, in general, have found pro-inflammatory responses and indications of damage in the lung cells after coal dust exposures [12], [23], [30], [60]. Also, a combination of in-vivo with subsequent in-vitro experiments has been used to analyze the lung lavages obtained from the animals after dust exposures [59], [60].

Another critical approach for toxicity assessments includes the study of oxidative stress. This feature plays a significant role in the study of RCMD toxicity and has gained relevance in the last decades [2], [21]. Oxidative stress occurs when reactive oxygen species (ROS) are produced in excess, and the body cannot clear them completely. This

causes their accumulation in cells and tissues, ultimately damaging the cell structures, promoting different diseases, or even causing cancer [30], [70].

It is well-accepted that inflammation produced by exposure to dust is induced by ROS accumulation (oxidative stress) [2], [22], [23], [30], [64]. For this reason, several studies have been conducted to assess the oxidative potential (OP) of dust particles [2], [21], [22], [30], [64]. Among others, these studies have found that pyrite and Fe contents in RCMD are linked to the production of ROS and lung inflammatory response; and potentially contribute to the development of CWP [2], [21]–[24].

Trechera et al. (2020) studied the OP of respirable dust samples collected from different coal mines in China. They found that Fe and sulfate minerals had a high correlation with the production of ROS, mainly related to the presence of pyrite in the samples [2].

Pyrite can remain in the lungs for a year, oxidizing to sulfuric acid and Fe oxides [2]. The mode of occurrence of Fe has been shown to influence the production of ROS [2]. In Jan et al. (1999) study carried out in rats exposed to coal fly ash, Fe in coal fly ash was identified as an enhancer of ROS production [59]. In vitro experiments have also indicated that iron mineralogy is relevant to lung cell dysfunction [23].

However, continuing the Trechera et al. (2020) work, Shangguan et al. (2022) studied the production of oxidative stress from mines with low pyrite and low sulfurs to determine their influence on the oxidative potential (OP). High production of reactive oxygen species was found even with the low presence of pyrite in the samples, creating controversy in the responsibility of Fe in producing reactive oxygen species [21]. Zosky et al. (2021), in a previous study, also found no evidence that links pyrite with lung cell cytotoxicity, inflammatory response, and cell proliferation [24].

Anatase (TiO_2) and other elements (Mg, Ca, Na, K, Cu, Mo, Cr, Pb, Zn, As, Ba, Rb, Sb, Cs, Mn, Co, Ni, and Sr) have been pointed as well to be relevant in terms of OP in coal and other dust types studies [2], [19], [21], [22], [71]

Now, studies in SLF look for the elemental bio-accessibility of inhaled RCMD, which means the elements that dissolve when the dust particles get in contact with the lung fluids and become accessible for different processes in the body. In these studies, it is measured first the bio-availability of each element by dissolving the complete sample and measuring the initial concentration of the elements. Then the dissolution in SLF experiments is conducted [12], [14].

To determine the bio-availability and bio-accessibility of elements (and also the OP) in different types of experiments, the most common techniques used to read major and trace elements in the solutions are Inductively-Coupled Plasma Atomic-Emission Spectrometry (ICP-AES) and Inductively-Coupled Plasma Mass Spectrometry (ICP-MS), respectively [2], [12], [14], [21]–[23], [30], [72]. For determining the major components in samples, such as total elemental C, Fe, and Si, X-ray fluorescence spectrometry and high-temperature combustion analysis have been used as well [19], [23].

Sarver et al. (2019) conducted a characterization of RCMD beyond the conventional metrics of samples from 8 underground mines. They included analysis in SLF, finding both the bio-availability and the bio-accessibility of elements to be low in

RCMD [14]. Salinas et al. (2022) studied the dissolution in SLF of lab-created RCMD from different regions in the U.S. They found that the dissolution of elements from the particles that come from the coal seam is even lower. they also suggested that, even if most of the elements dissolving in SLF can be toxic to human health, the body's overload is very unlikely due to the concentrations were below the body's toxicity levels [12]. Nevertheless, studies of RCMD toxicity using SLF remain scarce, and more efforts are needed to assess better the elemental bio-accessibility of RCMD and its relationship with its toxicity [64].

Novel techniques have been recently studied to improve the assessment of the implications in health of RCMD exposure, such as the use of SLF instead of water for measuring the OP of dust particles since some of the ligand compounds present in the SLF decrease their OP when compared with water extractions [64]. Another technique is using confocal Raman spectrometry in lung tissue and cells, which identifies the biochemical changes in CWP lungs and potential biomarkers of inflammation and fibrosis [68].

Until now, despite the efforts made to study RCMD toxicity, the specific characteristics and factors involved in its toxicity remain unclear [12], [15].

2.3 Toxicity of Metals Overload[3]

2.3.1 Aluminum

Aluminum is the third most abundant element in the Earth's crust (8%) and the most abundant metal [73]–[77], but it is a too reactive element to be found free in nature. Aluminum has no biological role and is a toxic nonessential metal to microorganisms [73], [77]. It may pose a significant threat to humans, animals, and plants, causing many diseases [73]. The absorption of aluminum is increased by low pH, enhancing aluminum species' solubility [77]. In humans, Mg^{2+} and Fe^{3+} are replaced by Al^{3+}, which causes many disturbances associated with intercellular communication, cellular growth, and secretory functions [73]. In adults, aluminum exposure has been linked to age-related neurological deficits and Alzheimer. A range of neurological disorders might arise due to exposure to aluminum, including Parkinson's disease and multiple sclerosis [75]–[81]. Aluminum has been found to be very harmful to nervous, osseous, and hemopoietic cells [73]. Most clinical evidence points to a massive overload of Al causing osteomalacia and adynamic bone disease [77]. Several studies show that in addition to accumulating in tissues traditionally associated with Al toxicity, such as the liver and bone, Al also accumulates in the kidney, producing renal function [79], [81], [82].

[3] This section is partially based on the author's paper V. Salinas *et al.*, "Characterization and Toxicity Analysis of Lab-Created Respirable Coal Mine Dust from the Appalachians and Rocky Mountains Regions," *Minerals*, vol. 12, no. 7, p. 898, Jul. 2022, doi: 10.3390/min12070898.

2.3.2 Silicon

Silicon is the second most abundant element after oxygen, the most abundant metal, and is present in almost all the rocks in the earth's crust [83], [84]. Orthosilicic acid is absorbed mainly by humans and is found in numerous tissues, including bone, tendons, aorta, liver, and kidney [83]. Silicon toxicity has been mostly related to producing adverse human effects when it is in the form of silica or asbestos, which affects the respiratory system. However, silica is used widely in the food and beverage industry as a food additive, so the human body obtains large loads of Si from dietary sources. Relatively insoluble forms of silica can release small but meaningful quantities of silicon into biological compartments. Still, Si exposure to humans is limited and mainly in chemical forms that are neither readily absorbed nor bioavailable [84]. Although the adverse effects known for silica, silicic acid has been associated with beneficial effects for bone [85], and also to reduction of Al toxicity and risk of Alzheimer's disease due to its high affinity to Al [86], [87].

2.3.3 Iron

Iron is the second most abundant metal on the earth's crust [73]. Iron is essential for fundamental vital activities, a crucial element for the growth and survival of almost all living organisms [73], [88]–[95]. The human body contains approximately 3–5 g of iron. Most of the iron in the body (~60–70%) is utilized within hemoglobin in circulating red blood cells [88]–[90]. The source of iron in the surface water is anthropogenic and is related to mining activities. The production of sulfuric acid and the discharge of ferrous (Fe^{2+}) takes place due oxidation of iron pyrites (FeS_2) that are common in coal seams and metal mines [73].

Excess of redox active iron (as well as copper) aggravates oxidative (and nitrosative) stress and leads to accelerated tissue degeneration [88]. When present in excess, iron threatens cells and tissues, and therefore iron homeostasis must be tightly controlled. Iron overload may be harmful, causing oxidative stress, DNA damage, and carcinogenesis. Iron's toxicity is based mainly on its ability to catalyze the generation of radicals, which attack and damage cellular macromolecules and promote cell death and tissue injury [88], [92], [93]. Except for the genetic overload disease, Wilson's disease [88], [91], [96], its toxicity is not so well known. Another disease related to iron overload is Hemochromatosis or transfusional siderosis. Pathological iron accumulation in the liver has also been linked to the development of hepatocellular cancer. Another human iron overload diseases are iron-loading anemias, dietary iron overload, and chronic liver disease [88], [93]. High iron concentrations are found in the brains of patients with frequently encountered conditions such as Parkinson's and Alzheimer's disease [88]. Iron dysregulation is closely associated with the initiation and development of several malignant tumors, including lung cancer [92], [94], [95].

2.3.4 Copper

Copper (Cu) is an essential trace element for humans. Cu plays a vital role in the function and maintenance of the human immune system [97]–[101]. The natural concentration of Cu in the soil is approximately 50 ppm Cu. Cu content of the

atmosphere ranges from 5 to 20 ng Cu/m^3, and natural water has a mean concentration of 4–10 µg Cu/L [98]. While copper and iron are essential nutrients for humans, animals, and plants, they can pose risks to human health with elevated exposure [88], [92], [100], [102]. In most severe forms, copper toxicity leads to rhabdomyolysis, cardiac and renal failure, methemoglobinemia, intravascular hemolysis, hepatic necrosis, encephalopathy, and ultimately death [103]. The lethal dose of ingested copper is 10 to 20 g [103]. Drinking water action level for copper at 1.3 mg Cu/L [102].

When Cu homeostasis is disrupted, excess or toxicity of Cu can occur. This is associated with the pathogenesis of the hepatic disorder, neurodegenerative changes, and other disease conditions. The capacity to initiate oxidative damage is most commonly attributed to Cu-induced cellular toxicity [98]. Excess of free copper ions can cause damage to cellular components. Excess copper induces oxidative stress and DNA damage and reduces cell proliferation. Ingestion of more than 1 g of copper sulfate results in symptoms of toxicity [101], [103]. In the brain, toxic levels of Cu^{2+} have been reported to cause oxidative stress, apoptosis, and astrocytosis in the hippocampus and frontal cortex, as well as impaired learning and memory. Altered levels of Cu^{2+} may result in detrimental effects, including cognitive dysfunction and accelerated disease progression [100].

2.3.5 Strontium

There are no harmful effects of stable strontium in humans at the levels typically found in the environment (typical concentration is 0.2 mg/kg). Disposing of coal ash, incinerator ash, and industrial wastes may increase strontium concentration in soil [104]. Sr-90 is a radioactive isotope of stable Sr, which is very dangerous for human health. Sr-90 has identical chemical properties and biological characteristics to stable Sr but is not common in nature [105]

Sr is a physicochemical analog of calcium and is an alkaline earth metal; thus, when Sr enters the bloodstream, it can replace calcium in the bone and in tooth [106]. Cumulated Sr can be eliminated from the body through urine, feces, and sweat, but it may be slow, taking long periods [104]. Strontium chloride hexahydrate destroys liver tissue structure. It results in hepatocyte enlargement, cell nucleus enlargement, blurred cytoplasmic boundaries, and the formation of a vacuolar liver [107].

2.3.6 Lead

Exposure to Pb and Cd is a major public health threat for people [108], [109]. Pb comprises 0.002% of Earth's crust and is the second most toxic metal after Arsenic (As), considered carcinogenic (Group 2B) to humans [110], [111]. the key pathways for human exposure of Pb salts and oxides are through atmospheric dust, automobile exhaust, paint, contaminated food, and water [111]. Contamination of air, soil, and water with Pb are related to several natural and anthropogenic causes, including mining activities [112]–[121].

Enhanced Pb concentration in the blood affects behavior and cognitive performance, and postnatal growth delays puberty and reduces hearing capacity in infants and children. In adults, Pb can cause cardiovascular, central nervous system, kidney, and

fertility problems. During pregnancy, Pb can also hamper fetal growth in the early stage [122]. Long-term exposure to Pb is associated with immune dysfunction, increased susceptibility to various diseases, and severe toxicities to various organs, such as the kidneys, heart, liver, brain, and lung [123], [124]. The lung is the primary organ exposed to air pollutants, including heavy metals. Pb exposure has been shown to induce oxidative stress and altered expression of genes related to inflammation. Previous studies have reported increased incidences of lung cancer among Pb smelters and workers at Pb battery plants [125]–[127]. In addition, studies on occupational hazards have demonstrated the increased risk of lung cancer in workers exposed to Pb [124], [128].

2.3.7 Barium

The abundance of barium is relatively high, the 14th most common element on the Earth's crust, but it is too reactive to be found free in nature. It is usually found in the form of salts such as sulfates and carbonates. The average concentration is 500 ppm, more abundant than zinc [129], [130].

Food is the primary source of human uptake of barium, containing, in general, less than 3 mg/100 g. The tolerable daily intake for humans is 0.2 mg Ba/kg bw/d [131], [132], but reported cases of barium poisoning remain somewhat limited [133]. This element does not have a recognized biological role in humans; however, an overdose of barium may be fatal, producing cardiac and respiratory failure [132]. Barium cation is extremely toxic and may produce gastrointestinal symptoms, paresthesia, hypertension, hypokalemia, and progressive flaccid muscular paralysis [134].

Barium also has been widely used as a rodenticide [135], [136]. Suicidal cases have been reported by ingestion of barium acetate and carbonate [135], [137], and even mass accidental poisoning [135].

CHAPTER 3

MATERIALS AND METHODS[4]

This study is divided into two sections: an analysis of the geographic location's influence on RCMD toxicity and a preliminary comparison of three sources on RCMD toxicity. The followings are the materials and methods used for both analyses. In the case of the source comparison, since it is a preliminary analysis, only a few characterization techniques were used.

3.1 Sample Collection

Bulk samples used in this study were collected from 5 mines in the United States, including three mines from the Appalachian region and two from the Rocky Mountains. The purpose of bulk sample collection was to create a representative collection of materials in a mine that are aerosolized and inhaled by the miners during their shifts. Samples for geographic location analysis were collected from the coal seam of the working face in order to collect material that closely matches the excavated coal rock. Samples for the source comparison were taken from the coal seam and the host rock surrounding the seam, including one sample from the roof and another from the floor of the production area.

Mines 1 and 2 correspond to the samples collected from the Rocky Mountains, and Mines 3, 4, and 5 to the ones collected from the Appalachian region. These five samples were used for the geographic location analysis. It is important to mention that Mine 1 is a surface mine; the rest are underground room and pillar mines. The descriptions of the mines' location, type, mining methods, coal rank, seam height, ash percentage, volatile matter, and sulfur content are shown in Table 1.

Table 1. Overall information of the samples collected for this research.

Region	Mine ID	Type	Mining Method	Coal Rank	Seam Height	Ash (%)	Volatile Matter (%)	Sulfur (%)
Rocky Mountains	Mine 1	S *	Open cut	Sub-bituminous	Low seam	16.90	32.00	1.08
	Mine 2	UG **	Room and pillar	Bituminous	High seam	11.64	33.39	0.55
Appalachians	Mine 3	UG	Room and pillar	Sub-bituminous	Low seam	5.85	16.26	1.07

[4] This chapter is based on large on the author's paper V. Salinas *et al.*, "Characterization and Toxicity Analysis of Lab-Created Respirable Coal Mine Dust from the Appalachians and Rocky Mountains Regions," *Minerals*, vol. 12, no. 7, p. 898, Jul. 2022, doi: 10.3390/min12070898.

	Mine 4	UG	Room and pillar	Sub-bituminous	Low seam	11.28	15.43	1.17
	Mine 5	UG	Room and pillar	Bituminous	High seam	N/A***	N/A	N/A

* S: Surface; ** UG: Underground; *** N/A: Not available.

For the source comparison, samples from the coal seam (CO), host roof (HR), and host floor (HF) collected in Mine 4 were used. It is important to note that the sample Mine 4 in the geographic location section is the same sample denoted as CO in the source comparison section.

3.2 Sample Preparation

The bulk sample size was initially reduced with a jaw crusher or mortar and pestle, depending on the initial size of the sample, until reaching 100% passing U.S.A. standard sieve No. 6 (3.35 mm, ASTM E11). After that, samples were air dried for at least 12 hours to eliminate the excess water.

The resulting sample was ground with a 755RMV jar mill of 9.5” in diameter and 8.5” in height, using media of zirconia 1/2” × 1/2” radius end cylinder, magnesia stabilized. First, the material was ground for six hours and sieved using U.S.A. standard sieve No. 120 (opening of 125 µm) to remove the big particles that the mill could not reduce. Then, the material passing the sieve was ground again.

Three grinding times of 6, 12, and 18 hours were used to determine the time required for the second grinding to achieve the desired percentage of particles less than 10 µm. Samples were analyzed with dynamic light scattering (DLS). The particle size distributions (PSD) found are shown in Figure 3.

The test showed that the same particle size distributions were achieved at different tested times of 6h, 12h, and 18h (Figure 3), indicating that after 6 hours of grinding, the ball mill had already reached its maximum capacity to grind the samples; thus, 6 hours were used as the time for the second grinding in the sample preparation procedure. Additionally, both samples obtained the same particle size distribution after 6 hours of grinding (Figure 4), indicating the replicability of the procedure within different samples. The fraction of the sample less than 10 µm achieved until this point was around 60%.

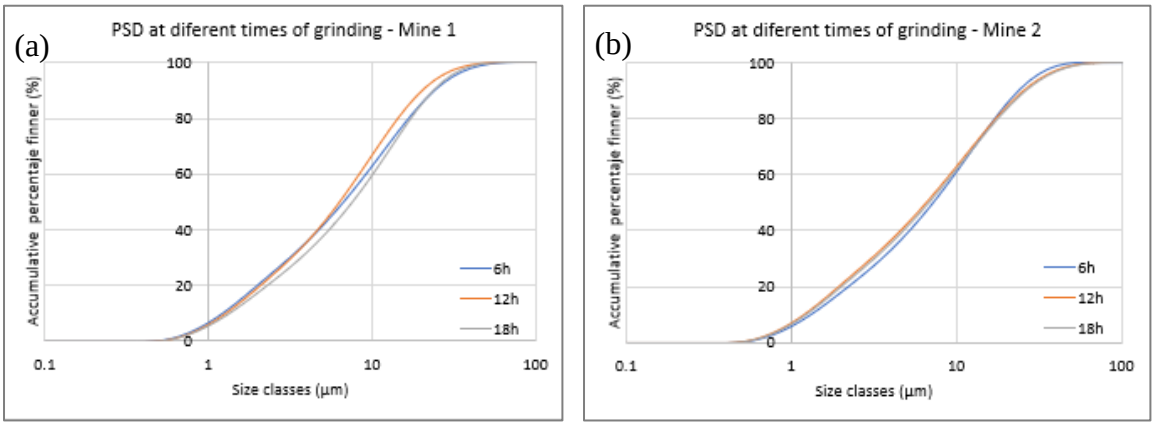

Figure 3. Particle size distributions. (a) Three times tested in Mine 1. (b) Three times tested in Mine 2.

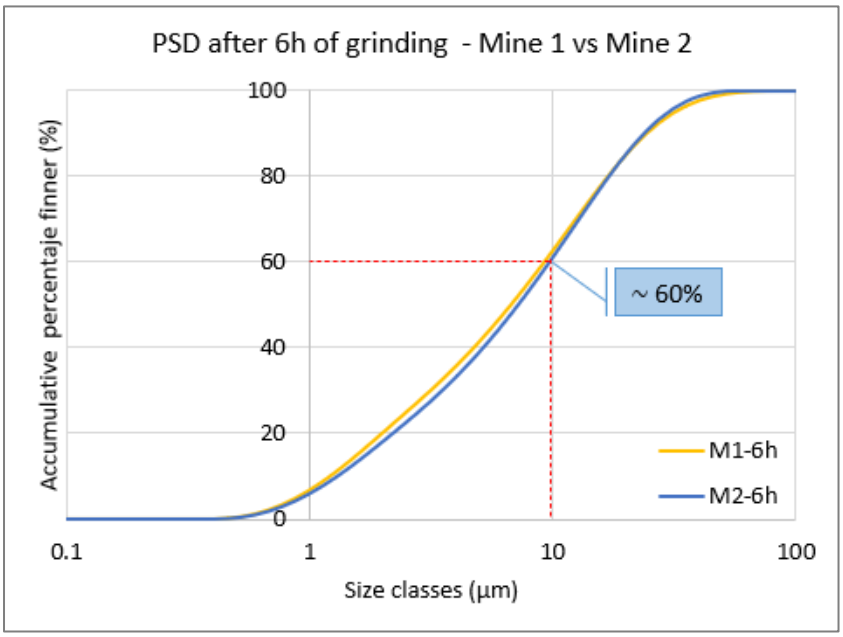

Figure 4. Mine 1 vs. Mine 2 with six hours of grinding

A RETSCH XRD-Mill McCrone was used to achieve a higher fraction of coal particles smaller than 10 µm. This process preserved the structure of the coal samples. The grinding was conducted for 5 min in a 4-step process, loading only 2 mL of sample per round and using agate as media. This mill brings four speeds, so in the first three speeds, the mill was left running for 15 seconds each, and lastly, the 5 min were completed at the maximum speed.

Finally, the fractions less than 10 µm in the samples (mass mean aerodynamic diameter) were separated at the College of Nursing, University of New Mexico-Health Sciences Center by Dr. Katherine Zychowski's team using a next-generation cascade impactor (NGI, model 170 NGI, MSP Corporation, Shoreview, Minnesota, USA) with an attached aerosolizer and gravimetric stages. Dust samples were weighed and placed in hydroxypropyl methylcellulose capsules. Samples were drawn through an induction port using a pump Copley Scientific (Copley Scientific, Nottingham, UK) operated at a flow rate of 60 L/min for 4 s. The fractions less than 10 µm were collected from multiple stages and used for the experiments in this research. PSD was verified using SEM.

3.3 Characterization

Different characterization techniques were carried out to obtain the samples' particle size distribution, functional groups, specific surface area, elemental content, mineralogy, and surface composition. The followings are the descriptions of each technique used to characterize the samples with their respective objectives.

3.3.1 Scanning Electron Microscope (SEM)

A NOVA-Nano-SEM-450 from the Center for Integrated Nanotechnologies (CINT) was used to collect low- and high-resolution SEM images to verify the particle size from the previous separation and to obtain the particle size distribution in the

samples. Between 10 – 15 low-resolution and 1 – 6 high-resolution images were taken for each sample. The images were analyzed for particle size using the software package ImageJ. An average of 80 particles were measured in width and length to plot histograms of the particle sizes for both dimensions. Particulate matter (PM) fractions were calculated using the width of the particles. Dr. Gayan Rubasinghege and Milton Das from the New Mexico Tech Department of Chemistry provided SEM results.

3.3.2 X-Ray Diffraction (XRD)

A PANalytical X'Pert Pro diffractometer, equipped with a Cu Kα source and a fixed divergence silt of 0.25°, was used to determine the mineral components in the samples. A small sample scoop was placed on the analytical plates and tamped to homogeneously flat the sample at the center of the plate (measurement area). Then, samples were placed in the sample holder and taken to the equipment to run the analysis. The analyses were conducted in a 40 min program with a continuous scan of 0.008° step size, operating at 45 kV and 40 mA, with a 2θ scan range from 5° to 70° and a scanning time of 40 sec/step. Raw data were analyzed with HighScore Plus software with a minimum significance of 2 and restricted to the dataset of minerals.

3.3.3 Total Microwave Digestion

The objective of this technique is to digest the samples completely and read from the solution obtained the concentration of several element components in the sample.

A high-performance microwave system from Milestone, model ETHOS UP, was used for the total digestion. The system is equipped with infrared and direct contactless temperature sensors and two 950-Watt magnetrons for a total power of 1900 Watts, which can operate up to 230° C and 100 bar. TFM vessels with high resistant PEEK shields were used in an SK-15 rotor.

The first step was to clean the vessels with 5 ml of a solution 50:50 of water and nitric acid trace metals grade. The vessels were capped, tightened, and placed in the microwave for 25 minutes. After that, the vessels were kept in the microwave and turned off for at least 2 hours until they cooled down. Then the acid solution was disposed of, and the vessels were left to air dry. When completely dry, the vessels were ready for running digestion.

SK-PE-017 was used to digest the coal samples. Digestion was performed in two steps since it is difficult to digest coal for up to 200 mg. The first step used 10 mL of HNO3 with a program of 190°C and 800W/1200W of power (for 3 or fewer vessels/4-8 vessels), using 10 min to reach the temperature and 15 min of standing time. The second step used 2 ml of HF with a program of 230°C using 20 min to reach the temperature and 15 min of standing time. For both steps, 800W was used with 3 or fewer vessels and 1200W when operating 4-8 vessels. The standard reference material (SRM) CLB-1 from the USGS was used for quality control [138]. After digestion, the solution was filtered and dissolved with RO water up to 50 ml of solution. Finally, elemental content was measured with an inductively coupled plasma mass spectrometer (ICP-MS), using a 1:10 and a 1:100 dilution to coal and host rock samples, respectively.

ICP-MS used was an Agilent Technologies model 7900. For the samples from the microwave digestion, an HF resistant set-up was used, equipped with a sapphire torch, a PFA spray chamber capable of cooling down up to 2° C, and a PFA Scott-type concentric nebulizer. The following 29 elements were analyzed with the method: Li, Be, Mg, Al, Si, K, Ca, Ti, V, Cr, Mn, Fe, Co, Ni, Cu, Zn, As, Se, Sr, Mo, Ag, Cd, Sn, Sb, Ba, Tl, Pb, Th, and U. Limit of detection of the method for Mg, K, Ca, and Fe was around 100 ppb, for Mo 2 ppb, and the rest of the elements 1 ppb.

3.3.4 Brunauer-Emmett-Teller (BET) Method

The BET method was used to analyze the dust samples' surface area and micro-pore. This method uses the physical adsorption of gas molecules on a solid surface to measure the specific surface area of samples [139].

300 mg of each sample were weighed in a piece of weight paper and then put in a glass cell. 300 milligrams of the sample are needed to obtain reliable micro-pore data. Below 100 mg of sample, surface area results would not be accurate, and over 300 mg are not readable for the equipment.

The cell with the sample was placed in the outgassing section of the equipment (Figure 5). The program for micro-pore analysis (which also reads the surface area) is set up in the computer using the software AS1WIN. First, the option "Outgasser" was run to eliminate any gaseous contamination in the sample and leave it completely clean. The equipment would read any contamination in the sample, giving additional surface area in the results. Samples were outgassed for over 24 hours at 150˚C. All contaminants are removed when the same amount of gas gets in and out of the cell. At this point, the samples are ready for surface area reading. The cell with the sample was weighed again after contamination removal.

Figure 5. Autosorb 1: Brunauer-Emmett-Teller analyzer.

The cell was placed in the surface area reading section of the equipment and submerged in liquid nitrogen during the test to maintain the temperature. Then, the test

was set in the software AS1WIN and run. Samples were analyzed in a 92 points (52 points N_2 adsorption and 40 points desorption) Brunauer-Emmet-Teller (BET) isotherm using a Quantachrome Autosorb-1 instrument. The surface area was obtained using 7 N_2 adsorption points from the linear region of the isotherm. The pore size analysis was performed using Quenched Solid Density Functional Theory (QSDFT), which considers the surface roughness and heterogeneity and offers a reliable pore size analysis for any unknown carbon sample.

3.3.5 X-Ray Photoelectron Spectroscopy (XPS)

X-ray photoelectron spectroscopy (XPS) was used to identify the particles' elemental components on the surface. A collaborator from Lehigh University (Dr. Jonas Baltrusaitis) recorded the data using a SPECS instrument equipped with Phoibos 1D-DLD hemispherical electron energy analyzer and 0.3 mm entrance aperture, XR50MF aluminum K-α X-ray source operating at 100 W with m-FOCUS 600 X-ray monochromator, and in ultra-high vacuum (UHV) mode. Survey spectra were acquired using 100 eV pass energy, while high-resolution scans were acquired using pass energy of 20 eV. Low energy electrons were used to neutralize the charge. Data processing was performed using CasaXPS software [140]. Charge calibration was performed using a 284.4 eV graphitic peak [141]. C1s spectrum peak fitted with synthetic components based on the literature data [142]. Elemental quantification was performed using relative sensitivity factors of 2.93 for O1s, and 1.0 for C1s with correction for the instrument transmission/escape depth applied.

3.3.6 Fourier-Transform Infrared Spectroscopy (FTIR)

This experiment was carried out to determine the functional groups in the dust sample using Fourier-Transform Infrared Spectroscopy (FTIR). FTIR spectra of the dust samples were collected using a Nicolet iS50 series FTIR equipped with Ge-ATR crystal. The sample was prepared in a small centrifuge tube.

FTIR equipment reads the functional groups present in the sample plus the bare crystal of the sample holder. To determine only the functional groups of the sample, it was necessary to run the FTIR test first in the bare crystal (with any sample on it) to get its spectrum and subtract it later from the sample reading. The bare crystal reading is known as "background" of the test.

About 10 mg of coal dust was sonicated for 20 minutes in 1 mL of isopropyl alcohol (IPA) and transferred to the ATR crystal, followed by air drying, which left a thin layer of dust on the ATR crystal. The parameters for the test were set in the software package OMNIC as shown in Table 2.

Table 2. Parameters for the characterization with FTIR experiment

Parameter	**Value**
Number of scans	250
Resolution	4
Final format	Single bean

Sample compartment	Main
Detector	MCT/B
Beam splitter	KBr
Source	IR
Accessory	ATR
Window	Ge
Max range limit	4000
Min range limit	400
Gain:4	4.0
Optical velocity	1.8988
Aperture	100
Attenuation	None

The crystal is placed in a sealed chamber where the CO_2 is extracted with the help of a pump (Figure 6). The beam refracts the CO_2, so it was necessary to eliminate the gas from the chamber where the analysis takes place. Before reading the samples, some inspection tests were run to check if all the CO_2 was gone Once the CO_2 was completely removed from the chamber, the actual measurements were taken, first for the bare crystal and then for the sample. The same parameters are used for both tests.

Collected spectra were processed against the spectra of bare crystal, and only the processed spectra were reported. For each sample, FTIR analysis was performed for the parent dust sample before any dissolution experiment as well as after the dissolution in both GS and ALF. For this purpose, we recollected undissolved dust after the dissolution experiment using filtration and a hot plate to dry it. The spectrum's peaks were matched with functional groups' peak references.

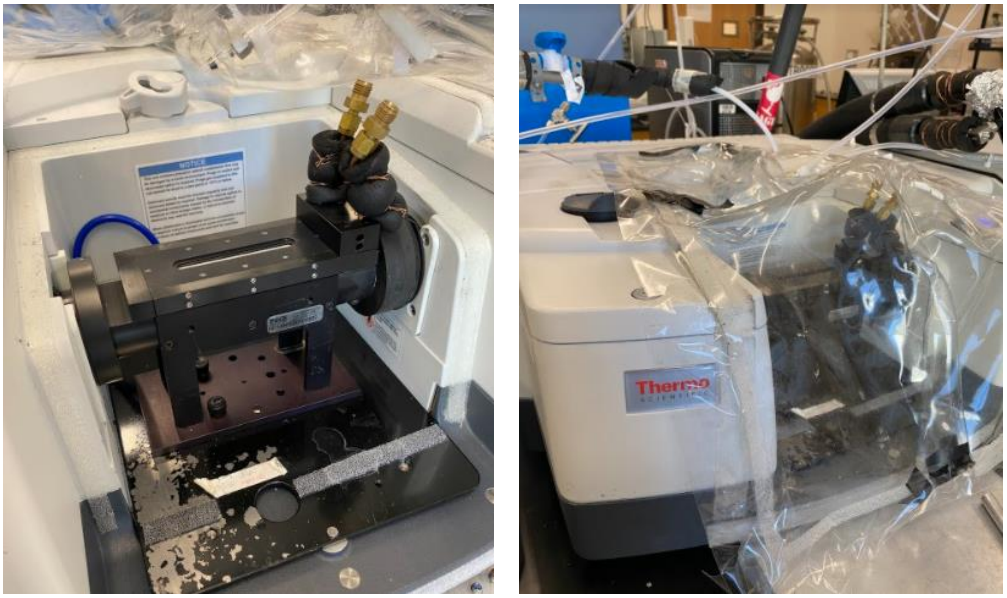

Figure 6. a. Sample holder inside the chamber. b. Chamber sealed with a plastic film.

3.4 Toxicity Analysis in Simulated Lung Fluids

The toxicity analysis of RCMD in simulated lung fluids (SLFs) comprises the preparation of the SLFs (gamble's solution and artificial lysosomal fluid), the dissolution experiment, and the reading of the elements dissolving after exposure with SLFs using ICP-MS. The followings are the descriptions of each procedure used in the toxicity analysis in SLFs of the samples with their respective objectives.

3.4.1 Simulated Lung Fluid Preparation

There are two types of simulated lung fluids: Gamble's solution (GS) and artificial lysosomal fluid (ALF). Both have different compositions and properties. GS simulated the pulmonary surfactants secreted by cells in the interstices of the lungs, and ALF simulated the acid fluid in macrophages that is in charge of trapping and eliminating foreign bodies [64], [9]. Table 3 shows the chemicals and the amount of each component used in the preparation of the SLFs used in the dissolution experiment.

Table 3. Simulated lung fluids used in the dissolution experiment [10], [143].

Composition	**Gamble Solution (GS) (g/L)**	**Artificial Lysosomal Fluid (ALF) (g/L)**
NaCl	6.779	3.21
Na_2HPO_4	-	0.071
$NaHCO_3$	2.268	-
Sodium citrate dehydrate	0.055	0.077
NH_4Cl	0.535	-
Glycine	0.375	0.059
NaH_2PO_4	1.872	-
L-Cysteine	0.121	-
NaOH	-	6
Citric acid	-	20.8
$CaCl_2.2H_2O$	0.026	0.128
Na_2SO_4	-	0.039
$MgCl_2.6H_2O$	-	0.05
Disodium tartrate	-	0.09
Sodium lactate	-	0.085
Sodium pyruvate	-	0.172

250 mL of Milli-Q water was poured into a volumetric flask (Figure 7. a) to prepare the simulated solution. Each solution component shown in Table 3 was weighted in an analytical balance (Figure 7. b) and poured carefully into the volumetric flask with the help of a glass funnel and Milli-Q water (Figure 8. a). Each component was dissolved separately before adding the next component by shaking the flask and using a sonicator to boost the dissolution (Figure 8. b). After diluting all the components, the volumetric flask was filled up to 500 ml, shaken, and put in the sonicator for 20 min to dissolve the smaller particles that may remain in the solution.

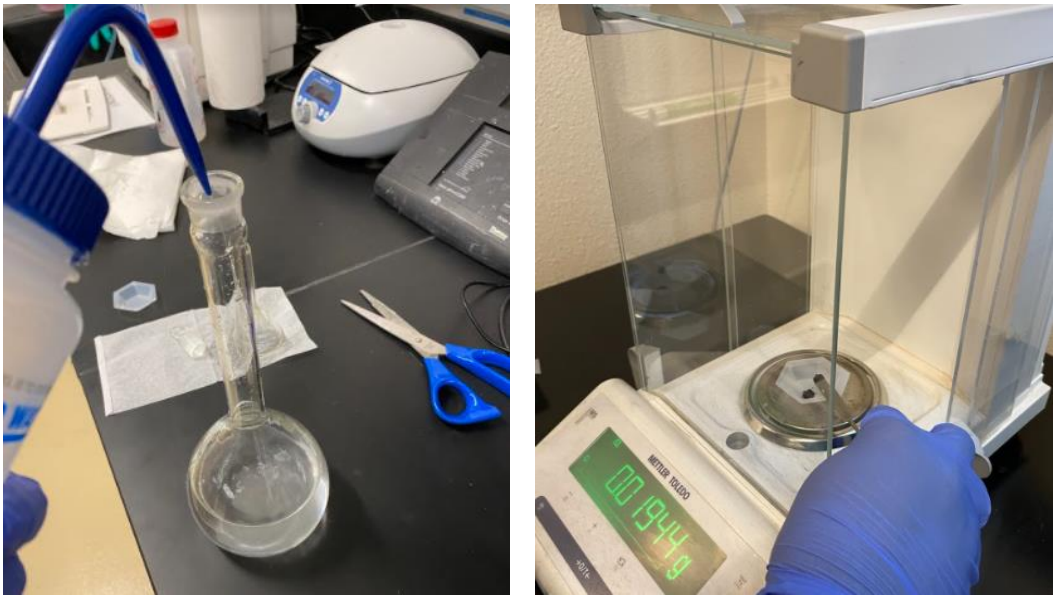

Figure 7. a. Pouring Milli-Q water into a volumetric flask. b. Weighting of the components in the balance.

Figure 8. a. Volumetric flask with glass funnel. b. Shaking the solution with a sonicator.

3.4.2 Dissolution of RCMD in SLFs Experiment

Dissolution experiments in SLFs were carried out to analyze the elements that dissolved from the dust samples that were in contact with the SLF for 24 hours. GS and ALF were used as SLFs, which were prepared as described previously. Some conditions inside the lungs were simulated, such as body temperature (37°C), the absence of light, and oxygenation. The experiment was carried out in a dark room to simulate better the absence of light in the lung environment (Figure 9. b.).

To set up the experiment, first, a wash bottle is filled with around 50 ml of the SLF solution and used to clean all the bottles and implements necessary to run the experiment, such as the graduated cylinder to measure, the double-walled jacketed reactors, the stirring magnets, and the collecting tubes.

100 ml of SLF was measured with the graduated cylinder and poured into a double-walled jacketed reactor (Figure 9. a.). Three of these bottles were prepared the same way to run three trials and obtain better accuracy in the results. Then, magnetos were inserted inside the bottles, and each one was fastened in a magnetic stirrer (Figure 9. b.). The three reactors were connected to each other with tubes to a controlled water bath, which recirculated water at 37°C across the bottle's jackets to maintain a constant temperature during the experiment to simulate the body's temperature.

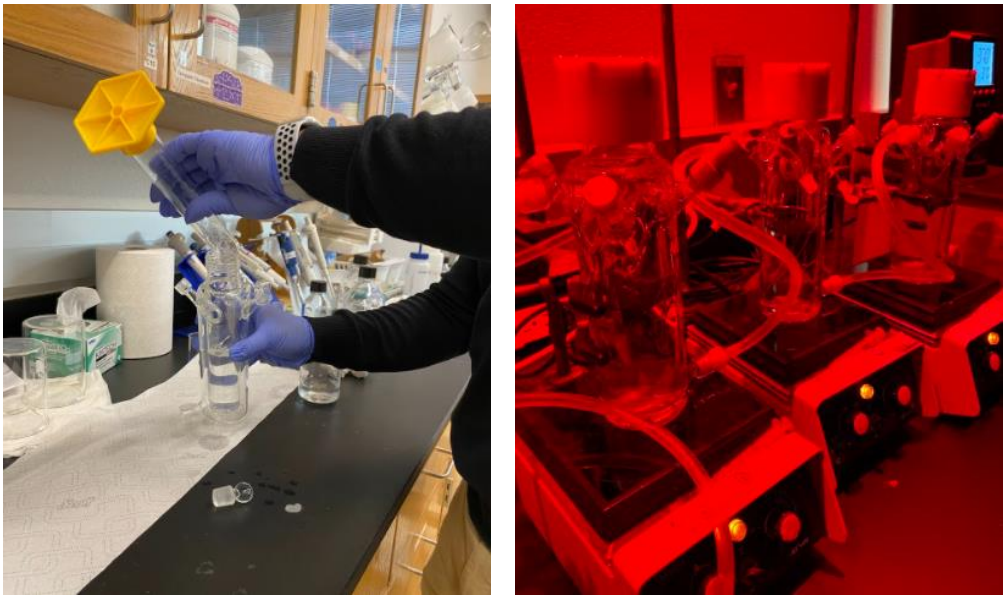

Figure 9. a. Pouring gamble's solution into a double-walled jacketed bottle. b. Bottles connected in dark room.

A collecting tube was placed fixed in an opening of each double-walled jacketed bottle to collect the samples during the experiment and ensure that the samples are collected at the same height of the solution each time. These collecting tubes were also used to oxygenate the SLF solutions at a rate of 5 L/min for 5 min before starting the experiment to saturate the solution with oxygen. In the lungs, the fluids are constantly in contact with oxygen, so it was necessary to oxygenate the solution to simulate the same conditions. Then, all the openings in the bottles were closed with paraffin paper.

Sample aliquots of 1.5 mL were collected from the bottles before adding the coal to the SLF (blanks, which help to know what was in the SLFs before starting the experiments), and right after adding 20 mg of coal to set the 0 h. Then, samples were collected at 1, 3, 6, 9, 12, 18, and 24 hours. Constant stirring at 1000 rpm was provided during the experiments. After collection, SLF samples were centrifuged for 2 minutes to sediment the suspended particles, filtered, and stored in a freezer until analyzed. After dissolution, undissolved samples were filtered and washed with Milli-Q water for further FTIR analysis (Figure 10).

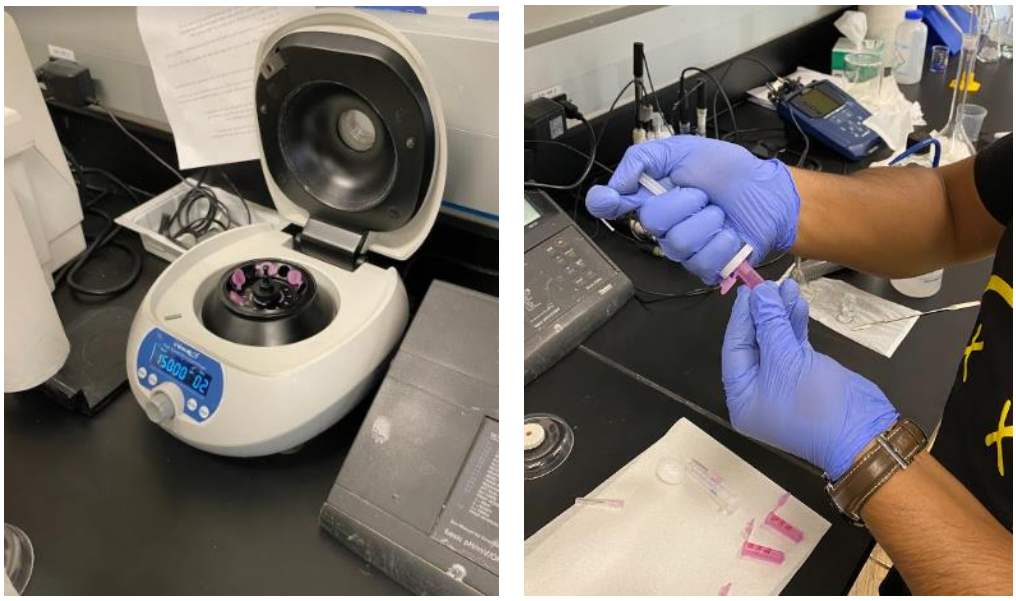

Figure 10. a. Centrifuging collected samples. b. Filtering a sample.

3.4.3 Inductively Coupled Plasma Mass Spectrometry (ICP-MS)

The same ICP-MS used previously for microwave digestion was used with a standard set-up to determine the elemental content in the SLF dissolution. The standard set-up used a quartz torch, quartz spray chamber, and borosilicate glass Scott-type concentric nebulizer. For this experiment, aliquots obtained from the dissolution of RCMD in the SLF experiment were used.

To run the experiment, first, the "matrix" was prepared (solution to dilute the aliquots). For this, 4 parts of reverse osmosis (RO) water and 1 part of SLF were used (5:1 v/v). The SLF solutions have numerous ions, so the solutions were diluted to avoid interference in the readings. The aliquots were diluted to a ratio of 5:1 v/v, i.e., 1 part of the aliquot and 4 of the matrix (Figure 11).

Test blanks and checking samples (standards) were prepared (Figure 12.a.) following the compositions described in Table 4. These are reference samples with known values that were used to check if the equipment was taking the readings properly during the analysis.

Then, all the samples, standards, and checking samples are placed in the test tube rack (Figure 12.b). The batch sheet is prepared in the software setting, showing each sample's location in the equipment rack. The batch sheet has four sections that must be filled, as shown in Table 5. The experiment parameters were set in the software to run the analysis, as shown in Table 6. Then, the experiment was started, and the data showed up on the screen as the experiment ran.

Figure 11. Samples' dilution.

Table 4. The blanks and checking samples compositions.

Standard sample	**Volume of NMGB-1 and NMGB-2 (each) (µL)**	**Diluted to ___ mL of matrix**
1 ppb	5	50
10 ppb	50	50
50 ppb	250	50
100 ppb	500	50
CCV	250	50
Tune solution	5	50
ICV	250 µL of CAS 250 µL of 10 ppm Al solution 250 µL of 10 ppm Th solution 50 mL of matrix	
Blanks	15 mL of matrix 2 blanks are prepared. The equipment will take ≈1 mL of blank after every 10 samples, so the volume of blank required would depend on the number of samples that will be analyzed.	
USGS T-225 check sample	A special solution prepared by the USGS. Contains most of the metals with specific concentrations.	

Table 5. Batch sheet information

Section	**Samples***
Calibration samples	2 blanks
	1 ppb
	10 ppb
	50 ppb
	100 ppb
Check samples	CCV
	ICV
	USGS T-225
	Blank
Unknown samples	The list of the samples to analyze with their concentrations
Check samples 2	CCV
	Blank

* For all the samples the location in the rack must be set in the batch sheet.

Figure 12. a. Blanks and checking samples preparation. B. Placing of blanks and checking samples.

Table 6. Parameters of the batch

Parameter of the plasma*	**Value**
RF Power	1600 W
RF Matching	1.50 V
Smpl Depth	8.0 mm
Nebulizer gas	0.74 L/min
Nebulizer pump	0.10 rps
S/C temperature	2
Gas switch	Dilution gas

* Most of the parameters remain as default.

3.5 In-vitro Toxicity

Dr. Katherine Zychowski's team at the College of Nursing, University of New Mexico-Health Sciences Center, conducted the experiments to analyze the inflammatory response of lung cells after RCMD exposures. The first step consisted of the cell culture. THP-1 (monocytic/macrophage), HL-60 (neutrophilic) and A549 (lung epithelial) cells (ATCC, Manassas, VA, USA) were incubated at 37OC in complete media according to the manufacturer's instructions. Cells were monitored for confluence and appropriately passaged periodically. THP-1 and HL-60 cells were seeded (2.0x105 cells per well) in 24 well plates and were then differentiated using 1.25% DMSO in media for five days. A549 cells were similarly seeded at 2.0x105 cells per well and did not require differentiation.

For PM in vitro exposures, HL-60 cells were treated with a low (5µg/ml), medium (10µg/ml), and high (20µg/ml) concentration of previously fractionated PM10. A549 and THP-1 cells were exposed to a low (10 µg/ml) and high (100 µg/ml) concentration of PM10. Each cell line was exposed to PM10 for four hours, and each PM-treatment was run in duplicate or triplicate technical replicates. Supernatants were then collected for further analysis.

Proinflammatory Panel 1 (Human) Kit V-Plex (K15049D-1, Meso Scale Discovery, Rockville, MD) was used to assess cytokine expression in the HL-60 and A549 cells from PM10 exposures. The following cytokines were evaluated for HL-60 and A549 cells: IFN-γ, IL-1β, IL-2, IL-4, IL-6, IL-8, IL-10, IL-12p70, IL-13, and TNF-α. Cytokine Panel 1 (Human) Kit V-Plex (K15050D-1, Meso Scale Discovery) was used to assess cytokine expression, including GM-CSF, IL-1α, IL-5, IL-7, IL-12/IL-23p40, IL-15, IL-16, IL-17A, TNF-β, and VEGF-A in THP-1 cells. Meso Scale plates were run according to the manufacturer's instructions. Briefly, the supernatant was collected and pipetted onto plates. These plates were incubated with gentle shaking for two hours at room temperature. Plates were washed three times with buffer solution. Detection antibodies were added to the wells and reacted at room temperature for one hour. A read buffer was added to each well, and plates were analyzed on a Meso Scale Discovery QuickPlex SQ instrument. Discovery Workbench software was used to calculate cytokine concentrations based on each cytokine standard curve. Change in protein expression was evaluated by the following equation: Log = exposed cell concentration/control and plotted according to each dust sample.

CHAPTER 4

RESULTS AND DISCUSSION

As mentioned before, this study is divided into two sections: an analysis of the geographic location's influence on RCMD toxicity[5] and a preliminary comparison of three sources on RCMD toxicity. The followings are the results obtained and the discussion carried out for both analyses.

4.1 Geographic Location Analysis

4.1.1 Particle Size Distribution

From the SEM analysis, it was verified that all samples were under 10 µm. Only a few particles were outside the range, representing a maximum of 1% of the total number of particles analyzed. Histograms with particle size distribution were built by the number of particles. Table 7 shows the information obtained from the SEM analysis, including the mean width and length of the particles, and the percentage fraction of the particulate matter (PM) less than 1 µm (PM1), 2.5 µm (PM2.5), 4 µm (PM4), and 10 µm (PM10).

Sub-micron and supra-micron fractions were extracted from the particle size information. It was observed that the majority of the particles were in supra-micron size. Only Mine 4 and Mine 5 had sub-micron particles, representing the 4% and 7% of the particles counted, respectively. However, it is important to mention that with the resolution of the images obtained, it was difficult to measure individual particles less than 1 µm or differentiate them from the structural layers in the coal, which may have led to an underestimating of the sub-micron fraction.

Both mines from the Appalachian region had a mean width and length smaller than samples from the Rocky Mountains, which were approximately 20% coarser. Considering that all the samples were prepared in the same way, the differences in the particle size distributions are attributed to the specific characteristics of each sample, such as the hardness and mineral contents. Additionally, significant differences in the percentages of PM4 and PM2.5 were found, indicating that the overall samples from the Appalachian region contain a higher number of finer particles.

[5] The geographic location analysis conducted in this chapter is based on large on the author's paper V. Salinas *et al.*, "Characterization and Toxicity Analysis of Lab-Created Respirable Coal Mine Dust from the Appalachians and Rocky Mountains Regions," *Minerals*, vol. 12, no. 7, p. 898, Jul. 2022, doi: 10.3390/min12070898.

Angular edges may considerably influence the interaction of the particles with lung tissue, increasing inflammation [1]. In the images (Figure 13), even if the particle shape was not extensively analyzed, it can be observed that overall, particles are not entirely sharp. All samples from different mines showed a transitional particle shape, according to the qualitative shape classification used by Sellaro, et al., 2015, which are particles in-between an angular and a rounded shape [8]. All samples were prepared following the same procedure, which may have provided similar particle shapes within the mines. In addition, the extensive hours of grinding may have rounded the edges of the particles, which is not necessarily the particle shape produced by the specific equipment and methods used in each mine. Since there are no significant differences in particle shapes between samples from mines, they may not be representative and were not considered as an influential factor for this study.

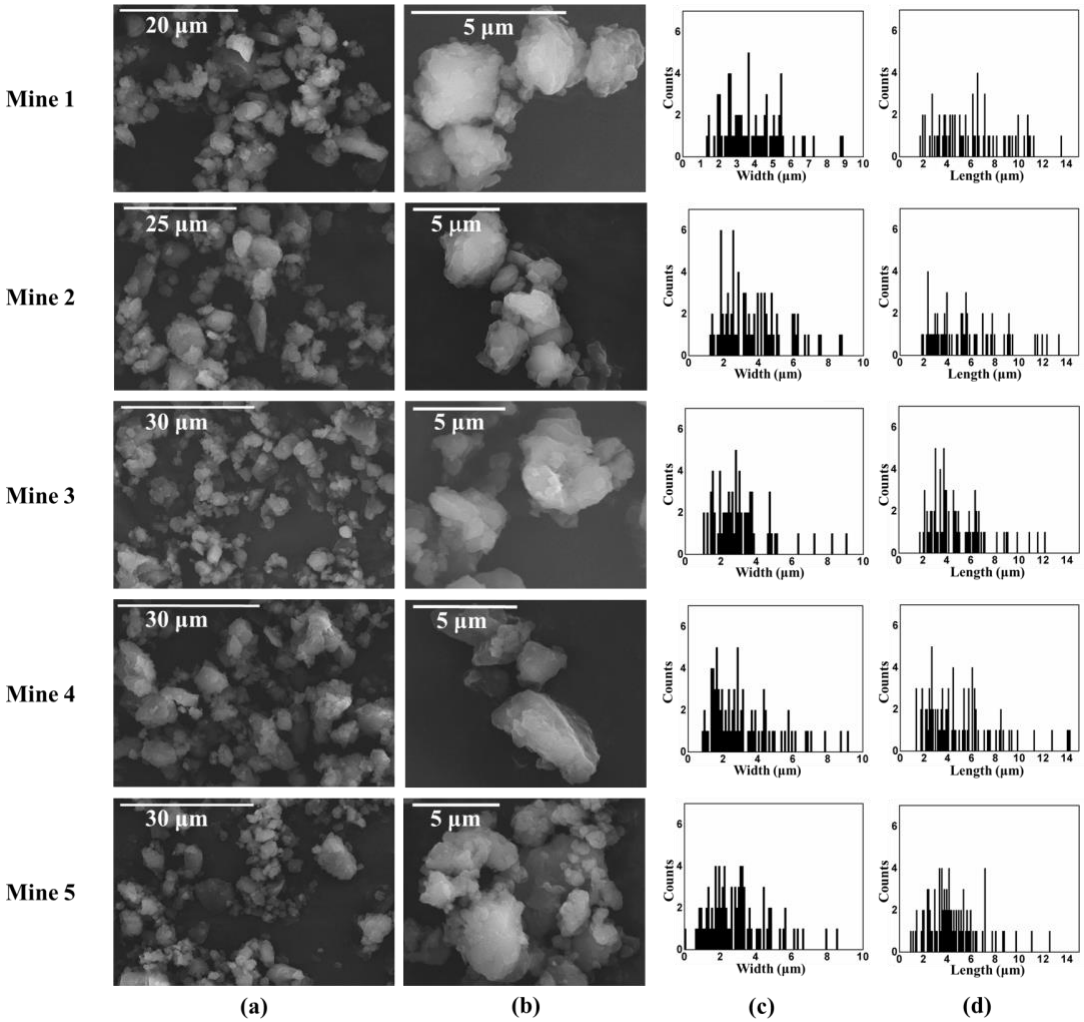

Figure 13. SEM results from the five mines. (a) SEM images. (b) Zoomed-in SEM images. (c) Particle size distribution based on width. (d) Particle size distribution based on length.

Table 7. Mean width and length of the particles and percentages of different particle fractions.

Mine ID	Mean Width (µm)	Mean Length (µm)	PM1 (%)	PM2.5 (%)	PM4 (%)	PM10 (%)
Mine 1	3.86 ± 1.62	6.03 ± 2.80	0	18	58	100
Mine 2	3.81 ± 2.06	5.70 ± 3.20	0	28	62	99
Mine 3	3.15 ± 1.76	4.82 ± 2.26	0	39	83	99
Mine 4	3.24 ± 2.00	5.07 ± 3.10	4	44	73	99
Mine 5	2.95 ± 1.65	4.43 ± 2.11	7	46	77	100

4.1.2 Mineral Composition

The mineral phases present in the coal samples are reported in Table 8. The XRD patterns obtained (Figure 14) showed that the five mines studied have in common the presence of quartz and kaolinite, as expected. Additionally, in all the samples except for Mine 5, pyrite was observed. These three minerals showed to be the main mineral components in the coal samples. Small peaks for siderite and calcite were also observed in Mines 4 and 5, respectively. The limitation of the method is that it is challenging to state the exact amount of each mineral, but relative abundances can be compared.

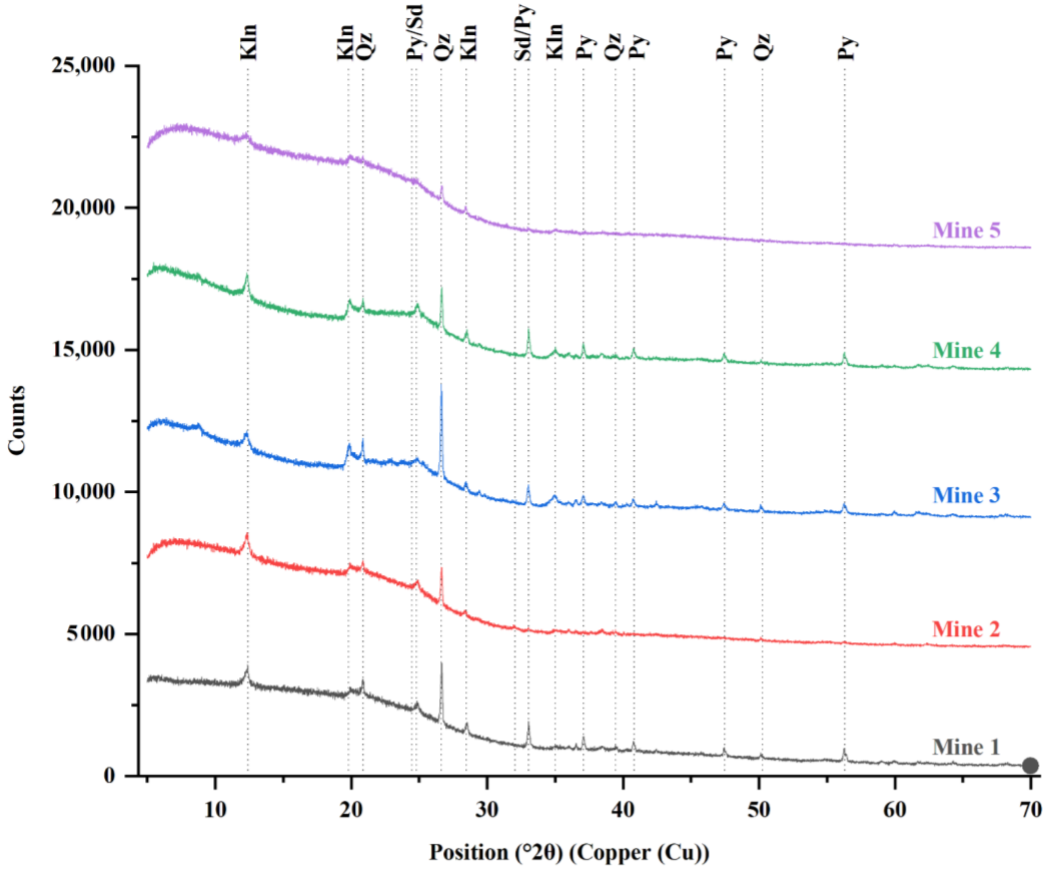

Figure 14. XRD patterns of coal samples from Mine 1, Mine 2, Mine 3, Mine 4, and Mine 5. Symbols according to [144], [145]: quartz (Qz), kaolinite (Kln), siderite (Sd), pyrite (Py), and calcite (Cal).

Table 8. Minerals, compound names, and chemical formulas of the crystalline phases present in Mine 1, Mine 2, Mine 3, Mine 4, and Mine 5.

			Mine ID				
Mineral	**Compound Name**	**Chemical Formula**	**Mine 1**	**Mine 2**	**Mine 3**	**Mine 4**	**Mine 5**
Quartz	Silicon Oxide	SiO_2	X	X	X	X	X
Kaolinite	Aluminum Silicate Hydroxide	$Al_2 (Si_2O_5) (OH)_4$	X	X	X	X	X
Pyrite	Iron Sulfide	FeS_2	X	X	X	X	
Siderite	Iron Carbonate	$Fe (CO_3)$		X			
Calcite	Calcium Carbonate	$CaCO_3$			X		

After plotting the raw data, a large wave in the spectrum at the beginning of the graph was observed. This hump in the XRD spectra is characteristic of amorphous materials due to the random molecular structures [146], [147]. It indicates the presence of considerable amounts of amorphous materials corresponding to the carbonaceous matter.

The relative abundance of the mineral phases was obtained from the intensity displayed by each one in the XRD patterns. The same peaks from the different samples were compared to identify which mine had more content of each mineral. Some peaks in the spectra were influenced by two minerals, so only the major peaks showing the influence of single minerals were considered for comparison. This helps to have an idea of the relative abundance of the minerals among the mines, but not a measured value. The overall idea is that, comparing the same peaks, the higher the intensity, the higher the abundance of the mineral in the samples since the beam found more atoms aligned in this direction. Table S2 in Appendix A shows the values of the counts for each mineral extracted from the software. Figure 15 shows the counts per mineral phase for the five mines. The major peak was located at $2\theta \sim 26.65°$, which corresponds to quartz. It is clear from Figure 14 that the peak for Mine 3 is significantly higher than for the rest of the samples, suggesting that Mine 3 has a higher amount of quartz in its composition. In the same way, Mine 5 has a smaller peak at this position, indicating a lower amount of quartz in the sample.

In Figure 14, one can observe that the peaks for kaolinite (position $2\theta \sim 12.38°$) have similar intensities. This can also be observed in Figure 15, where the major peaks for each mineral were compared. The relative amount within the mines is very similar, except Mine 5, which had fewer counts in the diffraction pattern. Pyrite was not observed in Mine 5 and showed a low intensity in Mine 2. The other three mines showed similar contents of pyrite.

Mine 5 was a relatively cleaner sample since it has only quartz and kaolinite, and peaks can barely be seen in the diffraction pattern, indicating small amounts of minerals. Concerning the geographic locations, quartz and pyrite vary within the mines in the Appalachian region with no trends. The same observation was achieved for samples from the Rocky Mountains. Considerable differences were found within the Appalachian region mines since Mine 5 was collected in north-central Appalachian, and Mine 3 and 4 were collected from northern Appalachia, which may indicate geological differences.

In underground mines, RCMD has contributions from different sources, mainly from the coal seam, host rock, diesel equipment, and rock dust. The final composition of

RCMD is a mixture of all these components, providing, in some cases, higher concentrations of quartz and other minerals (compared to the dust from only the coal seam), especially in the production areas [14]. In this study, only the coal samples from the seam were used, so small mineral contributions were expected in the dust samples.

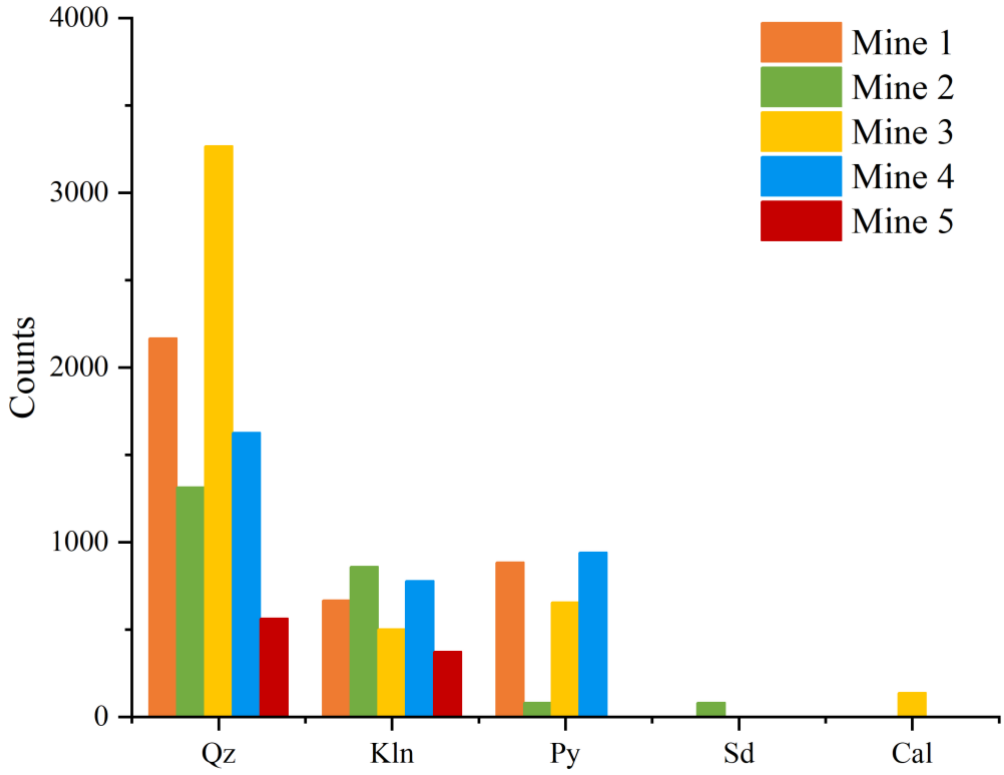

Figure 15. Relative abundance of the minerals in Mine 1, Mine 2, Mine 3, Mine 4, and Mine 5. Quartz (Qz), Kaolinite (Kln), Siderite (Sd), Pyrite (Py), and Calcite (Cal).

4.1.3 Elemental Composition

From the original raw data, Be, Co, Se, Mo, Ag, Cd, Sn, Sb, Tl, Th, and U were not included in the results since all of them showed readings under 10 ppb, which is lower than the limit of detection for the method with the dilution used. Additionally, after mass normalization, almost all of the above-mentioned elements resulted in under 5 ppm, suggesting that these elements were in negligible concentrations or not present in the samples.

The SRM sample was digested completely, and the total concentration of the analyzed elements was obtained. The results from the method and the information of the SRM were compared, and reliable data were obtained for 14 elements: Al, Si, Fe, Ti, Sr, Ba, Pb, Mn, Ni, Cu, As, V, and Cr (Table 9). Most of them met the allowable error described in the SRM information when available or remained between 1% and 15% when the error was not reported in the SRM data. Only Si, Al, and Fe were out of range but, within 1%–15% of the relative difference with the SRM, so they were included in the results.

Table 9. Summary of element content of dust samples.

Mine ID	Al	Si	Fe	Ti	Sr	Ba	Pb	Mn	Ni	Cu	Zn	As	V	Cr
	%	%	%	µg/g	µg/g	µg/g	µg/g	µg/g	µg/g	µg/g	µg/g	µg/g	µg/g	µg/g
Mine 1	0.66	1.18	0.65	608	127.4	53.3	20.4	28.7	7.5	20.8	24.0	6.8	9.3	8.0
Mine 2	0.73	1.13	0.20	503	21.6	8.9	23.5	7.2	7.4	11.7	12.6	1.0	4.8	7.1
Mine 3	0.90	3.53	0.89	1114	41.2	56.6	16.6	24.4	21.8	20.4	52.7	27.8	36.9	26.3
Mine 4	1.03	2.46	1.13	1040	69.2	45.0	8.7	8.0	16.0	13.0	36.3	14.8	55.4	26.1
Mine 5	0.65	0.91	0.12	310	75.5	45.1	10.6	4.9	11.3	23.2	3.7	1.2	11.6	7.5

Li, Mg, K, and Ca showed relatively high concentrations. Still, were not included in the results because when using the SRM to verify the accuracy. It was found that the relative difference was between 30% and 44%, which is very high to be accepted. These elements were under or very close to their detection limit, which may have led to spreading in the results. The information and results of the SRM are shown in Table S3 in Appendix A. Zn and Sr were not reported in the SRM information, so it was not possible to verify their reliability, but the results were in the same order as the digested SRM in the lab, so they were included for reference. The results are shown in Figure 16. They are separated into major and trace element components and in Appendix A, Figure S1 at the same scale.

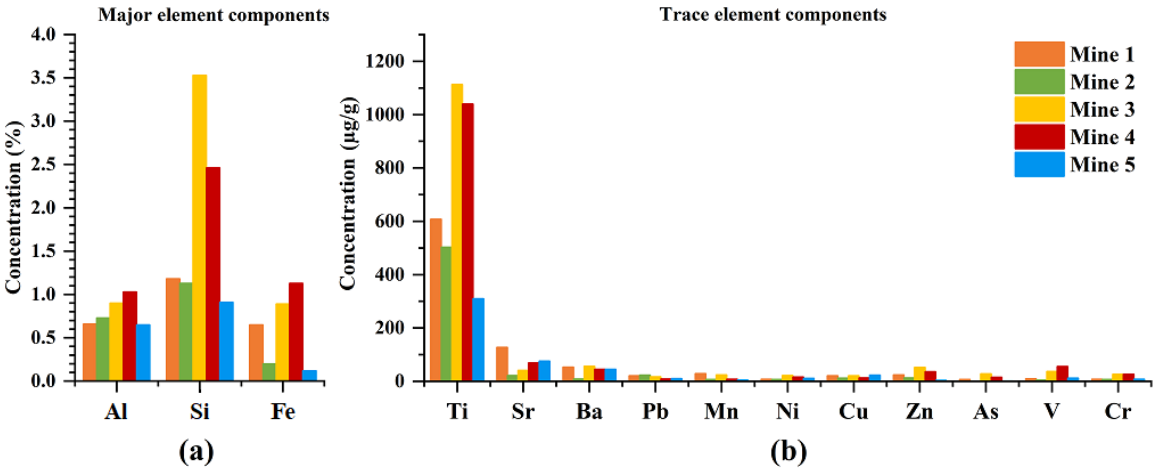

Figure 16. (a) Major and trace element components in the samples. (b) Trace element components in the samples.

Most elements had higher concentrations in Mine 3 and Mine 4, from the Appalachian region. Mine 5, overall, had the lowest concentrations, except for Cu and Sr, which were higher than in other mines. Al, Si, and Fe were the major elements in all the samples, corresponding to the major components of the minerals found in the XRD analysis. The rest of the elements were in very low concentrations, so it could be said that they are present in trace levels. Al showed similar concentrations among the coal from the different mines, similar to the XRD results. Fe was in a lower concentration in Mine 2 and Mine 5, and Si significantly higher in Mine 3, both in accordance with the XRD results.

4.1.4 Surface Composition

A typical coal dust sample exhibited strong peaks due to the carbon and oxygen, with small peaks due to the iron also observed in the elemental content and dissolution studies. The C1s region was fitted using the asymmetric Doniach–Sunjic–Shirley profile as described in recent literature [142]. The C1s region shown in Figure 17a was dominated by a graphitic carbon peak and an sp^3 hybridized carbon peak. Carbon–oxygen bonds (C-O and C=O) corresponded to about 2.4% of the total carbon. This was much less than the total oxygen content obtained from the O1s/C1s ratio shown in Table 10. The O1s region was broad and did not allow an exact spectrum fitting. This suggests that coal dust samples also contained a significant amount of oxygen associated with hydroxyl groups or trapped water. The total oxygen content was comparable in all samples but for Mine 3, which was markedly lower.

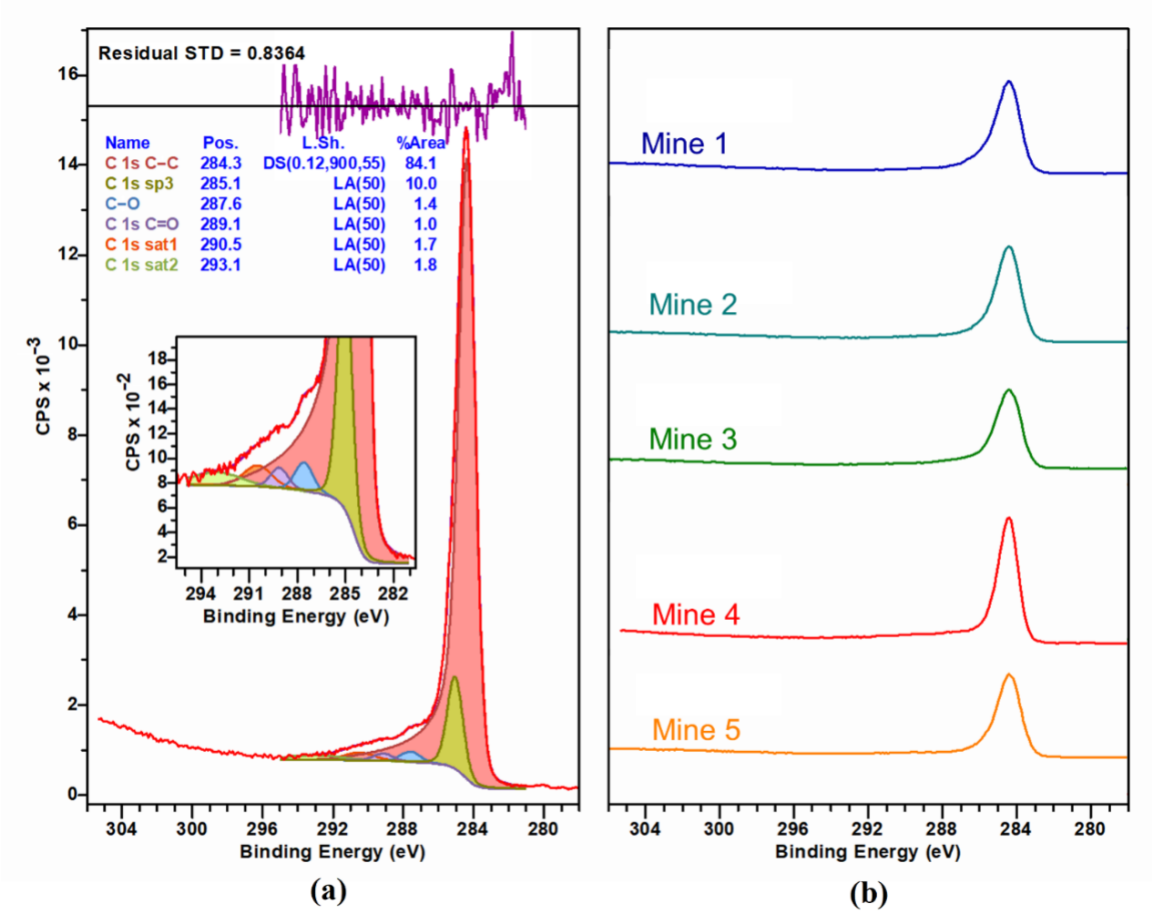

Figure 17. (a) High-resolution C1s spectrum of Mine 4, peak fitted with synthetic components based on the literature data [142]. (b) C1s spectra of the dust samples.

The results are shown in Table 10. As expected, the main component in the samples' surface was C1s. Si2p had a composition according to the results from the total digestion. In the case of Al, the results were not according to the total digestion. Mine 3 had a high concentration of Al in the total digestion, close to the concentration of Mine 4, but here the percentage of Al in Mine 3 was significantly lower. The same was seen for

Mine 5, which had a similar concentration to Mine 1, but here it was shown to be around five times less than Mine 1. This may be explained by the minerals present in the selected samples. Al is related to kaolinite, which occurs in nature packed in layers, so Al may not be exposed on the surface in all cases. Fe was found with the total digestion and XRD, but it did not appear exposed on the particles' surface according to the XPS results.

Table 10. Elemental composition on the surface of the coal dust.

Mine ID	**Al (2p) %**	**C (1s) %**	**O (1s) %**	**Si (2p) %**
Mine 1	0.90767	86.5527	11.7515	0.788068
Mine 2	1.3677	87.0865	10.4115	1.13433
Mine 3	0.827133	90.9843	6.74449	1.44407
Mine 4	1.89306	87.7379	9.26774	1.10128
Mine 5	0.174653	90.8217	8.27811	0.725521

When analyzing the trends by geographic location, the samples regarding Al and Si did not follow a clear pattern. The only significant differentiation was for O, which presented a lower exposure in the particle surface for the mines in the Appalachian region.

4.1.5 Specific Surface Area and Micro-Pore Analysis

The specific surface area of dust samples was determined using a seven-point N2 adsorption isotherm. The measured surface area was similar for all the samples, ranging from 6.80 to 7.77 m^2/g. The surface area was 7.77 ± 0.45, 7.66 ± 0.15, 6.80 ± 0.10, 7.11 ± 0.23, and 7.58 ± 0.33 m^2/g for Mine 1, Mine 2, Mine 3, Mine 4, and Mine 5, respectively. Further, micro-pore analysis was performed, and all the samples were mesoporous with a half pore size distribution found at 58.81 Å. The summary of the results is shown in Table 11.

Table 11. Specific surface area and half-pore width of samples.

Mine ID	**Specific Surface Area (m^2/g)**	**Half Pore Width (Å)**
Mine 1	7.77 ± 0.45	58.81
Mine 2	7.66 ± 0.15	58.81
Mine 3	6.80 ± 0.10	58.81
Mine 4	7.11 ± 0.23	58.81
Mine 5	7.58 ± 0.33	58.81

The specific surface area and micro-pore analysis of the dust samples are important because they give the area that is in contact with the SLF in the dissolution experiments. The formation of the surface complexes is highly dependent on the exposed surface area and thus governs the dissolution process. The same mass (20 mg) was used for each dissolution experiment. Therefore, a big difference in the specific surface area among the samples may influence the final dissolutions of the elements because it is presumed that a larger exposed area to the SLF can result in more dissolution and, finally biased results. In this case, the specific surface area of the samples was very close to each

other, representing the minimum influence of the exposed area in the dissolution experiments.

4.1.6 Initial Functional Groups

FTIR spectra of coal dust were collected from a 4000 to 600 cm^{-1} wavenumber range. In general, FTIR spectra of coal show four bands: 3800–3000 cm^{-1} for the hydroxyl structures, 3000–2800 cm^{-1} for the aliphatic structures, 1800–1000 cm^{-1} for the oxygen-containing functional groups, and 900–700 cm^{-1} for the aromatic structures. However, the collected spectra showed no prominent peak in the hydroxyl and aliphatic regions. Hence, spectra are reported within 2000 to 700 cm^{-1} wavenumbers. The results are shown later in Figure 20, and their respective peak assignments are reported in in Table 14.

The absorption peak starting around 1200–1000 cm^{-1} is the most obvious, indicating that the presence of oxygen-containing functional groups in the coal dust are the highest. The peak coming at 1120–1080 cm^{-1} is associated with S=O stretching. The peaks in the range of 1060–1020 cm^{-1} are associated with Si-O-Si or Si-O-C stretching. The doublet coming at 799–779 cm^{-1} is a representative peak for Si-O-Si bridging, which is the characteristic peak for low-temperature quartz and is also used for the quantitative determination of silica. The peak at 913 cm^{-1} is associated with kaolinite, a common clay mineral. The peak at 1602 cm^{-1} is for benzene ring C=C stretching, whereas the peak at 1445 cm^{-1} is associated with antisymmetric $–CH_3$ deformation [148].

4.1.7 Dissolution in Simulated Lung Fluids

Variable dissolutions of elements across the samples and within the same SLF were found. This may be influenced by several factors, such as the particle size, the surface area, the availability of the elements (elemental composition), the surface composition, and/or the mineralogy. Figure 18 shows the elements dissolving in GS, and Figure 19 in ALF. Dissolutions were mass normalized, and each panel used the same scale to visualize the mines that presented more dissolution of the main elements. The data were fitted to the Langmuir-type model. Surface area normalization was carried out to eliminate the particle size and surface area influence, and the results are shown in Figures S2 and S3 in Appendix A. The surface area was very similar for all the samples, so the same behavior of dissolutions was obtained in the results.

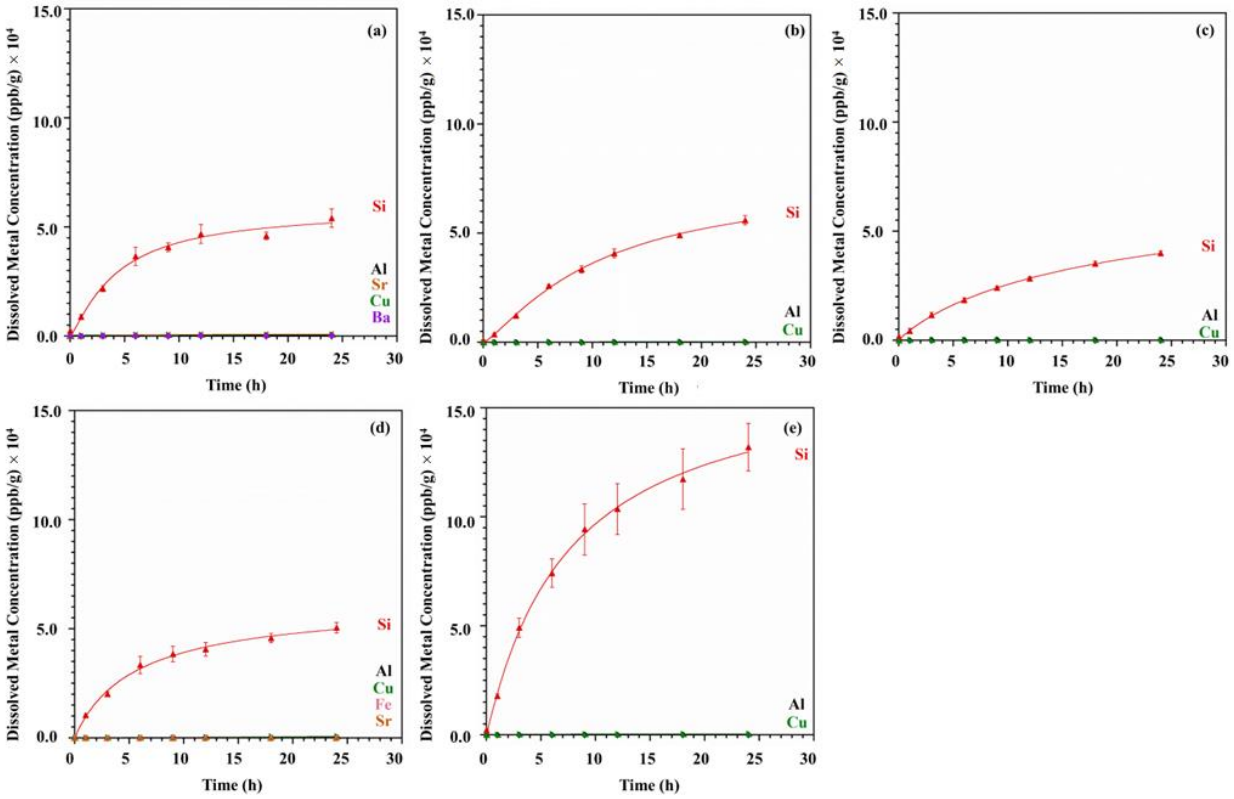

Figure 18. Mass normalized dissolution of metals as a function of time in GS from (a) Mine 1, (b) Mine 2, (c) Mine 3, (d) Mine 4, and (e) Mine 5.

The ICP-MS analysis showed Si being the most dissolved element in GS for all the coal samples. Significantly lower dissolutions of Al, Cu, and in some cases, Fe, Ba, and Sr were found after 24 h of the dissolution experiment. For ALF, higher dissolutions were found for Fe, Al, Si, and Cu, which showed increased concentration with the reaction time for all the coal samples. Very low dissolutions of Sr, Cr, Ba, Pb, and Ni were consistently found as well in ALF. The total dissolutions of the most dissolved elements after 24 h are shown in Table 12.

It was observed that some of the element dissolutions were influenced by the pH of the SLF used. In general, Al, Fe, Sr, and Pb, showed higher dissolutions in ALF than in GS, indicating a strong influence of the pH of the SLF used. Al and Fe showed 4 to 16-fold and >50-fold higher dissolutions in ALF, respectively. Higher dissolutions for Si (9 to 48-fold higher) and slightly higher for Cu were found in GS. The higher dissolution of Si in GS may be explained by the fact that part of the Si may come from the quartz (SiO_2) present in the sample. Quartz, an acid oxide dissolves slowly in alkaline solutions [149]. The GS pH is 7.3, placed in the alkaline side of the pH scale. The ALF pH is 4.5, representing a more acid media for the Si dissolutions (giving less dissolution) but providing better conditions of pH for the dissolution of other components (i.e., Fe, Al, Sr, and Pb).

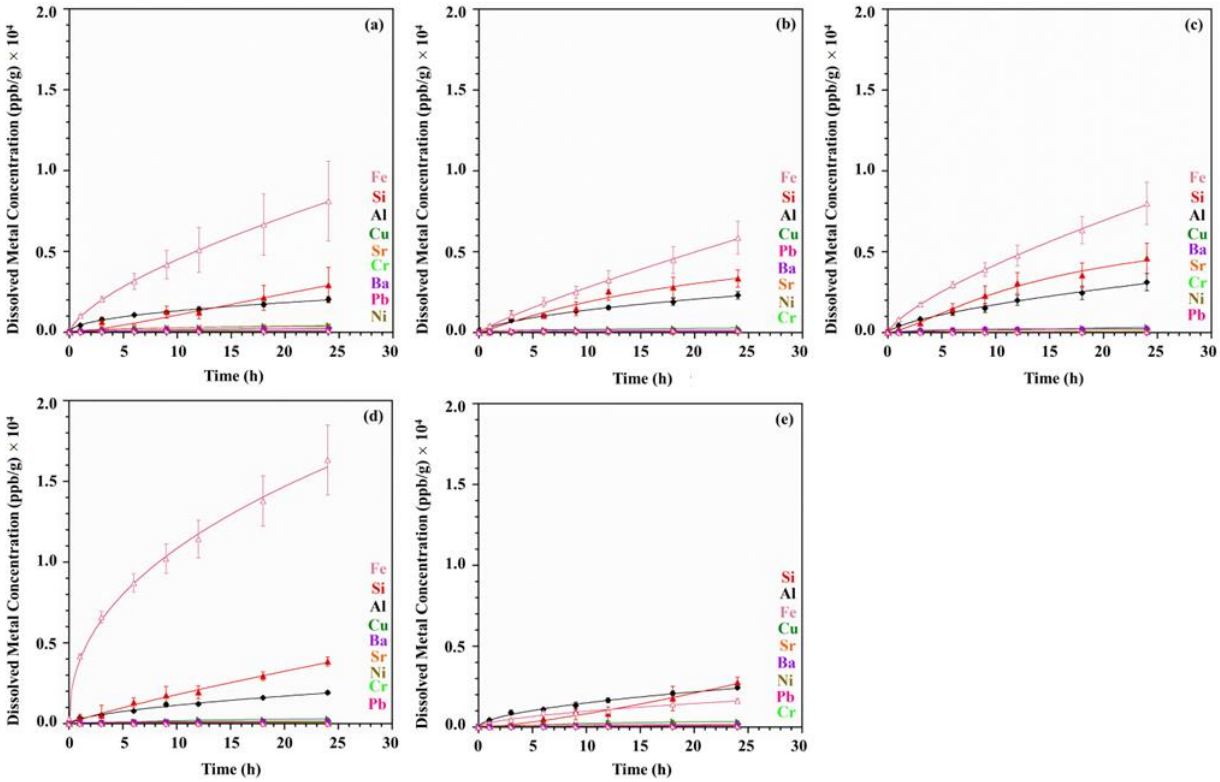

Figure 19. Mass normalized dissolution of metals as a function of time in ALF from (a) Mine 1, (b) Mine 2, (c) Mine 3, (d) Mine 4, and (e) Mine 5.

Table 12. Final metals concentration after 24 h of dissolution in SLF. Values in ppb/g.

	Al		Si		Fe		Cu		Sr		Pb	
Mine ID	**ALF**	**GS**	**ALF**	**GS**	**ALF**	**GS**	**ALF**	**GS**	**ALF**	**GS**	**ALF**	**GS**
Mine 1	2317	142.6	3351	56,006	5879	-	292	324	83.1	-	160	-
Mine 2	2059	555.8	2919	54,117	8118	7.7	436	692	392	-	110	-
Mine 3	3136	210.2	4591	39,918	7993	-	354	245	189	-	47.6	-
Mine 4	1926	468.1	3851	50,577	16,329	315	309	753	108	-	22.5	-
Mine 5	2444	162.5	2764	131,966	1633	-	335	547	203	-	56.4	-

Characterization experiments indicated that Al, Si, and Fe were the main components of the samples, which gave the higher dissolutions as well in SLF, so overall, the initial availability of the metals in the samples plays an important role in the dissolutions in SLF (the more the availability, the higher the concentration after dissolution in SLF). However, comparing the magnitude of the initial concentration vs. the total dissolution in SLF (availability normalization) for the major element components (Al, Si, and Fe) and some of the trace elements (Sr and Pb), a very small percentage of the initial amount was dissolved. This represented less than 0.5% in most cases for both GS and ALF, many even below 0.1%. The availability comparison is shown in Table S4 in Appendix A. On the other hand, Cu, which was found as a trace element, having a lower availability in the samples, and, thus, a low concentration after the dissolutions in SLF, showed values ranging from 1.2 to 5.9% of the initial concentrations. So, Cu was more soluble than the other elements since a higher

percentage of the initial available Cu was digested in both GS and ALF. Sarver et al. [14] found much higher dissolutions of elements when RCMD samples collected in the filter were dissolved in SLF. Si, Al, Cu, and Fe were found to have 75, 26, 90, and 5% or less of the total initial concentration dissolved in SLF, respectively. This previous study is based on dust samples collected on the filter, while the current research was conducted using bulk coal samples collected from the mines and then prepared in the lab; therefore, the composition of the dust is different. According to the mean mineralogy distributions found for the samples collected in the filter (larger particles: 400–10,000 nm), the carbonaceous mineralogy class represented less than 15% of the composition for all the mines and sample locations studied [14]. Characterization results indicate that samples used in this study were mainly carbonaceous materials with very few mineral contributions. In the case of the major elements found by Sarver et al. [14], the total element concentrations (acid-soluble) ranged from 10 to 200 mg/g, while the samples used in this study ranged from 1.2 to 35.3 mg/g (0.12%–3.53%) as shown in Table 9. These significant differences in sample compositions might explain the difference in the results between the two studies.

Dissolutions of Al in GS and Si, Fe, and Pb in ALF were higher when the initial availability was higher, indicating that dissolutions in these cases are directly related to the initial availability of the metal in the sample. This behavior was not observed in the rest of the dissolutions, which in general, were led by the pH of the solution. Only for Cu was observed that the dissolutions were not driven by the initial availability nor by the pH of the solutions. In this case, the dissolution may have been driven by the chemical affinity of the Cu with the free ions in the SLF solutions. The mode of occurrence and oxidation state of the elements in the RCMD have an important role in the dissolution process, improving or impairing their affinity with the free ions and solvent agents in the SLF solutions.

Sarver et al. [14] studied the associated dissolution in the SLF of these elements with the contribution of the geologic strata in the mine or the rock dusting products applied to the RCMD [14]. This study only studied coal from the seam (no strata or rock dust influence); thus, it can be concluded that the coal seam also contributes to the final concentrations of elements found after dissolution experiments in the SLF, but probably in small quantities.

A clear trend was not observed when comparing by geographic location , since the dissolution were led by different factors (Table 13). Even if samples from the Appalachian region had a higher initial availability in most cases, the dissolutions experiments varied behavior in the final concentration after being dissolved in SLF.

Table 13. Factors influencing dissolutions in SLF. Av: availability.

Al		**Si**		**Fe**		**Cu**		**Sr**		**Pb**	
ALF	**GS**	**ALF**	**GS**	**ALF**	**GS**	**ALF**	**GS**	**ALF**	**GS**	**ALF**	**GS**
pH	pH + Av.	Av.	pH	Av. + pH	pH	Possible Affinity	Possible Affinity	pH	pH	pH	pH

In summary, from the dissolution experiment, it was obtained that the main elements dissolving from the dust samples when in contact with the SLF were Al, Si, Fe,

Cu, Sr, and Pb. The overloading in the human body of Al, Fe, Cu, and Pb has been related to different diseases and health issues, as described below.

The quantities of metals dissolved in SLF that were found are lower than the recommended dietary allowance (RDA), tolerable upper intake levels (UL), or average intake (AI) usually found for these elements, which are in almost all the cases in the order of mg/day (Al-AI: 10 mg/day [150], Fe-UL: 1.1 mg/day [151], Cu-UL: 10 mg/day [151], Sr-AI: 1.9 mg/day [152], and Pb-UL: 1.75 mg/week [153]), except for Si, for which there is no evidence of adverse health effects or UL [151].

Compared with the results, the values found were lower since the results are given in ppb/g. In addition, the concentrations obtained are per gram of coal dust, so considering that the permissible exposure limit (PEL) for RCMD is 1 mg/m^3 [1], if we set a scenario where a mine folds five times the PEL (i.e., 5 mg/m^3), it would take a long time for a miner to inhale 1 g of RCMD. An average breath carries around 0.5 L of air [154], and the normal number of respirations for a healthy adult range from 12 to 20 breaths per min [155]. This means that considering the extreme (20 breaths/min), a person could breathe around ~5 m^3 of air in 8 h (normal shift), resulting in a total dose of ~25 mg/8-h of RCMD, so it would take several days to achieve 1 g inhaled, not considering the fraction that is exhaled or expelled from the body. Thus, the concentrations found in the dissolution experiments are difficult to reach in short periods from RCMD, and more, concentrations in toxic levels.

However, the direct release of these elements to the cells and the direct contact with tissues may play a role in cell damage. It was found in the literature that free Cu ions can cause cell damage, replacements by Al^{+3} cause disturbances in the cell communication and growth, and Pb exposures alter the expression of genes related to inflammation. Therefore, the effects of the direct contact of these elements with the cells should be further studied to determine how they may affect their functionality and be involved in the development of diseases.

4.1.8 Changes in Functional Groups

FT-IR analysis was carried out on the samples after dissolution in SLF experiments. The spectra collected for the coal dust that has been dissolved in SLF and recollected showed similar spectral bands to the initial spectra found in the samples before dissolution but with lower intensities. The spectra of the dust after dissolution indicate that oxygen-containing functional groups are the most consumed. The spectra obtained for samples before and after SLF dissolution are shown in Figure 20, and the peak assignments are in Table 14.

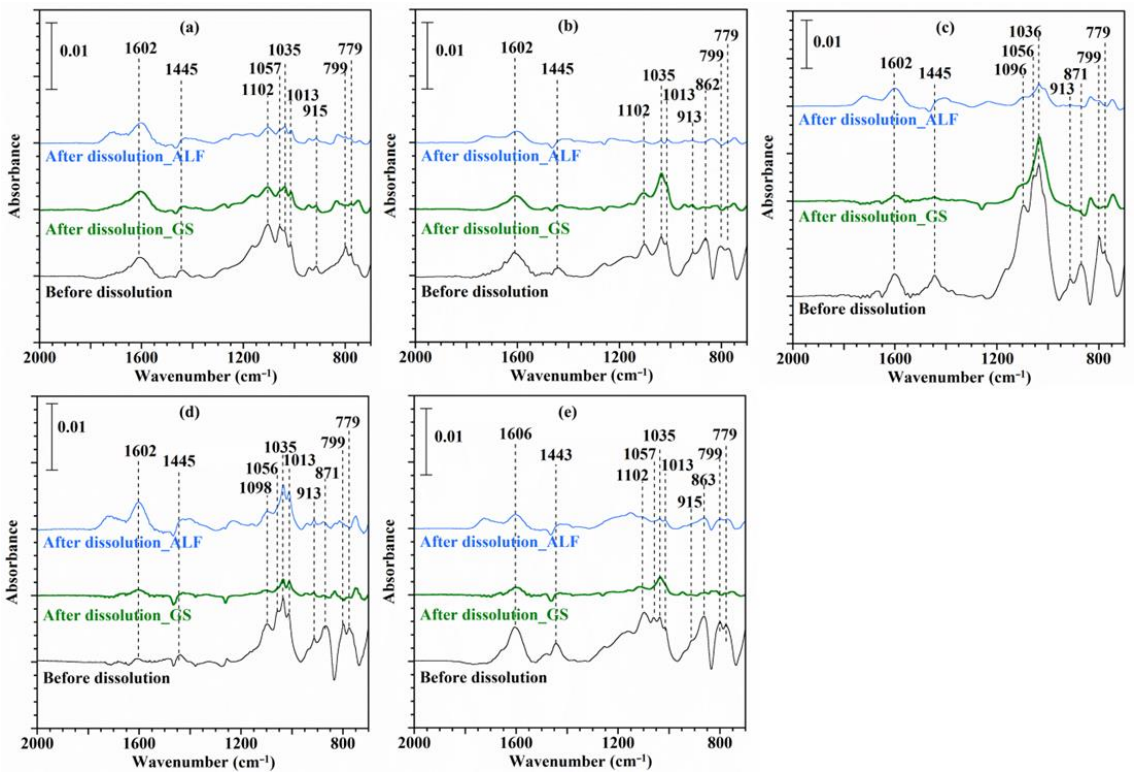

Figure 20. FTIR spectra. (a) Mine 1, (b) Mine 2, (c) Mine 3, (d) Mine 4, and (e) Mine 5.

Table 14. Peak assignments from FT-IR.

Wavenumber (cm^{-1})	**Peak Assignment**
779 and 799	Quartz
913	Kaolinite
1000–1200	Si=O, Si-O-Si, Si-O-C, C-O-C
1445	Antisymmetric–CH_3 deformation
1602	Benzene C=C stretching

4.1.9 In vitro Inflammatory Response

Existing literature has focused on the development of pulmonary fibrosis in pneumoconiosis, largely examining the role of fibroblasts in the development of CWP [156]–[158]. Instead of merely examining the role of fibroblasts, we assessed the impact of coal-based PM10 on epithelial (A549), neutrophilic (HL-60), and macrophage (THP-1) cells. The results of the PM10 coal dust in vitro exposures for cells HL-60, A549, and THP-1 are shown in Figure 21, Figure 22, and Figure 23, respectively.

After four hours of in vitro dust exposure, HL-60 cells indicated mostly a decrease in cytokine expression. Interferon gamma (IFN-γ), interleukin-10 (IL-10), interleukin 12p70 (IL-12p70), interleukin-13 (IL-13), interleukin-4 (IL-4), and interleukin-6 (IL-6) demonstrated a diminished expression across low (5µg/mL), medium (10µg/mL), and high (20µg/mL) treatment groups, relative to controls (no dust exposure). These cytokines are biological signaling molecules frequently involved in chronic inflammatory conditions, including CWP. Overall, the three concentrations did not

demonstrate a dose response relationship, only IL-1β showed a decrease in the cytokine expression when the dose increased for almost all the mines. Interestingly, IL-2 expression mostly increased across treatment groups, with Mine 2 and Mine 5 demonstrating the greatest relative IL-2 expression. IL-8 and IL-1β indicated mixed results, with both up and downregulation across all three treatment groups.

For A549 cells, after 4 h of in vitro dust exposure, they showed mixed results but with mostly a decrease in cytokine expression. IFN-γ, IL-10, IL-12p70, IL-2, and IL-8 demonstrated either a diminished or a very low (<0.05) expression across both low (10µg/mL) and high (100µg/mL) treatment groups. IL-4 and IL-6 were the most responsive cytokines, displaying consistent responses among low and high-treatment groups in most cases. IL-6 has been linked to CWP and silicosis in previous studies [156]. Data from IL-4 is limited. IFN-γ and IL-1β indicated a dose response, showing an increased expression when the dose was increased. The rest of the cytokines showed a mixed dose response, increasing and decreasing expressions when treated with a higher concentration.

THP-1 cells also displayed mixed results in cytokine expression after four hours of in vitro dust exposure. Still in this case, all the cytokines had an increase in cytokine expression in at least two mines, either in the low (10 µg/mL) or high (100 µg/mL) treatment groups, except for interleukin-17A (IL-17A) and tumor necrosis factor-β (TNF-β), which had only one and with very low expression. Overall, the two concentrations did not demonstrate a dose response consistently across all the mines; only TNF-β showed an increase in the cytokine expression when the dose increased.

Selected cytokines were selected based on their role in pneumoconiosis. Chronic inflammation is a key symptom of pneumoconiosis in lung tissues and bronchoalveolar lavage fluid [159]. Pneumoconiosis is characterized by pulmonary injury and the recruitment of inflammatory cells such as monocytes, macrophages, and neutrophils [160]–[162]. Neutrophils are known for being the most abundant leukocytes in the blood, and for that, they are used as the first line of defense in the immune system in several situations. From the circulation, they are quickly mobilized to sites of inflammation [163], [164]. In pneumoconiosis, neutrophils respond to several inflammatory cell chemoattractants generated by activated macrophages. Neutrophils migrate from the vascular compartment to the alveolar space [160], [161]. Once inside the alveolar space, recruited neutrophils secrete toxic oxygen radicals or proteolytic enzymes. As a result, they induce an inflammatory response by avoiding lung colonization from agents such as silica, asbestos fibers, and coal dust [160], [161], [165].

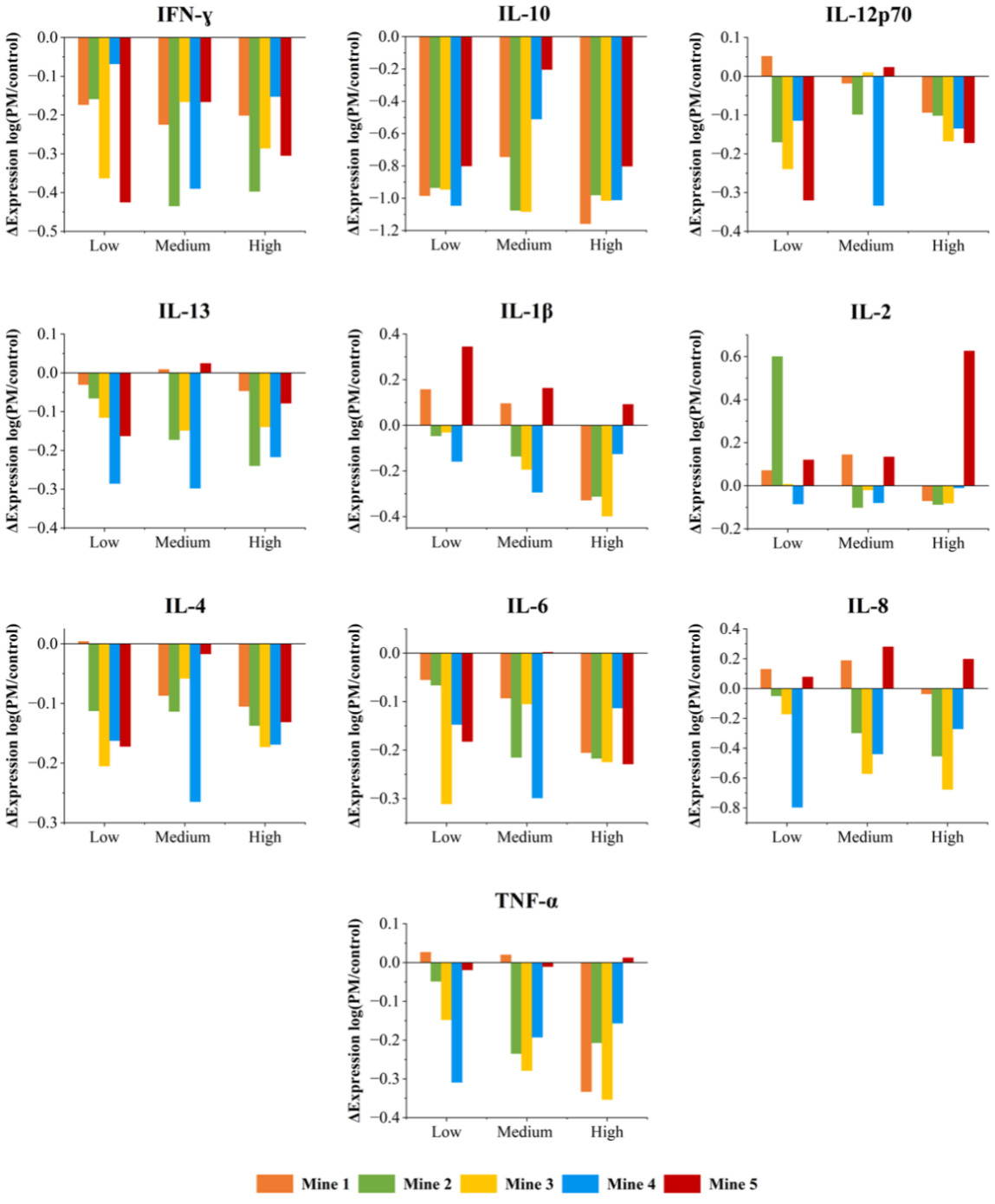

Figure 21. Results of PM10 coal dust exposures to HL-60 cells using low (5 µg/mL), medium (10 µg/mL), and high (20 µg/mL) concentrations.

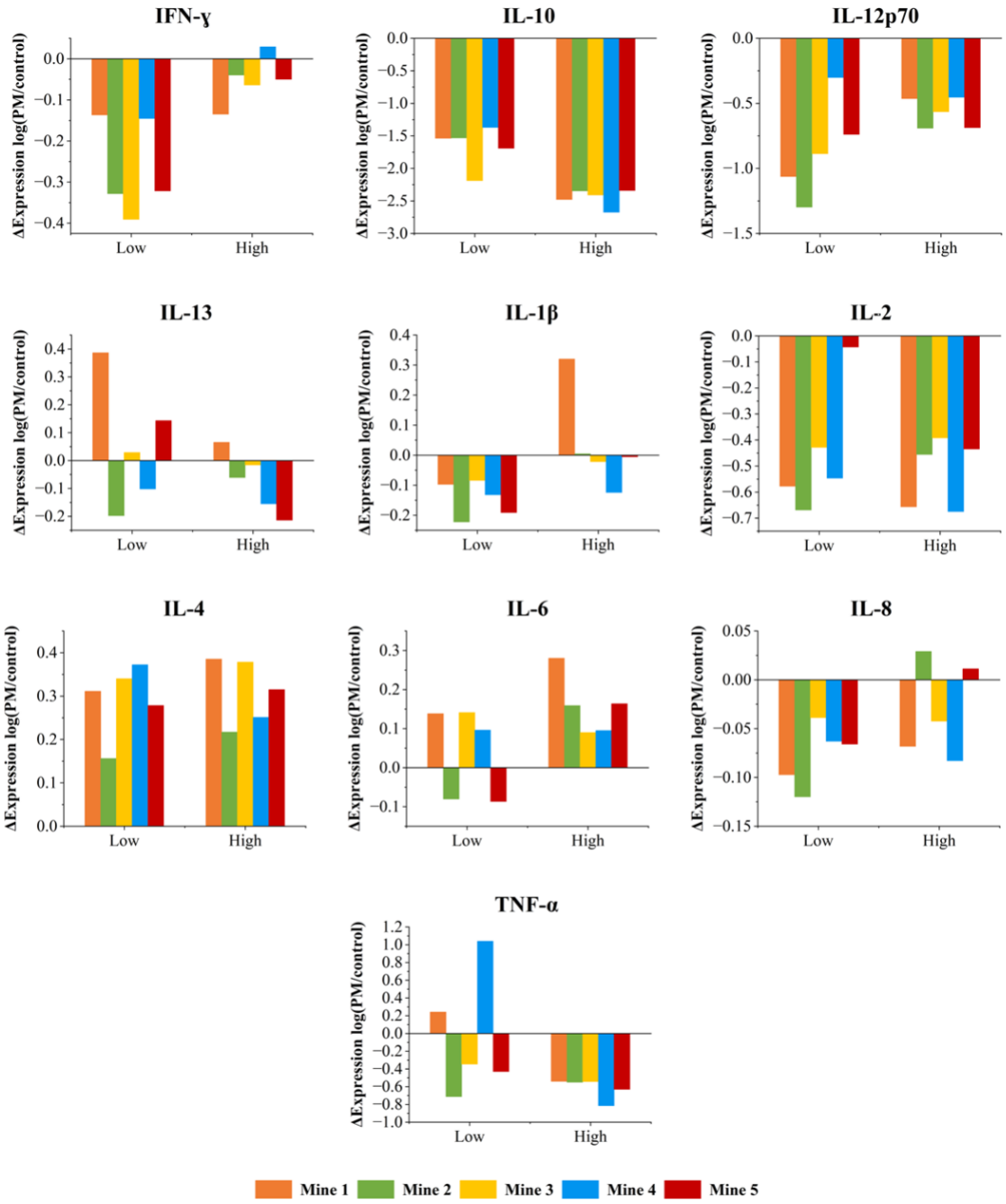

Figure 22. Results of PM10 coal dust exposures to A549 cells using low (10 µg/mL) and high (100 µg/mL) concentrations.

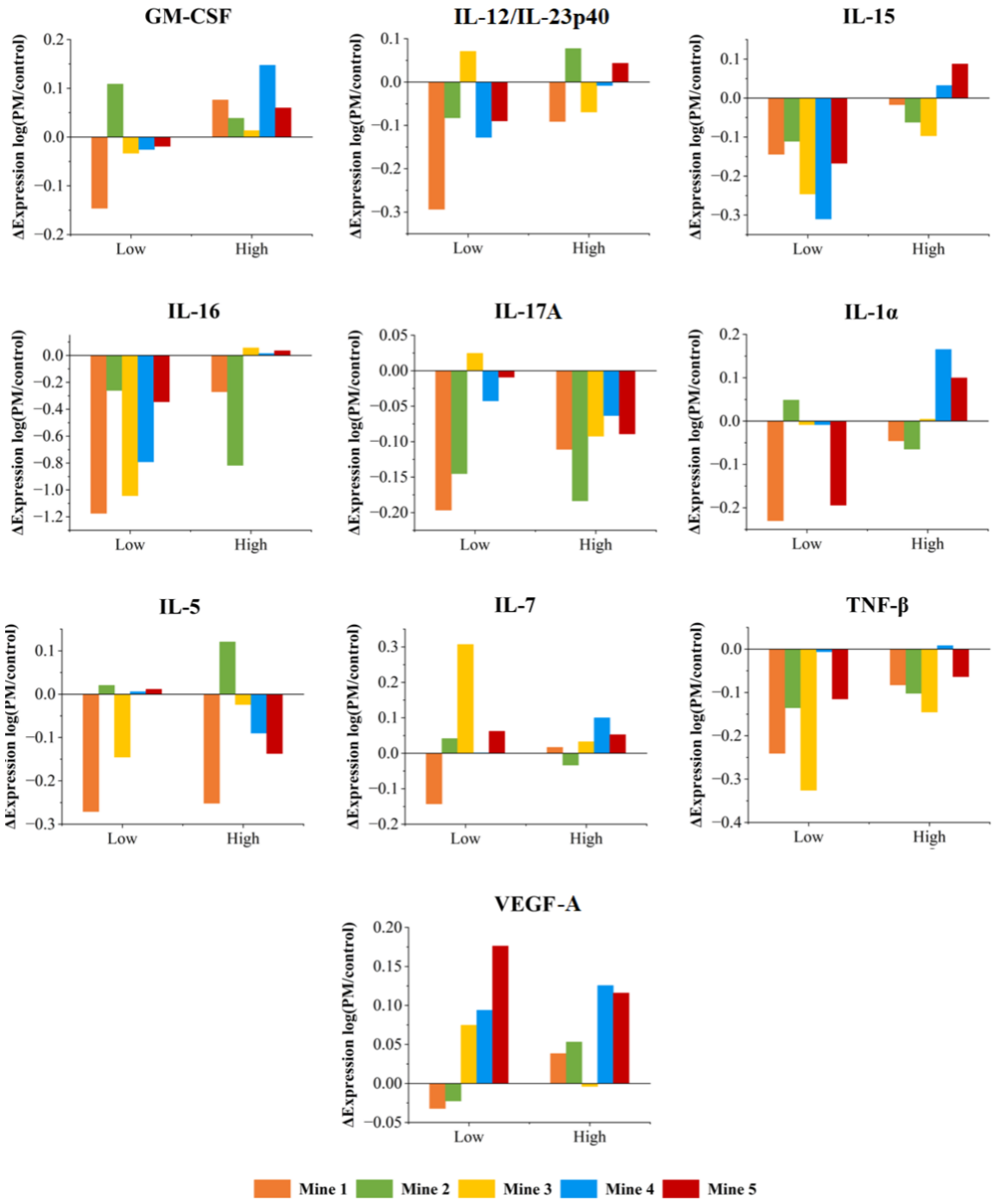

Figure 23. Results of PM10 coal dust exposures to THP-1 cells using low (10 µg/mL) and high (100 µg/mL) concentrations.

Dust particles under 5 µm escape mucociliary clearance and deposit in the terminal bronchioles and alveoli [165], [166]. Then, lung epithelial cells play a huge role in avoiding lung colonization by these agents (silica, asbestos fibers, or coal dust). They recognize microbial molecules through specialized receptors, such as toll-like receptors, pattern recognition receptors (PRRs), and CD14 receptors [167]. The detection of foreign

material by the epithelial cells triggers the immune system response, resulting in the activation of alveolar macrophages, which accept the smaller particles via phagocytosis and collect in the interstitium along the perivascular and peribronchiolar regions of the lung [165]. It also results in the release of cytokines that stimulate inflammation, such as IL-1 and TNF-α, the generation of free radicals, and the augmentation of cell-signaling pathways. As a result, the different cytokines result in the promotion of fibrosis [165], [166], [168]. Following this, once the inflammation process is complete, the fibrotic process initiates by stimulating growth factors. Then, type 1 pneumocytes grow over the collected alveolar macrophages and enclose them in the interstitium. Fibroblasts become stimulated to cause fibrosis and tissue remodeling by producing ECM and matrix metalloproteinases [165]. Fibrocytes can also induce chemotaxis and attract inflammatory factors and chemokines to increase the immune response trying to prevent the establishment of these pathogenic microorganisms [165]. By the end of the fibrotic process, there is an overproduction of fibronectin and collagen, resulting in scar tissue formation in the lungs [165], which is less compliant than normal lung tissue, making it harder to breathe over time [169]. These reactions take place for years before showing any symptoms [169]. Heppleston's theory states that the death and disintegration of macrophages engulfing dust results in fibrosis [159].

TNF, IL-6, and IL-8 are some of the mediators that may be involved in the pathogenesis of coal workers' pneumoconiosis [156]. TNF participates in the initiation and regulation of inflammatory reactions, and the regulation of fibrotic reactions, while IL-6 and IL-8 in the chemotaxis and activation of lymphocytes and the chemotaxis of inflammatory cells, respectively [156] Previous literature has found TNF-α, IL-6, and IL-1 highly related to CWP and silicosis after conducting in vitro, in vivo animals, and human studies from patients with these lung diseases [156], [170]–[174]. The increase in both TNF-α and IL-12p40 has been associated with silicosis development and severity [174]. TNF seems to play a crucial role in controlling of the inflammatory and fibrotic response of the lungs to RCMD and RCS [156], [175], [176] [77,96,97]. Furthermore, it has been found that IL-8 (important as neutrophil attractants and adhesion molecules) is associated with PMF [161].

Davis G.S. et al. studied IFN-γ (a lymphocyte cytokine that acts in macrophage activation) and IL-4 (involved in the differentiation of T cells and eosinophilic inflammation [177]) in mice exposed to silica, finding an immune–inflammatory response from IFN-γ but not from IL-4 [178]. IFN-γ also may help in the production of fibroblast growth factors by macrophages, but its influence remains in discussion [156].

IL-12 has multiple biological activities and is a key factor that drives Th1 responses and IFN- production. IL-12 may provide protection against bacterial and viral infections. IL-13, which is linked to inflammatory diseases and appears to contribute to the development of pulmonary fibrosis and the formation of granulomas, was found upregulated in a study when mice were exposed to silica, relating this cytokine to lung diseases [179].

IL-2 is a signaling molecule involved in T-cell proliferation. Previous literature suggests that bronchoalveolar lavage fluid samples from pneumoconiosis patients have tested positive for IL-1α and β, TGF-β, IL-5, IL-2, and IL-10 [180]. IL-12 has a variety

of biological functions and is a critical regulator of Th1 responses and IFN-γ production; also, it may play a key role in protecting against bacterial and viral infections [181].

In these current results, TNF-α, IL-2, IL-1β, IL-8, IL-6, and IL-10 were upregulated mainly for Mine 1 and Mine 5 in the neutrophilic cells. In the case of the epithelial cells, IFN-γ, IL-13, IL-1β, IL-4, IL-6, IL-8, and TNF-α were upregulated, but IL-4 and IL-6 showed to be cytokines with higher inflammatory stimulation from dust exposures. All cytokines in macrophage cells were also upregulated for different mines, showing significantly high expression for Mine 3 in IL-7, Mine 5 in VEGF-A at low concentrations, and Mine 4 in IL-1α at high concentrations. IL-6 and IL-4 were upregulated in epithelial cells for almost all the mines but were downregulated in neutrophilic cells, not displaying any trend.

From the data obtained, in some of the cytokines studied in the neutrophilic and epithelial cells, an immune suppressive effect was found (a downregulated response), but in general, the cytokines of the macrophage, and some of the neutrophilic and epithelial cells showed an upregulated response, indicating an inflammatory response when exposed to different concentrations of PM10 coal dust. This inflammatory response obtained from the mentioned cytokines may lead to the activation of the mechanisms that produce scar tissue formation and, thus, lung diseases. In general, no trends were found related to the geographic location. Based on our results, further research is warranted on cytokine production in non-fibroblast cell types in pneumoconiosis models, including neutrophils, lung epithelial cells, and macrophages.

4.2 Preliminary Source Comparison

4.2.1 Mineral Composition

The XRD results are shown in Table 15 and Figure 24. The analysis showed that all the samples have quartz in their mineral composition. As mentioned before, this mineral is very common in rocks and coal mines. However, it is noticeable that the quartz peaks (e. g. the one at ~26.7° in Figure 24) in the host rocks (HR and HF) are considerably more significant than the quartz peak for the coal sample (CO). This means that the host rock has a much higher content of quartz, behavior also observed in the peaks for muscovite and kaolinite, indicating a more significant amount of minerals in the host rock. These results are expected since the CO sample might be compounded mainly by organic material. This organic material is evidenced in the CO pattern with the amorphous hump that can be observed at the graph's beginning. Regarding the rest of the mineral components, it was observed that the CO composition was limited to kaolinite, pyrite, and calcite, while the HR and HF had in their composition a variety of minerals that are usually found in the latest stages of rock disintegration forming sedimentary rocks such as shales and limestone, which are typically found interlaying the seams in coal deposits.

Table 15. Minerals, compound names, and chemical formulas of the crystalline phases present in CO. HR, and HF

	Mine ID		
Mineral	**CO**	**HR**	**HF**
Quartz	X	X	X
Kaolinite	X	X	
Pyrite	X	X	
Muscovite		X	X
Microcline			+/-
Chlorite		Trace	X
Calcite	X		X

+/- Under detection limit (2.5%). The sample may or may not contain the mineral.

The following abbreviations represent the different minerals in Figure 24: Quartz (Q), Kaolinite (K), Pyrite (P), Muscovite (Mu), and Calcite (Ca). Microcline and chlorite are present in the samples in very small quantities, so they cannot be observed without zooming in on the patterns.

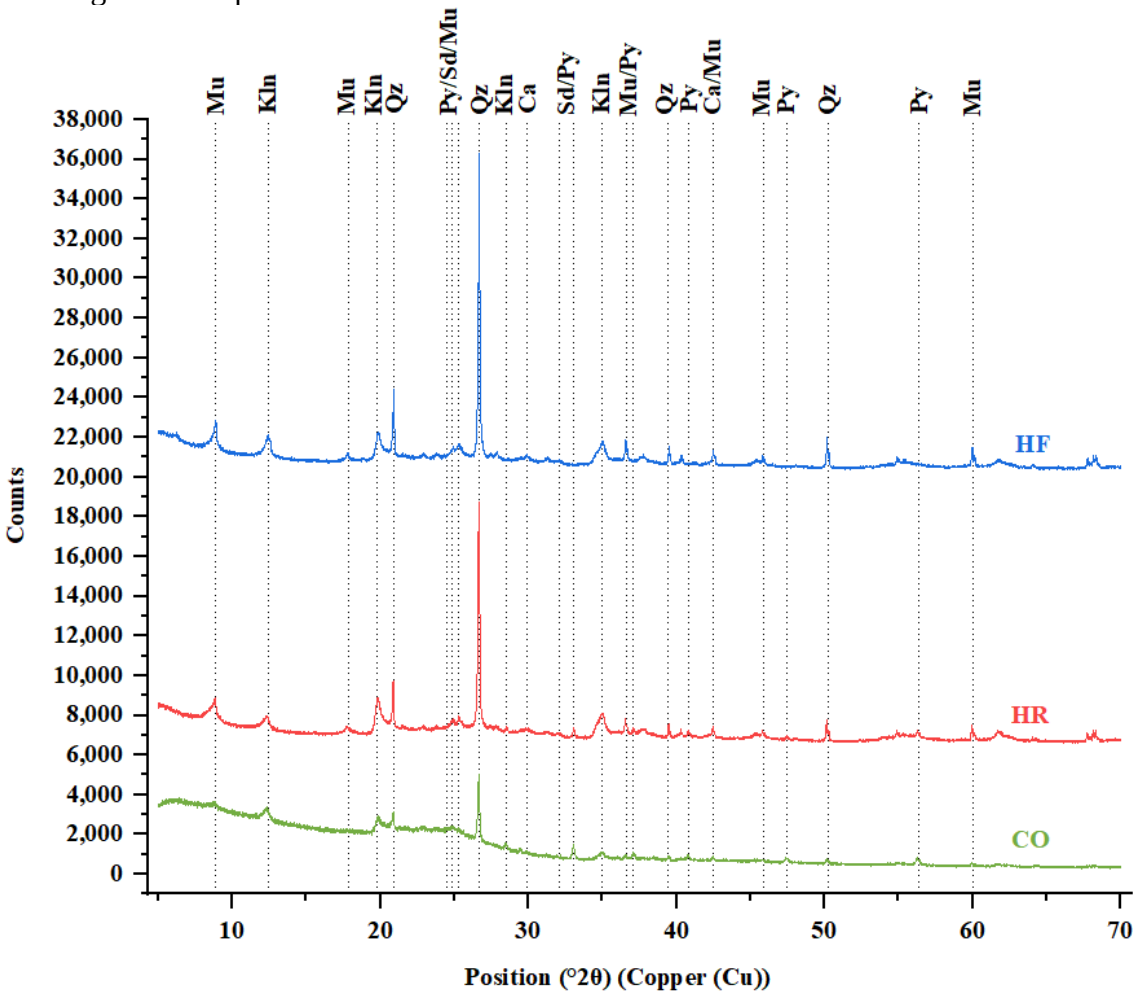

Figure 24. XRD patterns of CO, HR, and HF samples

4.2.2 Elemental Composition

The microwave digestion provided information regarding the elemental composition of the samples. In the same way as the XRD results, this analysis showed a significantly higher concentration of most elements analyzed in the host rock (HR and HF), especially for Si, Ti, Ba, V, and Cr. The major elements found in the samples were Al, Si, Fe, K, and Ti, and the trace elements were Sr, Mg, Ba, Pb, Mn, Ni, Cu, Zn, As, V, and Cr. Many of these elements have been associated with the production of reactive oxygen species, which have been related to RCMD toxicity [2], [21], [71]. Table 16 shows the concentration of each element analyzed.

Table 16. Elemental concentrations in CO, HR, and HF samples.

Mine ID	Al	Si	Fe	K	Ti	Sr	Mg	Ba	Pb	Mn	Ni	Cu	Zn	As	V	Cr
	%	%	%	%	%	µg/g	µg/g	µg/g	µg/g	µg/g	µg/g	µg/g	µg/g	µg/g	µg/g	µg/g
CO	0.90	3.53	0.9	N.A.	0.11	41.2	N.A.	56.6	16.6	24.4	21.8	20.4	52.7	27.8	36.9	26.3
HR	0.6	23.8	1.1	2.35	0.63	256.7	237	442.9	27.5	57.5	46.5	48.3	51.2	18.9	179.0	92.2
HF	0.5	25.0	1.7	2.04	0.72	53.4	125	341.7	1.1	160.2	42.9	35.1	138.7	3.3	170.1	94.9

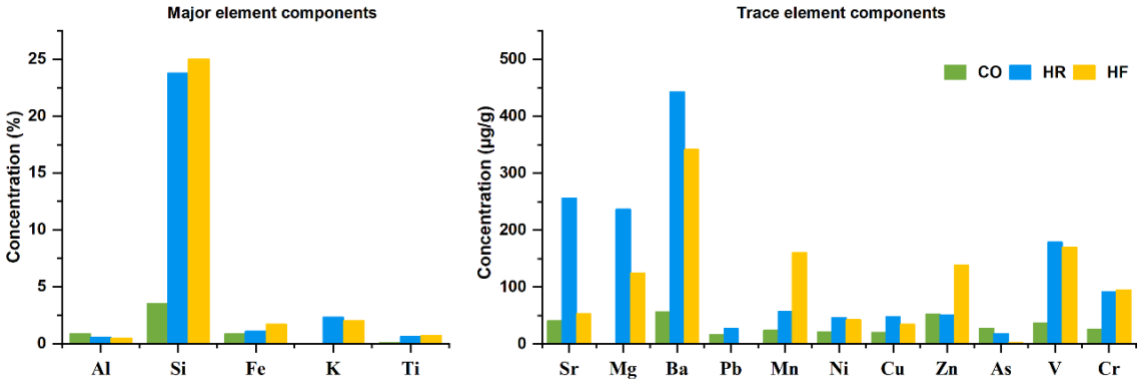

Figure 25. Major and trace element components in the samples.

4.2.3 Initial Functional Groups and Changes after Dissolution

The FTIR analysis was carried out on the samples before and after dissolution to determine the functional groups in the samples' composition and their changes after exposure to SLF. Figure 26 and Table 17 show the FTIR spectra obtained and the peak assignments, respectively. In the first graph (a), which corresponds to the CO sample, it can be observed that on the left side, numerous peaks are missing in the samples HR and HF. These peaks belong to antisymmetric–CH_3 deformation (1445 cm^{-1}) and the benzene C=C stretching (1602 cm^{-1}) which are characteristics of the carbonaceous material present in CO. Also, it can be observed that most of the peaks decrease after the dissolution experiment, indicating that those functional groups are actually dissolving, especially the ones for quartz (779 and 799 cm^{-1}) and kaolinite (913 cm^{-1}). These peaks are pretty much gone after dissolution. This behavior was also observed in the previous work where the influence of geographic location was evaluated [12].

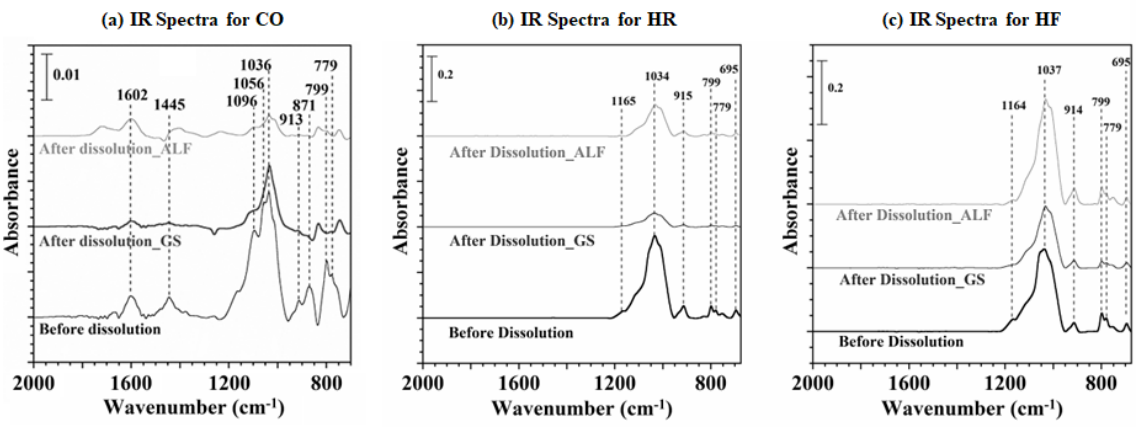

Figure 26. FTIR spectra of (a) CO, (b) HR, and (c) HF

Table 17. Peak assignments from FT-IR [148].

Wavenumber (cm^{-1})	**Peak Assignment**
779 and 799	Quartz
913	Kaolinite
1000–1200	Si=O, Si-O-Si, Si-O-C, C-O-C
1445	Antisymmetric–CH_3 deformation
1602	Benzene C=C stretching

4.2.4 Dissolution in Simulated Lung Fluids

Dissolution experiments were carried out for 24 h in gambles' solution (GS) and artificial lysosomal fluid (ALF). The results of the dissolution experiments in GS and ALF are shown in Figure 27 and Figure 28, respectively. Only Si and Al were dissolving in GS, including a little Cu from the CO sample. On the other hand, in ALF, there is a long list of elements dissolving, including Al, Si, Fe, Cu, Ba, Sr, Ni, Pb, and Mn. This indicates that the elements in dust samples are more bio-accessible when exposed to ALF. The dissolution of elements in GS showed to be negligible for most of the elements, representing lower risk compared to the exposure to ALF.

The dissolution of elements in GS was generally low, similar to the ones obtained in the previous work for the CO sample, even whit significantly higher initial availability of most of the elements. For example, in the case of the Si, the initial availability in HR and HF was around seven times the initial availability of CO, but the dissolutions of HR and HF was just slightly higher in GS.

In contrast, the dissolutions in ALF had a significant increase. The final concentrations after 24 hours increased in an order of 10, which means that the initial availability of elements in the samples played an important role in the dissolutions in ALF. This also indicates that the elements in dust samples are more bio-accessible when exposed to ALF. Additionally, these higher dissolutions obtained in ALF indicate that the dust coming from the host rock (HR and HF) is more toxic than the one coming from the coal seam (CO). Still, even with these higher concentrations, the chances of intoxication or to present adverse effects due to metal overload remain questionable. However,

releasing these elements in the human body may activate the production of reactive oxygen species, which cannot be dismissed as an enhancer of toxicity.

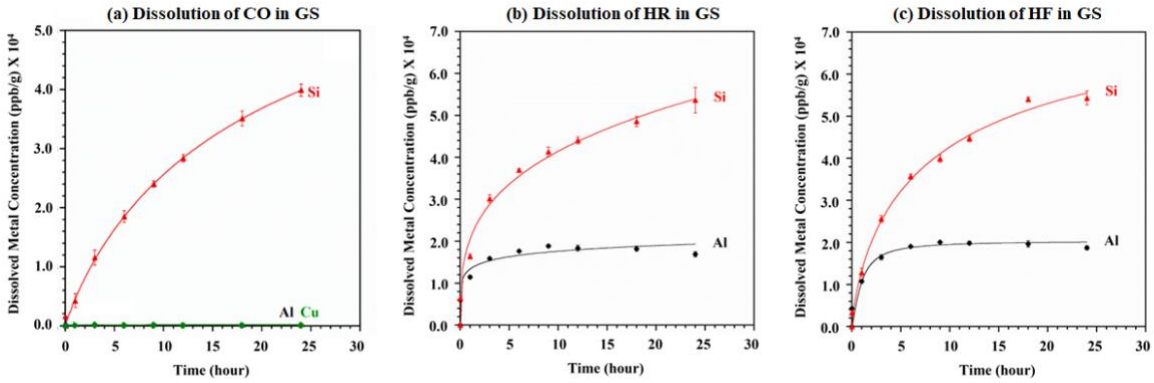

Figure 27. Mass normalized dissolution of metals in GS vs time from (a) CO, (b) HR, (c) HF.

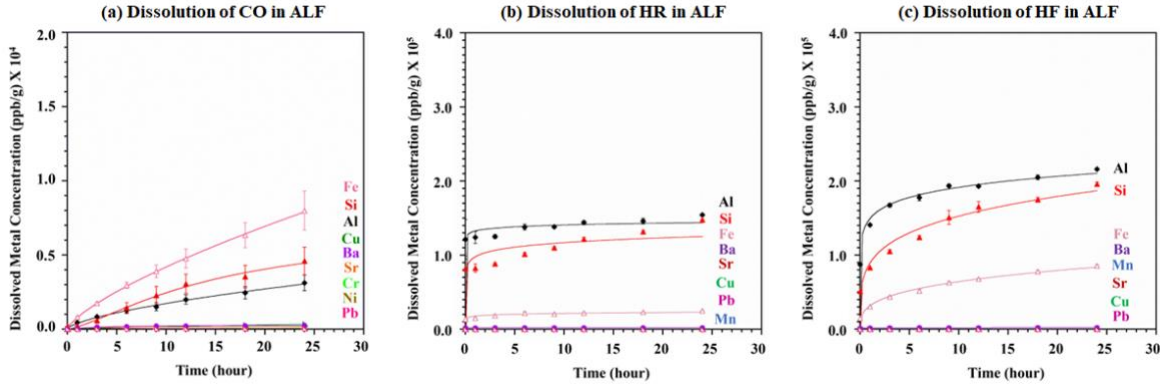

Figure 28. Mass normalized dissolution of metals in ALF vs time from (a) CO, (b) HR, (c) HF.

4.2.5 In-vitro Inflammatory Response

In vitro experiments were conducted to assess the inflammatory response in different human cells involved in lung disease development. In total, ten cytokines were analyzed for each one of the cells HL-60, A549, and THP-1, as follows:

- HL-60 and A549 cells: IFN-γ, IL-1β, IL-2, IL-4, IL-6, IL-8, IL-10, IL-12p70, IL-13, and TNF-α.
- THP-1 cells: GM-CSF, IL-1α, IL-5, IL-7, IL-12/IL-23p40, IL-15, IL-16, IL-17A, TNF-β, and VEGF-A

The results of selected cytokines for cells HL-60, A549, and THP-1 are shown in Figure 29.

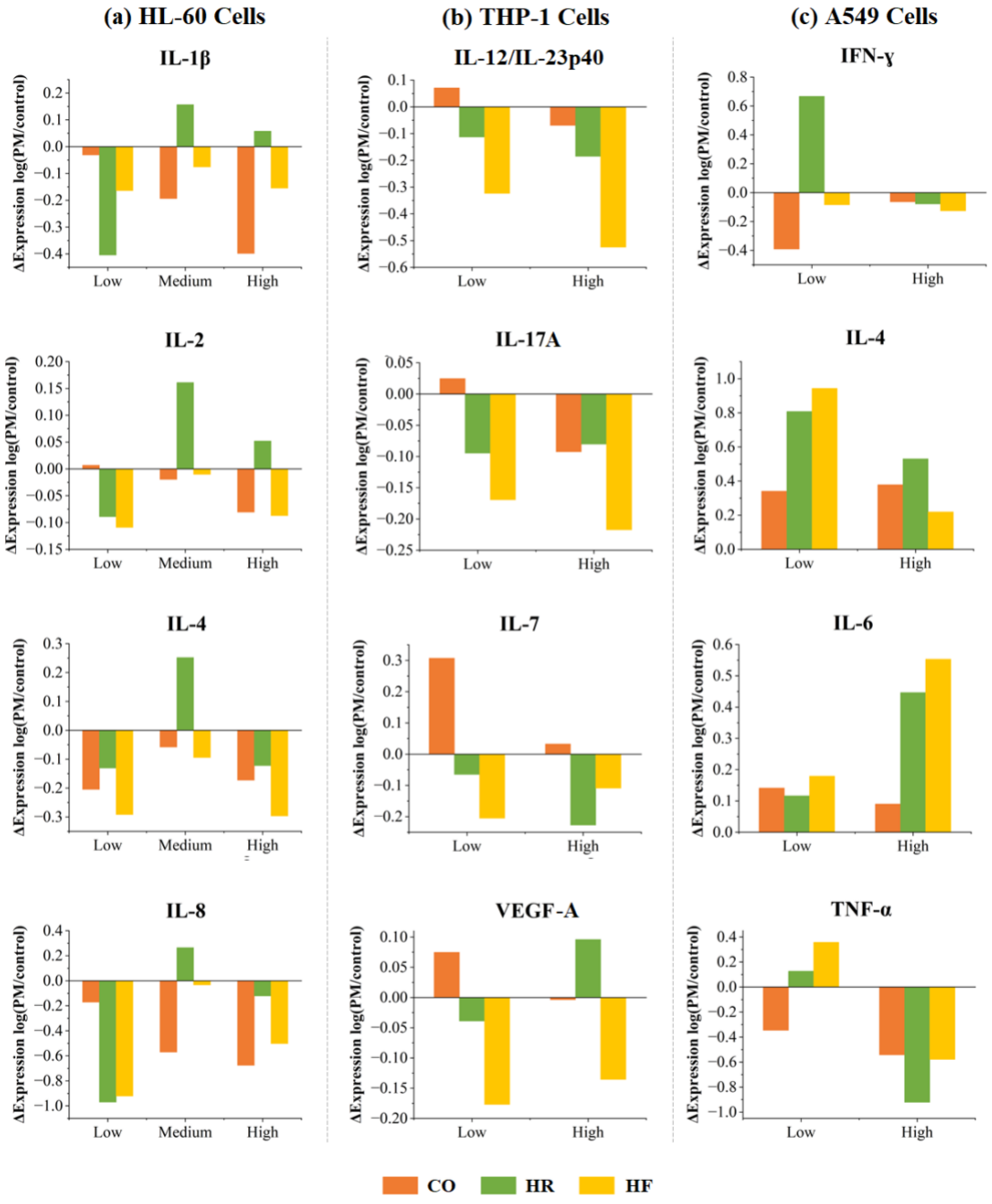

Figure 29. Results of dust exposures to (a) HL-60 cells using low (5 µg/mL), medium (10 µg/mL), and high (20 µg/mL) concentrations, and (b) THP-1 cell and (c) A549 cells using low (10 µg/mL) and high (100 µg/mL) concentrations.

In HL-60 cells (neutrophilic), 6/10 cytokines had at least one proinflammatory response among the three samples and the different concentrations of exposure (IL-1β, IL-2, IL-4, IL-8, IL-12p70, and TNF-α). In general, almost all the reactions were obtained from HR. In A549 cells (lung epithelial), 8/10 cytokines had at least one proinflammatory response (IFN-γ, IL-1β, IL-2, IL-4, IL-6, IL-8, IL-13, and TNF-α), and

two of them had a reaction from all the samples under all the concentrations tested (IL-4 and IL-6). In these last two cytokines, the reactions were mostly higher from the samples HR and HF. For the other six cytokines, the reaction came from either HR or HF, displaying a major affinity to display a proinflammatory response with exposures of the host rock (HR and HF). In THP-1 cells (macrophage), 8/10 cytokines had at least one proinflammatory response, from which seven had a reaction from the CO sample. This indicates, opposite to the other cells, that the coal sample (CO, even with less element and mineral content) is the activator of inflammation in the macrophage cells, although the expressions were low. Additionally, HF was the sample with the highest content of Fe. It has been mentioned in previous research that Fe may enhance the toxicity of RCMD [2], [21]–[24], but in this case, only some of the lung epithelial cytokines displayed an inflammatory response (IL-1β, IL-4, IL-6, IL-8, and TNF-α), but not with a remarkable trend, and in the macrophage and neutrophilic cells, almost any cytokine reacted to HF. Thus, this study does not demonstrate whether Fe influences RCMD toxicity.

CHAPTER 5

CONCLUSIONS AND RECOMMENDATIONS

This study provides characterization and human health impacts information of RCMD from two regions in the US (the Appalachian region and the Rocky Mountains). In this study the characteristics and toxicity of the RCMD fractions coming from the coal seams were analyzed. The differences between samples from the Appalachian and the Rocky Mountains regions were compared to identify the trends related to the geographic location[6]. From the results obtained, the main conclusions are:

- The samples particle size distribution was finer for those coming from the Appalachian region. Appalachian region samples were suggested to have more minerals and higher elemental concentrations, indicating that these samples would be more resistant to the reduction process, however, contrary to what was expected, these samples reached finer samples when reduced under the same procedure. For samples from the Appalachian region, even particles smaller than 1 micron were found, but not for samples from the Rocky Mountains;
- The XRD experiment showed that quartz, kaolinite, and pyrite were the main mineral components of the samples. These results were in accordance with the elemental content results, where Si, Al, and Fe were the elements with higher concentrations in the samples and the main element components of the minerals observed in the XRD. Additionally, XRD and elemental content results showed, in general, that samples from the Appalachian region had more mineral and elemental contents compared to the samples from the Rocky Mountains;
- As for XRD analysis, Si followed the same trend for its exposure on the surface as the elemental content. However, Al did not show any trend related to the initial concentration or the geographic location, indicating that not the same proportion of Al was exposed on the particle surfaces and that Al atoms may be packed inside the particles or the distinctive layers of the clay minerals (kaolinite). Fe was not observed to the particle surfaces, but it was dissolved later in the dissolution

[6] Conclusions regarding the geographic location analysis in this chapter are based on large on the author's paper V. Salinas *et al.*, "Characterization and Toxicity Analysis of Lab-Created Respirable Coal Mine Dust from the Appalachians and Rocky Mountains Regions," *Minerals*, vol. 12, no. 7, p. 898, Jul. 2022, doi: 10.3390/min12070898.

experiment, so the Fe atoms, even if they were not exposed in the surface, were reached by the SLFs and partially digested;

- Kaolinite and quartz showed decreases in the peaks of the FT-IR spectra after dissolution in both GS and ALF, indicating that the SLFs are actually digesting these minerals and the dissolution of Al and Si obtained in SLF came from them;
- The main factors influencing the dissolutions were the pH of the SLF and the initial availability of the elements in the samples. The specific surface area did not affect the general behavior of the dissolutions;
- The elements with the higher availability in the samples (AL, Si, and Fe) gave the higher total dissolutions in the SLFs, but the percentage dissolved from the initial contents did not exceed 0.5% in most of the cases. In contrast, Cu (trace elements) was dissolved from 1.2 to 5.9% of the initial content in the samples, so it can be concluded that normalized to the initial availability, Cu is more bio-accessible than the other elements;
- The toxicity of the samples based on the metal dissolutions could not be related to the geographic location since the factors influencing the dissolutions in SLF varied from the different samples and within the elements dissolved. So, the higher incidence of lung diseases in the Appalachian region may be related to other factors such as the exposure to RCMD, the particle size distribution of the actual RCMD in each mine, and the mineral contributions from the different sources in the mine to the RCMD that the miners inhale, which may be significantly different in each region;
- In-vitro studies indicated a proinflammatory response of the cytokines, especially in the macrophage cells. That suggests possible participation from these cell types in pneumoconiosis and lung diseases development. However, no trends were found related to the geographic location.

Regarding the preliminary source analysis, this study compared the characteristics and toxicity of dust samples from different sources in the mine: coal seam and host rock, to determine if the dust coming from the host rock is more toxic. The following are the main conclusions found:

- When the composition was compared, as expected, it was found that the host rock has a significantly higher content of elements (especially Si, Ti, Ba, V, and Cr) and minerals (quartz, kaolinite, and muscovite), which may influence in its final toxicity;
- Dissolution experiments showed no significant differences between the dissolutions in coal and host rock samples when GS was used. The element concentrations remained similar regardless of the initial bioavailability. However, when tested with ALF, more elements were dissolved, and the dissolutions increased in the order of magnitude of 10 (from $\times 10^4$ to $\times 10^5$) when comparing coal and host rock samples. This indicates that the elemental bio-accessibility is higher in samples from the host rock, and thus, their toxicity;

- In the neutrophilic cells, the inflammatory response was moderate across the cytokines analyzed, and the responses came mainly from HR. Lung epithelial cells displayed major affinity to respond to host rock samples, while the macrophage cells' response was associated with the CO samples, but low. This indicates that the host rock is more likely to activate the cytokines from the neutrophilic and lung epithelial cells but not much from the macrophages. Macrophage cells were more likely to be activated by the coal samples that were considered less toxic regarding composition and elemental dissolution in SLF.

It is essential to mention that all the mentioned results in the geographic location analysis are from samples taken from the coal seam. It is known that RCMD contains different contributions from other sources, so the results obtained are related only to the coal contribution in the RCMD, which means that no relationship was found between RCMD toxicity, and the geographic location corresponds only to the coal fraction and does not consider other sources. Other sources of RCMD in the different mines studied may or not be responsible for the increased rates of CWP in the Appalachian region. From the preliminary source analysis, only one mine was studied, so further study into the relationship of the different sources across different mines in the RCMD toxicity is needed to complement this study.

The following are proposed as recommendations for future research:

- It is recommended to conduct further study on the influence of the geographic location of the mines on RCMD toxicity from samples coming from different sources than coal, such as host rock.
- Further research is needed using different sets of samples from different mines to determine if the trends found in the source analysis in this research are consistent from mine to mine. Also, including additional sources such as rock dust or DPM would be beneficial for further analysis.
- Particle size may play an important role in RCMD toxicity. RCMD is composed of particles with a size below 10 μm. In this range, particles of different sizes may expose different toxicities. Smaller particles may have a more extensive specific area exposed to the lung tissue when inhaled, which may help the elements that compound the samples to dissolve more. So, smaller dust particles have higher metal/elemental dissolution than larger particles in simulated lung fluids. Also, smaller particles may not contribute much to the weight of RCMD collected in filter cassettes during monitoring but may be more toxic. Thus, further research into the toxicity of different particle fractions in RCMD is needed.
- Finally, additional examination of the implications of metal release in the body is required to understand better their interactions with the body processes and their relationship with RCMD toxicity.

APPENDIX A

Supplementary Information[7]

The following supporting information is provided in the current document, Table S1: Composition of the SLFs used; Table S2: Percentages of the relative mineral abundance, total counts, and counts per mineral in XRD data; Table S3: SRM verification (µg/g); Table S4. Percentage dissolves from the initial availability of the elements (dissolved/available); Figure S1. Elemental content of the sample in the same scale; Figure S2. Mass and surface area normalized dissolution of metals as a function of time in GS from (a) Mine 1, (b) Mine 2, (c) Mine 3, (d) Mine 4, and (e) Mine 5; Figure S3. Mass and surface area normalized dissolution of metals as a function of time in ALF from (a) Mine 1, (b) Mine 2, (c) Mine 3, (d) Mine 4, and (e) Mine 5.

Table S1. Composition of the SLFs used [10], [143].

Composition	Gamble Solution (GS) (g/L)	Artificial Lysosomal Fluid (ALF) (g/L)
NaCl	6.779	3.21
Na_2HPO_4	-	0.071
$NaHCO_3$	2.268	-
Sodium citrate dehydrate	0.055	0.077
NH_4Cl	0.535	-
Glycine	0.375	0.059
NaH_2PO_4	1.872	-
L-Cysteine	0.121	-
NaOH	-	6
Citric acid	-	20.8
$CaCl_2.2H_2O$	0.026	0.128
Na_2SO_4	-	0.039
$MgCl_2.6H_2O$	-	0.05
Disodium tartrate	-	0.09
Sodium lactate	-	0.085
Sodium pyruvate	-	0.172

[7] This appendix is based on large on the author's paper supplementary information V. Salinas *et al.*, "Characterization and Toxicity Analysis of Lab-Created Respirable Coal Mine Dust from the Appalachians and Rocky Mountains Regions," *Minerals*, vol. 12, no. 7, p. 898, Jul. 2022, doi: 10.3390/min12070898.

Table S2. Percentages of the relative mineral abundance, total counts, and counts per mineral in XRD data.

	Counts of major peak					Peak position (°2θ)
Mineral	Mine 1	Mine 2	Mine 3	Mine 4	Mine 5	
Quartz	2167.11	1316.02	3266.8	1626.2	564.32	26.65°
Kaolinite	341.11	394.53	697.91	609.89	312.64	12.38°
Pyrite	885.48	81.46	657.47	942.21	0	33.04°
Siderite	0	81.53	0	0	0	32.02°
Calcite	0	0	138	0	0	29.44°

Table S3. SRM verification (μg/g).

Element	**Li**	**Mg**	**Al**	**Si**	**K**	**Ca**	**Ti**	**V**	**Cr**	**Mn**	**Fe**	**Ni**	**Cu**	**As**	**Ba**	**Pb**
SRM CLB-1 Digested	5.7	157.5	6815	10465	440	1095	452	12.24	9.29	8.4	8309.6	18.1	8.5	13.6	31.6	5.1
SRM CLB-1 Information	8.0	279.133	7991	11734	631	1572	467	12.0	9.70	8.0	8742.5	18.0	10.0	13.000	34.000	5.100
Allowable error	N.R.	18	212	982	41.5	71.5	18	1	1.2	N.R	350	2	N.R.	N.R.	5.000	0.700
Difference	2.31	122	1176	1269	191	477	15.45	-0.24	0.41	-0.4	432.9	-0.10	1.52	-0.56	2.371	0.033
Relative difference (%)	29%	44%	15%	11%	30%	30%	3%	-2%	4%	-4%	5%	-1%	15%	-4%	7%	1%

Table S4. Percentage dissolves from the initial availability of the elements (dissolved/available).

Mine	**Al**		**Si**		**Fe**		**Cu**		**Sr**		**Pb**	
ID	**ALF**	**GS**	**ALF**	**GS**	**ALF**	**GS**	**ALF**	**GS**	**ALF**	**GS**	**ALF**	**GS**
Mine 1	0.0350%	0.0022%	0.0284%	0.4745%	0.0902%	-	1.4014%	1.5558%	0.0652%	-	0.7853%	-
Mine 2	0.0283%	0.0076%	0.0259%	0.4793%	0.4076%	0.0004%	3.7256%	5.9179%	1.8139%	-	0.4677%	-
Mine 3	0.0347%	0.0023%	0.0130%	0.1131%	0.0893%	-	1.7373%	1.2010%	0.4585%	-	0.2867%	-
Mine 4	0.0187%	0.0045%	0.0156%	0.2055%	0.1443%	0.0028%	2.3777%	5.7885%	0.1566%	-	0.2586%	-
Mine 5	0.0376%	0.0025%	0.0306%	1.4618%	0.1309%	-	1.4431%	2.3560%	0.2687%	-	0.5321%	-

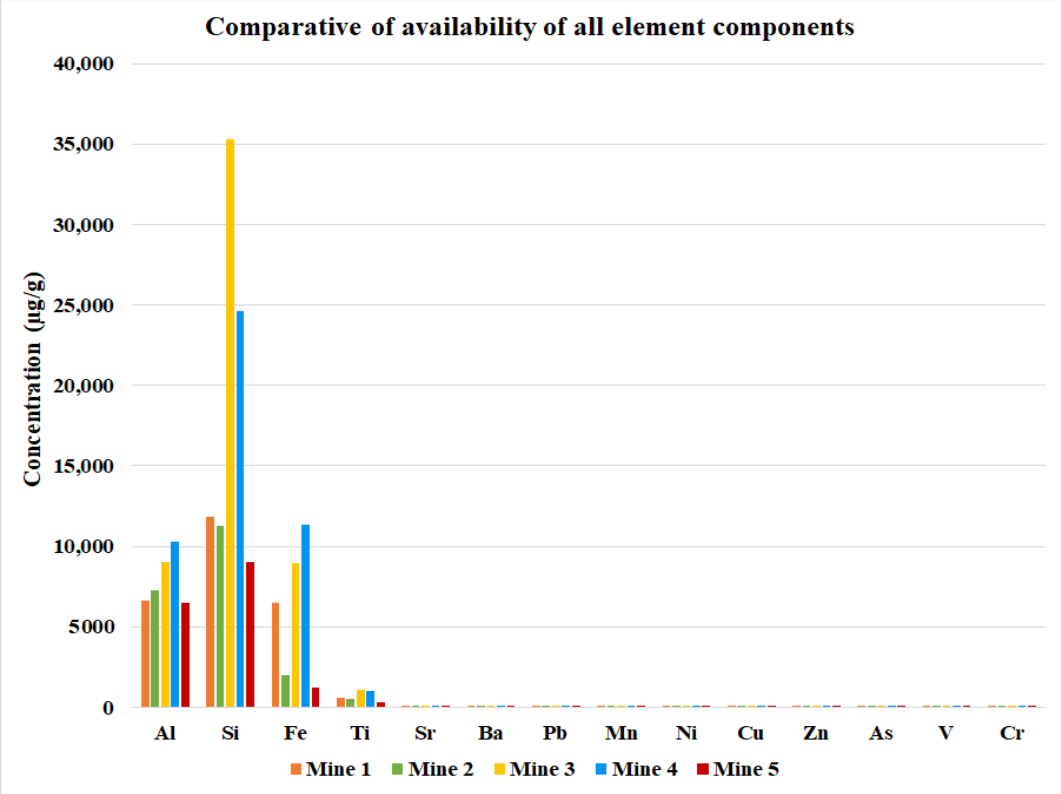

Figure S1. Elemental content of the sample in same scale.

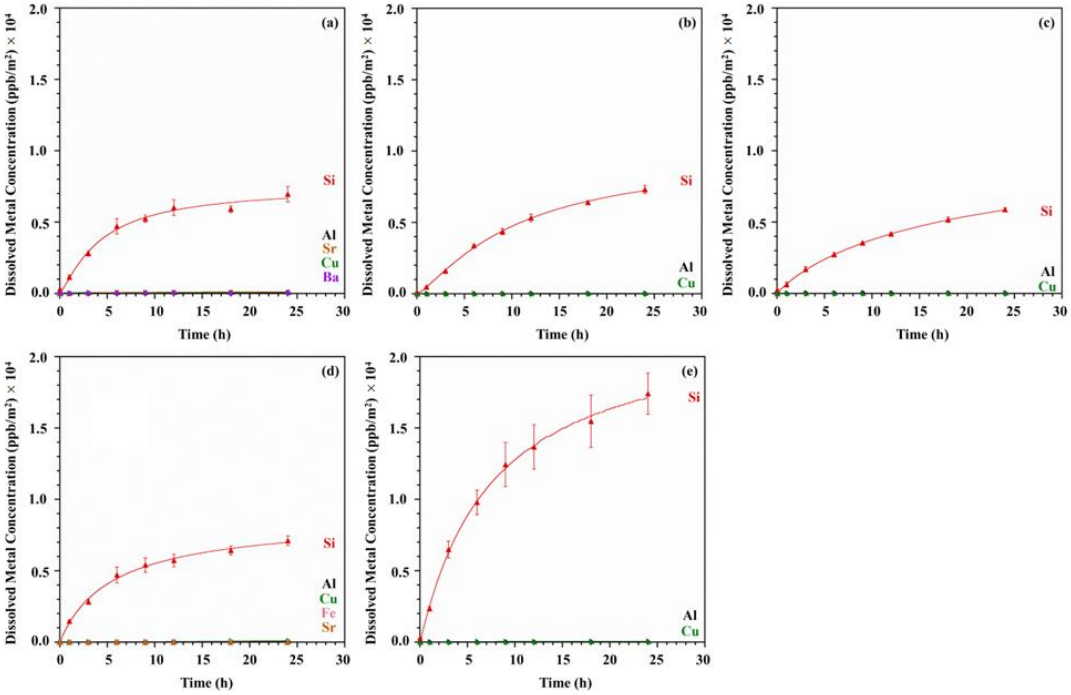

Figure S2. Mass and surface area normalized dissolution of metals as a function of time in GS from (a) Mine 1, (b) Mine 2, (c) Mine 3, (d) Mine 4, and (e) Mine 5.

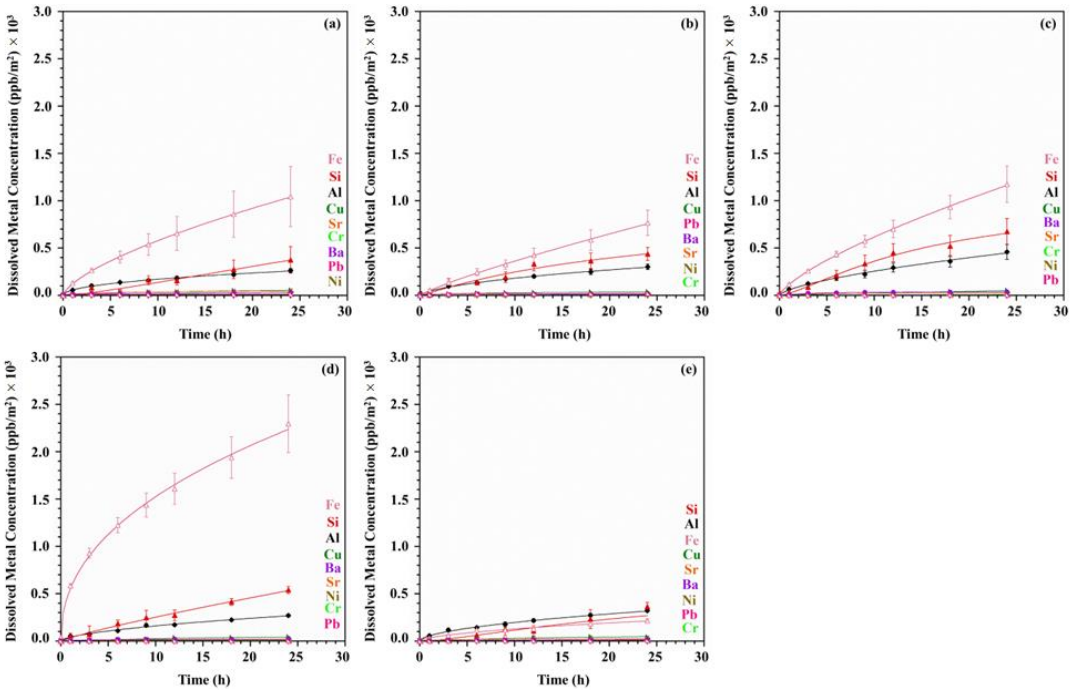

Figure S3. Mass and surface area normalized dissolution of metals as a function of time in ALF from (a) Mine 1, (b) Mine 2, (c) Mine 3, (d) Mine 4, and (e) Mine 5.

REFERENCES

[1] Y. Shekarian, E. Rahimi, M. Rezaee, W.-C. Su, and P. Roghanchi, "Respirable Coal Mine Dust: A Review of Respiratory Deposition, Regulations, and Characterization," *Minerals*, vol. 11, no. 7, p. 696, Jun. 2021, doi: 10.3390/min11070696.

[2] P. Trechera *et al.*, "Mineralogy, geochemistry and toxicity of size-segregated respirable deposited dust in underground coal mines," *J Hazard Mater*, vol. 399, p. 122935, Nov. 2020, doi: 10.1016/j.jhazmat.2020.122935.

[3] E. Sarver, Ç. Keleş, and S. G. Afrouz, "Particle size and mineralogy distributions in respirable dust samples from 25 US underground coal mines," *Int J Coal Geol*, vol. 247, p. 103851, Nov. 2021, doi: 10.1016/j.coal.2021.103851.

[4] J. S. Brown, T. Gordon, O. Price, and B. Asgharian, "Thoracic and respirable particle definitions for human health risk assessment," *Part Fibre Toxicol*, vol. 10, no. 1, pp. 1–12, 2013, doi: 10.1186/1743-8977-10-12.

[5] J. F. Colinet, C. N. Halldin, and J. Schall, "Best practices for dust control in coal mining, second edition.," Pittsburgh, PA, U.S., Aug. 2021. doi: 10.26616/NIOSHPUB2021119.

[6] Y. Shangguan *et al.*, "Mineralogical and geochemical variations from coal to deposited dust and toxicity of size-segregated respirable dust in a blasting mining underground coal mine in Hunan Province, South China," *Int J Coal Geol*, vol. 248, p. 103863, Dec. 2021, doi: 10.1016/j.coal.2021.103863.

[7] P. Thakur, "Characteristics of Respirable Coal Dust Particles," in *Advanced Mine Ventilation*, Elsevier, 2019, pp. 105–122. doi: 10.1016/B978-0-08-100457-9.00008-0.

[8] R. Sellaro, E. Sarver, and D. Baxter, "A standard characterization methodology for respirable coal mine dust using SEM-EDX," *Resources*, vol. 4, no. 4, pp. 939–957, 2015, doi: 10.3390/resources4040939.

[9] A. P. Nesterova *et al.*, "Endocrine, nutritional, and metabolic diseases," in *Disease Pathways*, Elsevier, 2020, pp. 121–218. doi: 10.1016/B978-0-12-817086-1.00004-X.

[10] E. Hettiarachchi, S. Paul, D. Cadol, B. Frey, and G. Rubasinghege, "Mineralogy Controlled Dissolution of Uranium from Airborne Dust in Simulated Lung Fluids (SLFs) and Possible Health Implications," *Environ Sci Technol Lett*, vol. 6, no. 2, pp. 62–67, Feb. 2019, doi: 10.1021/acs.estlett.8b00557.

[11] EIA, "U.S. energy facts explained," 2022. https://www.eia.gov/energyexplained/us-energy-facts/ (accessed Oct. 04, 2022).

[12] V. Salinas *et al.*, "Characterization and Toxicity Analysis of Lab-Created Respirable Coal Mine Dust from the Appalachians and Rocky Mountains Regions," *Minerals*, vol. 12, no. 7, p. 898, Jul. 2022, doi: 10.3390/min12070898.

[13] E. and M. National Academies of Sciences, “Monitoring and Sampling Approaches to Assess Underground Coal Mine Dust Exposures,” Washington, DC, USA, 2018.
[14] E. Sarver, C. Keles, and M. Rezaee, “Beyond conventional metrics: Comprehensive characterization of respirable coal mine dust,” *Int J Coal Geol*, vol. 207, pp. 84–95, Apr. 2019, doi: 10.1016/j.coal.2019.03.015.
[15] E. Rahimi, “Investigation of respirable coal mine dust (RCMD) and respirable crystalline silica (RCS) in the U.S. underground and surface coal mines,” New Mexico Institute of Mining and Technology, Socorro, 2020. Accessed: Oct. 10, 2022. [Online]. Available: https://nmt.idm.oclc.org/login?url=https://www.proquest.com/dissertations-theses/investigation-respirable-coal-mine-dust-rcmd/docview/2468128535/se-2
[16] D. W. Porter, M. Barger, V. A. Robinson, S. S. Leonard, D. Landsittel, and V. Castranova, “Comparison of low doses of aged and freshly fractured silica on pulmonary inflammation and damage in the rat,” *Toxicology*, vol. 175, no. 1–3, pp. 63–71, Jun. 2002, doi: 10.1016/S0300-483X(02)00061-6.
[17] NIOSH, “Health Effects of Occupational Exposure to Respirable Crystalline Silica,” 2002.
[18] E. D. Kuempel *et al.*, “Pulmonary inflammation and crystalline silica in respirable coal mine dust: Dose-response,” *J Biosci*, vol. 28, no. 1, pp. 61–69, 2003, doi: 10.1007/BF02970133.
[19] B. Abbasi *et al.*, “Review of Respirable Coal Mine Dust Characterization for Mass Concentration, Size Distribution and Chemical Composition,” *Minerals*, vol. 11, no. 4, p. 426, Apr. 2021, doi: 10.3390/min11040426.
[20] E. Tarbuck and F. Lutgens, *Ciencias de la tierra, una introducción a la geología física*. 2005.
[21] Y. Shangguan *et al.*, “Characterization of deposited dust and its respirable fractions in underground coal mines: Implications for oxidative potential-driving species and source apportionment,” *Int J Coal Geol*, vol. 258, p. 104017, Jun. 2022, doi: 10.1016/j.coal.2022.104017.
[22] P. Trechera *et al.*, “Geochemistry and oxidative potential of the respirable fraction of powdered mined Chinese coals,” *Science of The Total Environment*, vol. 800, p. 149486, Dec. 2021, doi: 10.1016/j.scitotenv.2021.149486.
[23] Y. Sun *et al.*, “Impact of reactive iron in coal mine dust on oxidant generation and epithelial lung cell viability,” *Science of The Total Environment*, vol. 810, p. 152277, Mar. 2022, doi: 10.1016/j.scitotenv.2021.152277.
[24] G. R. Zosky, E. J. Bennett, M. Pavez, and B. B. Beamish, “No association between pyrite content and lung cell responses to coal particles,” *Sci Rep*, vol. 11, no. 1, p. 8193, Dec. 2021, doi: 10.1038/s41598-021-87517-z.
[25] Y. Shekarian, E. Rahimi, N. Shekarian, M. Rezaee, and P. Roghanchi, “An analysis of contributing mining factors in coal workers’ pneumoconiosis prevalence in the United States coal mines, 1986–2018,” *Int J Coal Sci Technol*, vol. 8, no. 6, pp. 1227–1237, Dec. 2021, doi: 10.1007/s40789-021-00464-y.
[26] NIOSH, “Work-Related Lung Disease Surveillance System (eWoRLD). 2014-763 U.S. Department of Health and Human Services, Centers for Disease Control and Prevention, National Institute for Occupational Safety and Health, Respiratory

Health Division," Sep. 2014. https://wwwn.cdc.gov/eWorld/Data/763 (accessed Nov. 09, 2022).
[27] V. C. dos S Antao, "Rapidly progressive coal workers' pneumoconiosis in the United States: geographic clustering and other factors," *Occup Environ Med*, vol. 62, no. 10, pp. 670–674, Oct. 2005, doi: 10.1136/oem.2004.019679.
[28] E. Sarver *et al.*, "Mineralogic Analysis of Respirable Dust from 24 Underground Coal Mines in Four Geographic Regions of the United States," in *A105. SILICA, INORGANIC DUST, AND MINING*, May 2020, pp. A2635–A2635. doi: 10.1164/ajrccm-conference.2020.201.1_MeetingAbstracts.A2635.
[29] V. Johann-Essex, C. Keles, and E. Sarver, "A Computer-Controlled SEM-EDX Routine for Characterizing Respirable Coal Mine Dust," *Minerals*, vol. 7, no. 1, p. 15, Jan. 2017, doi: 10.3390/min7010015.
[30] M. A. Zazouli *et al.*, "Physico-chemical properties and reactive oxygen species generation by respirable coal dust: Implication for human health risk assessment," *J Hazard Mater*, vol. 405, p. 124185, Mar. 2021, doi: 10.1016/j.jhazmat.2020.124185.
[31] Y. Shekarian, "An investigation of the effects of mining parameters on the prevalence of coal Worker's pneumoconiosis (CWP) risks among the US coal miners," New Mexico Institute of Mining and Technology, Socorro, 2020. Accessed: Oct. 10, 2022. [Online]. Available: https://nmt.idm.oclc.org/login?url=https://www.proquest.com/dissertations-theses/investigation-effects-mining-parameters-on/docview/2467855260/se-2
[32] D. Drolet and G. Beauchamp, *Sampling Guide for Air Contaminants in the Workplace*, 8th ed. Montréal, Québec: The Institut de recherche Robert-Sauvé en santé et en sécurité du travail (IRSST), 2013.
[33] J. W. Cherrie, L. M. Brosseau, A. Hay, and K. Donaldson, "Low-Toxicity Dusts: Current Exposure Guidelines Are Not Sufficiently Protective," *Ann Occup Hyg*, vol. 57, no. 6, pp. 685–691, Jul. 2013, doi: 10.1093/annhyg/met038.
[34] A. Benabed and A. Boulbair, "PM10, PM2.5, PM1, and PM0.1 resuspension due to human walking," *Air Qual Atmos Health*, vol. 15, no. 9, pp. 1547–1556, Sep. 2022, doi: 10.1007/s11869-022-01201-3.
[35] W. F. Jr. Watts, K. J. Baumgard, B. K. Cantrell, and K. L. Rubow, "Control of Diesel Particulate Matter in Underground Coal Mines," 1989. Accessed: Nov. 10, 2022. [Online]. Available: https://stacks.cdc.gov/view/cdc/10384/cdc_10384_DS1.pdf
[36] B. H. Kaye, "Particle size characterization," in *Handbook of Podwer Science & Technology*, Chapman & Hall, Ed. New York, 1997.
[37] X. Woodward, A. Kostinski, S. China, C. Mazzoleni, and W. Cantrell, "Characterization of dust particles' 3D shape and roughness with nanometer resolution," *Aerosol Science and Technology*, vol. 49, no. 4, pp. 229–238, 2015, doi: 10.1080/02786826.2015.1017550.
[38] TSI, "Aerodynamic particle sizer (APS) spectrometer 3321," 2020. https://tsi.com/products/particle-sizers/particle-size-spectrometers/aerodynamic-particle-sizer-(aps)-spectrometer-3321/

[39] L. Pan *et al.*, “Characterization of Particle Size and Composition of Respirable Coal Mine Dust,” *Minerals*, vol. 11, no. 3, p. 276, Mar. 2021, doi: 10.3390/min11030276.
[40] S. Bonnamy and A. Oberlin, “Transmission Electron Microscopy,” in *Materials Science and Engineering of Carbon*, Elsevier, 2016, pp. 45–70. doi: 10.1016/B978-0-12-805256-3.00004-0.
[41] K. Song, “Interphase characterization in rubber nanocomposites,” in *Progress in Rubber Nanocomposites*, Elsevier, 2017, pp. 115–152. doi: 10.1016/B978-0-08-100409-8.00004-8.
[42] B. J. Inkson, *Scanning Electron Microscopy (SEM) and Transmission Electron Microscopy (TEM) for Materials Characterization*. Elsevier Ltd, 2016. doi: 10.1016/B978-0-08-100040-3.00002-X.
[43] D. K. Smith, “Evaluation of the detectability and quantification of respirable crystalline silica by X-ray powder diffraction methods,” *Powder Diffr*, vol. 12, no. 4, pp. 200–227, 1997, doi: 10.1017/S0885715600009775.
[44] Code of Federal Regulations, “Air Contaminants, 29 CFR § 1910.1000.” 1974. Accessed: Nov. 10, 2022. [Online]. Available: https://www.ecfr.gov/current/title-29/subtitle-B/chapter-XVII/part-1910/subpart-Z/section-1910.1000
[45] Code of Federal Regulations, “Respirable crystalline silica, 29 CFR § 1910.1053.” 2018. Accessed: Dec. 01, 2022. [Online]. Available: https://www.ecfr.gov/current/title-29/subtitle-B/chapter-XVII/part-1910/subpart-Z/section-1910.1053
[46] Code of Federal Regulations, “Respirable crystalline silica, 29 CFR § 1926.1153.” 2017. Accessed: Dec. 01, 2022. [Online]. Available: https://www.ecfr.gov/current/title-29/subtitle-B/chapter-XVII/part-1926/subpart-Z/section-1926.1153
[47] Code of Federal Regulations, “Respirable dust standard when quartz is present, 30 CFR § 70.101.” 2014. Accessed: Nov. 10, 2022. [Online]. Available: https://www.ecfr.gov/current/title-30/section-70.100
[48] P. B. Raja, K. R. Munusamy, V. Perumal, and M. N. M. Ibrahim, “Characterization of nanomaterial used in nanobioremediation,” in *Nano-Bioremediation : Fundamentals and Applications*, Elsevier, 2022, pp. 57–83. doi: 10.1016/B978-0-12-823962-9.00037-4.
[49] R. Sindhu, P. Binod, and A. Pandey, “Microbial Poly-3-Hydroxybutyrate and Related Copolymers,” in *Industrial Biorefineries & White Biotechnology*, Elsevier, 2015, pp. 575–605. doi: 10.1016/B978-0-444-63453-5.00019-7.
[50] D. Titus, E. James Jebaseelan Samuel, and S. M. Roopan, “Nanoparticle characterization techniques,” in *Green Synthesis, Characterization and Applications of Nanoparticles*, Elsevier, 2019, pp. 303–319. doi: 10.1016/B978-0-08-102579-6.00012-5.
[51] P. Mohamed Shameer and P. Mohamed Nishath, “Exploration and enhancement on fuel stability of biodiesel,” in *Advanced Biofuels*, Elsevier, 2019, pp. 181–213. doi: 10.1016/B978-0-08-102791-2.00008-8.
[52] H. Saka, “Transmission Electron Microscopy,” in *Carbon Alloys*, Elsevier, 2003, pp. 223–238. doi: 10.1016/B978-008044163-4/50014-0.

[53] S. Ebnesajjad, “Surface and Material Characterization Techniques,” in *Surface Treatment of Materials for Adhesive Bonding*, Elsevier, 2014, pp. 39–75. doi: 10.1016/B978-0-323-26435-8.00004-6.
[54] C. O. Colpan, Y. Nalbant, and M. Ercelik, “4.28 Fundamentals of Fuel Cell Technologies,” in *Comprehensive Energy Systems*, Elsevier, 2018, pp. 1107–1130. doi: 10.1016/B978-0-12-809597-3.00446-6.
[55] J. Bergström, “Experimental Characterization Techniques,” in *Mechanics of Solid Polymers*, Elsevier, 2015, pp. 19–114. doi: 10.1016/B978-0-323-31150-2.00002-9.
[56] B. Ji, Q. Li, and W. Zhang, “Rare earth elements (REEs) recovery from coal waste of the Western Kentucky No. 13 and Fire Clay Seams. Part I: Mineralogical characterization using SEM-EDS and TEM-EDS,” *Fuel*, vol. 307, p. 121854, Jan. 2022, doi: 10.1016/j.fuel.2021.121854.
[57] D. B. Warheit, R. Kreiling, and L. S. Levy, “Relevance of the rat lung tumor response to particle overload for human risk assessment—Update and interpretation of new data since ILSI 2000,” *Toxicology*, vol. 374, pp. 42–59, Dec. 2016, doi: 10.1016/j.tox.2016.11.013.
[58] R. Zhang, S. Liu, and S. Zheng, “Characterization of nano-to-micron sized respirable coal dust: Particle surface alteration and the health impact,” *J Hazard Mater*, vol. 413, p. 125447, Jul. 2021, doi: 10.1016/j.jhazmat.2021.125447.
[59] J. M. van Maanen *et al.*, “In vitro effects of coal fly ashes: hydroxyl radical generation, iron release, and DNA damage and toxicity in rat lung epithelial cells.,” *Inhal Toxicol*, vol. 11, no. 12, pp. 1123–41, Dec. 1999, doi: 10.1080/089583799196628.
[60] M. Mu *et al.*, “Coal dust exposure triggers heterogeneity of transcriptional profiles in mouse pneumoconiosis and Vitamin D remedies,” *Part Fibre Toxicol*, vol. 19, no. 1, p. 7, Dec. 2022, doi: 10.1186/s12989-022-00449-y.
[61] C. Keles, N. Pokhrel, and E. Sarver, “A Study of Respirable Silica in Underground Coal Mines: Sources,” *Minerals*, vol. 12, no. 9, p. 1115, Aug. 2022, doi: 10.3390/min12091115.
[62] Code of Federal Regulations, “30 CFR Part 70 - MANDATORY HEALTH STANDARDS - UNDERGROUND COAL MINES.” https://www.ecfr.gov/current/title-30/chapter-I/subchapter-O/part-70 (accessed Oct. 04, 2022).
[63] F. Turci *et al.*, “Revisiting the paradigm of silica pathogenicity with synthetic quartz crystals: the role of crystallinity and surface disorder,” *Part Fibre Toxicol*, vol. 13, no. 1, p. 32, Dec. 2015, doi: 10.1186/s12989-016-0136-6.
[64] A. Calas *et al.*, “The importance of simulated lung fluid (SLF) extractions for a more relevant evaluation of the oxidative potential of particulate matter,” *Sci Rep*, vol. 7, no. 1, p. 11617, Dec. 2017, doi: 10.1038/s41598-017-11979-3.
[65] Medical News Today, “What is the difference between in vivo and in vitro? ,” 2020. https://www.medicalnewstoday.com/articles/in-vivo-vs-in-vitro#summary (accessed Oct. 10, 2022).
[66] Humane Society International, “About Animal Testing ,” Oct. 05, 2022. https://www.hsi.org/news-media/about/ (accessed Oct. 04, 2022).

[67] D. L. Hickman, J. Johnson, T. H. Vemulapalli, J. R. Crisler, and R. Shepherd, "Commonly Used Animal Models," in *Principles of Animal Research*, Elsevier, 2017, pp. 117–175. doi: 10.1016/B978-0-12-802151-4.00007-4.
[68] W. Wang *et al.*, "Inflammation and fibrosis in the coal dust-exposed lung described by confocal Raman spectroscopy," *PeerJ*, vol. 10, p. e13632, Jun. 2022, doi: 10.7717/peerj.13632.
[69] J. G. Ayres *et al.*, "Evaluating the Toxicity of Airborne Particulate Matter and Nanoparticles by Measuring Oxidative Stress Potential—A Workshop Report and Consensus Statement," *Inhal Toxicol*, vol. 20, no. 1, pp. 75–99, Jan. 2008, doi: 10.1080/08958370701665517.
[70] G. Pizzino *et al.*, "Oxidative Stress: Harms and Benefits for Human Health.," *Oxid Med Cell Longev*, vol. 2017, p. 8416763, 2017, doi: 10.1155/2017/8416763.
[71] T. Moreno *et al.*, "Trace element fractionation between PM10 and PM2.5 in coal mine dust: Implications for occupational respiratory health," *Int J Coal Geol*, vol. 203, pp. 52–59, Feb. 2019, doi: 10.1016/j.coal.2019.01.006.
[72] S. J. Schatzel, "Identifying sources of respirable quartz and silica dust in underground coal mines in southern West Virginia, western Virginia, and eastern Kentucky," *Int J Coal Geol*, vol. 78, no. 2, pp. 110–118, Apr. 2009, doi: 10.1016/j.coal.2009.01.003.
[73] M. Jaishankar, T. Tseten, N. Anbalagan, B. B. Mathew, and K. N. Beeregowda, "Toxicity, mechanism and health effects of some heavy metals," *Interdiscip Toxicol*, vol. 7, no. 2, pp. 60–72, Jun. 2014, doi: 10.2478/intox-2014-0009.
[74] A. Haug and C. E. Foy, "Molecular aspects of aluminum toxicity," *CRC Crit Rev Plant Sci*, vol. 1, no. 4, pp. 345–373, Jan. 1984, doi: 10.1080/07352688409382184.
[75] C. A. Shaw and L. Tomljenovic, "Aluminum in the central nervous system (CNS): toxicity in humans and animals, vaccine adjuvants, and autoimmunity," *Immunol Res*, vol. 56, no. 2–3, pp. 304–316, Jul. 2013, doi: 10.1007/s12026-013-8403-1.
[76] A. Campbell, D. Hamai, and S. C. Bondy, "Differential Toxicity of Aluminum Salts in Human Cell Lines of Neural Origin: Implications for Neurodegeneration," *Neurotoxicology*, vol. 22, no. 1, pp. 63–71, Feb. 2001, doi: 10.1016/S0161-813X(00)00007-3.
[77] A. Becaria, A. Campbell, and S. Bondy, "Aluminum as a toxicant," *Toxicol Ind Health*, vol. 18, no. 7, pp. 309–320, Aug. 2002, doi: 10.1191/0748233702th157oa.
[78] R. J. Mailloux, J. Lemire, and V. D. Appanna, "Hepatic response to aluminum toxicity: Dyslipidemia and liver diseases," *Exp Cell Res*, vol. 317, no. 16, pp. 2231–2238, Oct. 2011, doi: 10.1016/j.yexcr.2011.07.009.
[79] R. A. Yokel, "The toxicology of aluminum in the brain: a review.," *Neurotoxicology*, vol. 21, no. 5, pp. 813–28, Oct. 2000.
[80] V. Frisardi *et al.*, "Aluminum in the Diet and Alzheimer's Disease: From Current Epidemiology to Possible Disease-Modifying Treatment," *Journal of Alzheimer's Disease*, vol. 20, no. 1, pp. 17–30, Mar. 2010, doi: 10.3233/JAD-2010-1340.
[81] E. Inan-Eroglu and A. Ayaz, "Is aluminum exposure a risk factor for neurological disorders?," *Journal of Research in Medical Sciences*, vol. 23, no. 1, p. 51, 2018, doi: 10.4103/jrms.JRMS_921_17.
[82] E. H. Jeffery, K. Abreo, and E. Burgess, "SYSTEMIC ALUMINUM TOXICITY: EFFECTS ON BONE, HEMATOPOIETIC TISSUE, AND KIDNEY," *J Toxicol*

Environ Health, vol. 48, no. 6, pp. 649–666, Aug. 1996, doi: 10.1080/009841096161122.
[83] K. R. Martin, "The chemistry of silica and its potential health benefits.," *J Nutr Health Aging*, vol. 11, no. 2, pp. 94–7, 2007.
[84] K. R. Martin, "Silicon: The Health Benefits of a Metalloid," in *Metal ions in life sciences*, vol. 13, 2013, pp. 451–473. doi: 10.1007/978-94-007-7500-8_14.
[85] M. Rondanelli *et al.*, "Silicon: A neglected micronutrient essential for bone health," *Exp Biol Med*, vol. 246, no. 13, pp. 1500–1511, Jul. 2021, doi: 10.1177/1535370221997072.
[86] S. Gillette Guyonnet, S. Andrieu, and B. Vellas, "The potential influence of silica present in drinking water on Alzheimer's disease and associated disorders.," *J Nutr Health Aging*, vol. 11, no. 2, pp. 119–24, 2007.
[87] J. D. Birchall, C. Exley, J. S. Chappell, and M. J. Phillips, "Acute toxicity of aluminium to fish eliminated in silicon-rich acid waters," *Nature*, vol. 338, no. 6211, pp. 146–148, Mar. 1989, doi: 10.1038/338146a0.
[88] G. Papanikolaou and K. Pantopoulos, "Iron metabolism and toxicity," *Toxicol Appl Pharmacol*, vol. 202, no. 2, pp. 199–211, Jan. 2005, doi: 10.1016/j.taap.2004.06.021.
[89] X. Huang, "Iron overload and its association with cancer risk in humans: evidence for iron as a carcinogenic metal," *Mutation Research/Fundamental and Molecular Mechanisms of Mutagenesis*, vol. 533, no. 1–2, pp. 153–171, Dec. 2003, doi: 10.1016/j.mrfmmm.2003.08.023.
[90] G. Sebastiani and K. Pantopoulos, "Disorders associated with systemic or local iron overload: from pathophysiology to clinical practice," *Metallomics*, vol. 3, no. 10, p. 971, 2011, doi: 10.1039/c1mt00082a.
[91] S. Fishbane, A. Mathew, and N. D. Vaziri, "Iron toxicity: relevance for dialysis patients," *Nephrology Dialysis Transplantation*, vol. 29, no. 2, pp. 255–259, Feb. 2014, doi: 10.1093/ndt/gft269.
[92] G. M. Sukiennicki *et al.*, "Iron levels, genes involved in iron metabolism and antioxidative processes and lung cancer incidence," *PLoS One*, vol. 14, no. 1, p. e0208610, Jan. 2019, doi: 10.1371/journal.pone.0208610.
[93] A. Pietrangelo, "Mechanism of Iron Toxicity," in *Iron Chelation Therapy. Advances in Experimental Medicine and Biology*, vol. 509, Boston, MA: Springer, 2002, pp. 19–43. doi: 10.1007/978-1-4615-0593-8_2.
[94] P. Chanvorachote and S. Luanpitpong, "Iron induces cancer stem cells and aggressive phenotypes in human lung cancer cells," *American Journal of Physiology-Cell Physiology*, vol. 310, no. 9, pp. C728–C739, May 2016, doi: 10.1152/ajpcell.00322.2015.
[95] Y. Kuang and Q. Wang, "Iron and lung cancer," *Cancer Lett*, vol. 464, pp. 56–61, Nov. 2019, doi: 10.1016/j.canlet.2019.08.007.
[96] G. J. Brewer, "Risks of Copper and Iron Toxicity during Aging in Humans," *Chem Res Toxicol*, vol. 23, no. 2, pp. 319–326, Feb. 2010, doi: 10.1021/tx900338d.
[97] S. Raha, R. Mallick, S. Basak, and A. K. Duttaroy, "Is copper beneficial for COVID-19 patients?," *Med Hypotheses*, vol. 142, p. 109814, Sep. 2020, doi: 10.1016/j.mehy.2020.109814.

[98] L. M. Gaetke, H. S. Chow-Johnson, and C. K. Chow, “Copper: toxicological relevance and mechanisms,” *Arch Toxicol*, vol. 88, no. 11, pp. 1929–1938, Nov. 2014, doi: 10.1007/s00204-014-1355-y.

[99] Y. Hong *et al.*, “Progress in the Research of the Toxicity Effect Mechanisms of Heavy Metals on Freshwater Organisms and Their Water Quality Criteria in China,” *J Chem*, vol. 2020, pp. 1–12, May 2020, doi: 10.1155/2020/9010348.

[100] D. C. Zamberlan, P. T. Halmenschelager, L. F. O. Silva, and J. B. T. da Rocha, “Copper decreases associative learning and memory in Drosophila melanogaster,” *Science of The Total Environment*, vol. 710, p. 135306, Mar. 2020, doi: 10.1016/j.scitotenv.2019.135306.

[101] S. Ouni, D. Askri, M. Jeljeli, H. Abdelmalek, M. Sakly, and S. Amara, “Toxicity and effects of copper oxide nanoparticles on cognitive performances in rats,” *Arch Environ Occup Health*, vol. 75, no. 7, pp. 384–394, Oct. 2020, doi: 10.1080/19338244.2019.1689376.

[102] A. A. Taylor *et al.*, “Critical Review of Exposure and Effects: Implications for Setting Regulatory Health Criteria for Ingested Copper,” *Environ Manage*, vol. 65, no. 1, pp. 131–159, Jan. 2020, doi: 10.1007/s00267-019-01234-y.

[103] A. Royer and T. Sharman, “Copper Toxicity,” *StatPearls [Internet]*, 2022. https://www.ncbi.nlm.nih.gov/books/NBK557456/ (accessed Nov. 29, 2022).

[104] A. F. Dorsey, M. E. Fransen, G. L. Diamond, and R. J. Amata, “Toxicological Profile for strontium,” Atlanta, GA, 2004. Accessed: Nov. 29, 2022. [Online]. Available: https://www.atsdr.cdc.gov/ToxProfiles/tp159.pdf

[105] S. Musilli *et al.*, “DNA damage induced by Strontium-90 exposure at low concentrations in mesenchymal stromal cells: the functional consequences,” *Sci Rep*, vol. 7, no. 1, p. 41580, Feb. 2017, doi: 10.1038/srep41580.

[106] D. K. Gupta and C. Walther, Eds., *Behaviour of Strontium in Plants and the Environment*. Cham: Springer International Publishing, 2018. doi: 10.1007/978-3-319-66574-0.

[107] Z. Liu, B. Chen, X. Li, L. Wang, H. Xiao, and D. Liu, “Toxicity assessment of artificially added zinc, selenium, and strontium in water,” *Science of The Total Environment*, vol. 670, pp. 433–438, Jun. 2019, doi: 10.1016/j.scitotenv.2019.03.259.

[108] C. Bartrem *et al.*, “Unknown risk: co-exposure to lead and other heavy metals among children living in small-scale mining communities in Zamfara State, Nigeria,” *Int J Environ Health Res*, vol. 24, no. 4, pp. 304–319, Jul. 2014, doi: 10.1080/09603123.2013.835028.

[109] J. Csavina *et al.*, “A review on the importance of metals and metalloids in atmospheric dust and aerosol from mining operations,” *Science of The Total Environment*, vol. 433, pp. 58–73, Sep. 2012, doi: 10.1016/j.scitotenv.2012.06.013.

[110] J. A. Arias, J. R. Peralta-Videa, J. T. Ellzey, M. Ren, M. N. Viveros, and J. L. Gardea-Torresdey, “Effects of Glomus deserticola inoculation on Prosopis: Enhancing chromium and lead uptake and translocation as confirmed by X-ray mapping, ICP-OES and TEM techniques,” *Environ Exp Bot*, vol. 68, no. 2, pp. 139–148, Apr. 2010, doi: 10.1016/j.envexpbot.2009.08.009.

[111] D. Romero-Estévez, G. S. Yánez-Jácome, K. Simbaña-Farinango, and H. Navarrete, “Distribution, Contents, and Health Risk Assessment of Cadmium, Lead, and Nickel in Bananas Produced in Ecuador,” *Foods*, vol. 8, no. 8, p. 330, Aug. 2019, doi: 10.3390/foods8080330.
[112] M. M. S. Cabral Pinto *et al.*, “An Inter-disciplinary Approach to Evaluate Human Health Risks Due to Long-Term Exposure to Contaminated Groundwater Near a Chemical Complex,” *Expo Health*, vol. 12, no. 2, pp. 199–214, Jun. 2020, doi: 10.1007/s12403-019-00305-z.
[113] M. Cabral Pinto and E. Ferreira da Silva, “Heavy Metals of Santiago Island (Cape Verde) Alluvial Deposits: Baseline Value Maps and Human Health Risk Assessment,” *Int J Environ Res Public Health*, vol. 16, no. 1, p. 2, Dec. 2018, doi: 10.3390/ijerph16010002.
[114] J.-W. Lee *et al.*, “Toxic effects of lead exposure on bioaccumulation, oxidative stress, neurotoxicity, and immune responses in fish: A review,” *Environ Toxicol Pharmacol*, vol. 68, pp. 101–108, May 2019, doi: 10.1016/j.etap.2019.03.010.
[115] Y. Hindarwati, T. Retnaningsih Soeprobowati, and Sudarno, “Heavy Metal Content in Terraced Rice Fields at Sruwen Tengaran Semarang - Indonesia,” *E3S Web of Conferences*, vol. 31, p. 03009, Feb. 2018, doi: 10.1051/e3sconf/20183103009.
[116] U. Zulfiqar *et al.*, “Lead toxicity in plants: Impacts and remediation,” *J Environ Manage*, vol. 250, p. 109557, Nov. 2019, doi: 10.1016/j.jenvman.2019.109557.
[117] A. Kumar *et al.*, “Fungal Phytoremediation of Heavy Metal-Contaminated Resources: Current Scenario and Future Prospects,” in *Recent Advancement in White Biotechnology Through Fungi. Fungal Biology.* , Springer, Cham, 2019, pp. 437–461. doi: 10.1007/978-3-030-25506-0_18.
[118] S. Kumar *et al.*, “Hazardous heavy metals contamination of vegetables and food chain: Role of sustainable remediation approaches - A review,” *Environ Res*, vol. 179, p. 108792, Dec. 2019, doi: 10.1016/j.envres.2019.108792.
[119] A. Kumar and M. N. V. Prasad, “Plant Genetic Engineering Approach for the Pb and Zn Remediation,” in *Transgenic Plant Technology for Remediation of Toxic Metals and Metalloids*, M. Prasad, Ed. Elsevier, 2019, pp. 359–380. doi: 10.1016/B978-0-12-814389-6.00017-1.
[120] N. Gupta, K. K. Yadav, V. Kumar, S. Kumar, R. P. Chadd, and A. Kumar, “Trace elements in soil-vegetables interface: Translocation, bioaccumulation, toxicity and amelioration - A review,” *Science of The Total Environment*, vol. 651, pp. 2927–2942, Feb. 2019, doi: 10.1016/j.scitotenv.2018.10.047.
[121] K. Kumar Yadav *et al.*, “Mechanistic understanding and holistic approach of phytoremediation: A review on application and future prospects,” *Ecol Eng*, vol. 120, pp. 274–298, Sep. 2018, doi: 10.1016/j.ecoleng.2018.05.039.
[122] O. Tarrago and M. Brown, “Case studies in environmental medicine (CSEM). Lead toxicity,” 2017. Accessed: Nov. 29, 2022. [Online]. Available: https://www.atsdr.cdc.gov/csem/lead/docs/CSEM-Lead_toxicity_508.pdf
[123] L. Järup, “Hazards of heavy metal contamination,” *Br Med Bull*, vol. 68, no. 1, pp. 167–182, Dec. 2003, doi: 10.1093/bmb/ldg032.

[124] A. Anttila *et al.*, “Excess lung cancer among workers exposed to lead,” *Scand J Work Environ Health*, vol. 21, no. 6, pp. 460–469, Dec. 1995, doi: 10.5271/sjweh.62.
[125] S. Kumar *et al.*, “Effect of automobile exhaust on the distribution of trace elements and its modulation following Fe, Cu, and Zn supplementation,” *Biol Trace Elem Res*, vol. 31, no. 1, pp. 51–62, Oct. 1991, doi: 10.1007/BF02990359.
[126] O. Wong and F. Harris, “Cancer mortality study of employees at lead battery plants and lead smelters, 1947-1995,” *Am J Ind Med*, vol. 38, no. 3, pp. 255–270, Sep. 2000, doi: 10.1002/1097-0274(200009)38:3<255::AID-AJIM4>3.0.CO;2-8.
[127] C.-M. Liu, Y.-Z. Sun, J.-M. Sun, J.-Q. Ma, and C. Cheng, “Protective role of quercetin against lead-induced inflammatory response in rat kidney through the ROS-mediated MAPKs and NF-κB pathway,” *Biochimica et Biophysica Acta (BBA) - General Subjects*, vol. 1820, no. 10, pp. 1693–1703, Oct. 2012, doi: 10.1016/j.bbagen.2012.06.011.
[128] N.-G. Lundström *et al.*, “Cumulative lead exposure in relation to mortality and lung cancer morbidity in a cohort of primary smelter workers,” *Scand J Work Environ Health*, vol. 23, no. 1, pp. 24–30, Feb. 1997, doi: 10.5271/sjweh.174.
[129] X.-Y. Nan *et al.*, “Barium isotopic composition of the upper continental crust,” *Geochim Cosmochim Acta*, vol. 233, pp. 33–49, Jul. 2018, doi: 10.1016/j.gca.2018.05.004.
[130] M. A. Zoroddu, J. Aaseth, G. Crisponi, S. Medici, M. Peana, and V. M. Nurchi, “The essential metals for humans: a brief overview,” *J Inorg Biochem*, vol. 195, pp. 120–129, Jun. 2019, doi: 10.1016/j.jinorgbio.2019.03.013.
[131] D. Poddalgoda, K. Macey, H. Assad, and K. Krishnan, “Development of biomonitoring equivalents for barium in urine and plasma for interpreting human biomonitoring data,” *Regulatory Toxicology and Pharmacology*, vol. 86, pp. 303–311, Jun. 2017, doi: 10.1016/j.yrtph.2017.03.022.
[132] A. A. Francis and C. S. Forsyth, “Formal Toxicity Summary for BARIUM,” Oct. 1997.
[133] B. S. Bhoelan, C. H. Stevering, A. T. J. van der Boog, and M. A. G. van der Heyden, “Barium toxicity and the role of the potassium inward rectifier current,” *Clin Toxicol*, vol. 52, no. 6, pp. 584–593, Jul. 2014, doi: 10.3109/15563650.2014.923903.
[134] J. C. U. Downs, D. Milling, and C. A. Nichols, “Suicidal Ingestion of Barium-Sulfide-Containing Shaving Powder,” *Am J Forensic Med Pathol*, vol. 16, no. 1, pp. 56–61, Mar. 1995, doi: 10.1097/00000433-199503000-00013.
[135] A. Ghose, A. A. Sayeed, A. Hossain, R. Rahman, A. Faiz, and G. Haque, “Mass barium carbonate poisoning with fatal outcome, lessons learned: a case series,” *Cases J*, vol. 2, no. 0, Sep. 2009, doi: 10.4076/1757-1626-2-9069.
[136] I. R. McNeill and K. Z. Isoardi, “Barium poisoning: an uncommon cause of severe hypokalemia,” *Toxicol Commun*, vol. 3, no. 1, pp. 88–90, Jan. 2019, doi: 10.1080/24734306.2019.1691340.
[137] E. M. Fenu, J. O. Brower, and T. E. O’Neill, “Suicide by an Unusual Compound,” *American Journal of Forensic Medicine & Pathology*, vol. 42, no. 3, pp. 286–288, Sep. 2021, doi: 10.1097/PAF.0000000000000663.

[138] S. A. Wilson, “Certificate of Analysis Coal, Lower Bakerstown CLB-1, U.S. Geological Survey Open File Report OFR 97-299,” 1997. doi: https://doi.org/10.3133/ofr97299.
[139] M. Naderi, “Surface Area,” in *Progress in Filtration and Separation*, Elsevier, 2015, pp. 585–608. doi: 10.1016/B978-0-12-384746-1.00014-8.
[140] N. Fairley *et al.*, “Systematic and collaborative approach to problem solving using X-ray photoelectron spectroscopy,” *Applied Surface Science Advances*, vol. 5, p. 100112, Sep. 2021, doi: 10.1016/j.apsadv.2021.100112.
[141] R. Blume, D. Rosenthal, J.-P. Tessonnier, H. Li, A. Knop-Gericke, and R. Schlögl, “Characterizing Graphitic Carbon with X-ray Photoelectron Spectroscopy: A Step-by-Step Approach,” *ChemCatChem*, vol. 7, no. 18, pp. 2871–2881, Sep. 2015, doi: 10.1002/cctc.201500344.
[142] B. Moeini *et al.*, “Definition of a new (Doniach-Sunjic-Shirley) peak shape for fitting asymmetric signals applied to reduced graphene oxide/graphene oxide XPS spectra,” *Surface and Interface Analysis*, vol. 54, no. 1, pp. 67–77, Jan. 2022, doi: 10.1002/sia.7021.
[143] A. Pelfrêne, M. Cave, J. Wragg, and F. Douay, “In Vitro Investigations of Human Bioaccessibility from Reference Materials Using Simulated Lung Fluids,” *Int J Environ Res Public Health*, vol. 14, no. 2, p. 112, Jan. 2017, doi: 10.3390/ijerph14020112.
[144] L. N. Warr, “IMA–CNMNC approved mineral symbols,” *Mineral Mag*, vol. 85, no. 3, pp. 291–320, Jun. 2021, doi: 10.1180/mgm.2021.43.
[145] D. L. Whitney and B. W. Evans, “Abbreviations for names of rock-forming minerals,” *American Mineralogist*, vol. 95, no. 1, pp. 185–187, Jan. 2010, doi: 10.2138/am.2010.3371.
[146] G. V. P. Bhagath Singh and K. V. L. Subramaniam, “Quantitative XRD study of amorphous phase in alkali activated low calcium siliceous fly ash,” *Constr Build Mater*, vol. 124, pp. 139–147, Oct. 2016, doi: 10.1016/j.conbuildmat.2016.07.081.
[147] R. K. Bund and R. W. Hartel, *Chemical Deterioration and Physical Instability of Food and Beverages*, 1st ed. Cambridge, UK: Woodhead Publishing, 2010.
[148] S. Lin *et al.*, “A study on the FTIR spectra of pre- and post-explosion coal dust to evaluate the effect of functional groups on dust explosion,” *Process Safety and Environmental Protection*, vol. 130, pp. 48–56, Oct. 2019, doi: 10.1016/j.psep.2019.07.018.
[149] J. G. Southwick, “Solubility of Silica in Alkaline Solutions: Implications for Alkaline Flooding,” *Society of Petroleum Engineers Journal*, vol. 25, no. 06, pp. 857–864, Dec. 1985, doi: 10.2118/12771-PA.
[150] R. Cuciureanu, A. Urzică, M. Voitcu, and A. Antoniu, “[Assessment of daily aluminum intake by food consumption].,” *Rev Med Chir Soc Med Nat Iasi*, vol. 104, no. 3, pp. 107–12, 2000.
[151] Institute of Medicine (US) Panel on Micronutrients, *Dietary Reference Intakes for Vitamin A, Vitamin K, Arsenic, Boron, Chromium, Copper, Iodine, Iron, Manganese, Molybdenum, Nickel, Silicon, Vanadium, and Zinc*. Washington, D.C.: National Academies Press, 2001. doi: 10.17226/10026.

[152] D. González-Weller *et al.*, “Dietary intake of barium, bismuth, chromium, lithium, and strontium in a Spanish population (Canary Islands, Spain).,” *Food Chem Toxicol*, vol. 62, pp. 856–8, Dec. 2013.
[153] O. Miedico, C. Pompa, S. Moscatelli, A. Chiappinelli, L. Carosielli, and A. E. Chiaravalle, “Lead, cadmium and mercury in canned and unprocessed tuna: six-years monitoring survey, comparison with previous studies and recommended tolerable limits,” *Journal of Food Composition and Analysis*, vol. 94, p. 103638, Dec. 2020, doi: 10.1016/j.jfca.2020.103638.
[154] S. Hallett, F. Toro, and J. V. Ashurst, *Physiology, Tidal Volume*. Treasure Island, FL: StatPearls Publishing, 2018. Accessed: Nov. 30, 2022. [Online]. Available: https://www.ncbi.nlm.nih.gov/books/NBK482502/
[155] T. Flenady, T. Dwyer, and J. Applegarth, “Accurate respiratory rates count: So should you!,” *Australasian Emergency Nursing Journal*, vol. 20, no. 1, pp. 45–47, Feb. 2017, doi: 10.1016/j.aenj.2016.12.003.
[156] D. Vanhée, P. Gosset, A. Boitelle, B. Wallaert, and A. B. Tonnel, “Cytokines and cytokine network in silicosis and coal workers’ pneumoconiosis.,” *Eur Respir J*, vol. 8, no. 5, pp. 834–42, May 1995.
[157] Y. Song, K. Southam, B. B. Beamish, and G. R. Zosky, “Effects of chemical composition on the lung cell response to coal particles: Implications for coal workers’ pneumoconiosis,” *Respirology*, vol. 27, no. 6, pp. 447–454, Jun. 2022, doi: 10.1111/resp.14246.
[158] Y. Zhang, L. Guan, Y. Zheng, L. Mao, S. Li, and J. Zhao, “Extracellular Histones Promote Pulmonary Fibrosis in Patients With Coal Workers’ Pneumoconiosis,” *J Occup Environ Med*, vol. 61, no. 2, pp. 89–95, Feb. 2019, doi: 10.1097/JOM.0000000000001473.
[159] X.-M. Qi *et al.*, “Pneumoconiosis: current status and future prospects,” *Chin Med J (Engl)*, vol. 134, no. 8, pp. 898–907, Apr. 2021, doi: 10.1097/CM9.0000000000001461.
[160] H. S. Ahn, J. H. Kim, H. S. Chang, K. A. Kim, and Y. Lim, “The Evaluation of IL-8 in the Serum of Pneumoconiotic patients,” *Tuberc Respir Dis (Seoul)*, vol. 43, no. 6, p. 945, 1996, doi: 10.4046/trd.1996.43.6.945.
[161] J. S. Lee, J. H. Shin, and B.-S. Choi, “Serum Levels of IL-8 and ICAM-1 as Biomarkers for Progressive Massive Fibrosis in Coal Workers’ Pneumoconiosis,” *J Korean Med Sci*, vol. 30, no. 2, p. 140, 2015, doi: 10.3346/jkms.2015.30.2.140.
[162] K. Donaldson *et al.*, “Contrasting bronchoalveolar leukocyte responses in rats inhaling coal mine dust, quartz, or titanium dioxide: Effects of coal rank, airborne mass concentration, and cessation of exposure,” *Environ Res*, vol. 52, no. 1, pp. 62–76, Jun. 1990, doi: 10.1016/S0013-9351(05)80151-3.
[163] W.-C. Lin and M. B. Fessler, “Regulatory mechanisms of neutrophil migration from the circulation to the airspace,” *Cellular and Molecular Life Sciences*, vol. 78, no. 9, pp. 4095–4124, May 2021, doi: 10.1007/s00018-021-03768-z.
[164] C. Rosales, “Neutrophils at the crossroads of innate and adaptive immunity,” *J Leukoc Biol*, vol. 108, no. 1, pp. 377–396, Jul. 2020, doi: 10.1002/JLB.4MIR0220-574RR.

[165] N. DeLigh and H. Sachs, *Pneumoconiosis*. Treasure Island, FL: StatPearls Publishing, 2021. Accessed: Nov. 30, 2022. [Online]. Available: https://www.ncbi.nlm.nih.gov/books/NBK555902/
[166] M. Mlika, R. Adigun, and B. S. Bhutta, *Silicosis*. Treasure Island, FL: StatPearls Publishing, 2022.
[167] B. Tonatiuh, M. Torres, K. Bobadilla, and E. Sada, "Papel de las células epiteliales en la respuesta inmune del pulmón," *Revista del Instituto Nacional de Enfermedades Respiratorias*, vol. 18, no. 4, pp. 321–326, 2005.
[168] I. Ates, B. Yucesoy, A. Yucel, S. H. Suzen, Y. Karakas, and A. Karakaya, "Possible effect of gene polymorphisms on the release of TNFα and IL1 cytokines in coal workers' pneumoconiosis," *Experimental and Toxicologic Pathology*, vol. 63, no. 1–2, pp. 175–179, Jan. 2011, doi: 10.1016/j.etp.2009.11.006.
[169] E. Svoboda, "What Is Pneumoconiosis? ," 2022. https://www.webmd.com/lung/what-is-pneumoconiosis (accessed Nov. 30, 2022).
[170] P. Lassalle *et al.*, "Abnormal Secretion of Interleukin-1 and Tumor Necrosis Factor α by Alveolar Macrophages in Coal Worker's Pneumoconiosis: Comparison between Simple Pneumoconiosis and Progressive Massive Fibrosis," *Exp Lung Res*, vol. 16, no. 1, pp. 73–80, Jan. 1990, doi: 10.3109/01902149009064700.
[171] V. Castranova and V. Vallyathan, "Silicosis and coal workers' pneumoconiosis.," *Environ Health Perspect*, vol. 108, no. suppl 4, pp. 675–684, Aug. 2000, doi: 10.1289/ehp.00108s4675.
[172] P. J. A. Borm, N. Palmen, J. J. M. Engelen, and W. A. Buurman, "Spontaneous and Stimulated Release of Tumor Necrosis Factor-alpha (TNF) from Blood Monocytes of Miners with Coal Workers' Pneumoconiosis," *American Review of Respiratory Disease*, vol. 138, no. 6, pp. 1589–1594, Dec. 1988, doi: 10.1164/ajrccm/138.6.1589.
[173] J.-S. Lee *et al.*, "Blood Levels of IL-Iβ, IL-6, IL-8, TNF-α, and MCP-1 in Pneumoconiosis Patients Exposed to Inorganic Dusts," *Toxicol Res*, vol. 25, no. 4, pp. 217–224, Dec. 2009, doi: 10.5487/TR.2009.25.4.217.
[174] E. Slavov, L. Miteva, G. Prakova, P. Gidikova, and S. Stanilova, "Correlation between TNF-alpha and IL-12p40-containing cytokines in silicosis," *Toxicol Ind Health*, vol. 26, no. 8, pp. 479–486, Sep. 2010, doi: 10.1177/0748233710373082.
[175] K. A. Kim *et al.*, "Tumor necrosis factor-alpha gene promoter polymorphism in coal workers' pneumoconiosis," *Mol Cell Biochem*, vol. 234/235, no. 1, pp. 205–209, 2002, doi: 10.1023/A:1015914409661.
[176] V. Castranova, "From Coal Mine Dust To Quartz: Mechanisms of Pulmonary Pathogenicity," *Inhal Toxicol*, vol. 12, no. sup3, pp. 7–14, Jan. 2000, doi: 10.1080/08958378.2000.11463226.
[177] M. Wang *et al.*, "Associations of IL-4, IL-4R, and IL-13 Gene Polymorphisms in Coal Workers' Pneumoconiosis in China: A Case-Control Study," *PLoS One*, vol. 6, no. 8, p. e22624, Aug. 2011, doi: 10.1371/journal.pone.0022624.
[178] G. S. Davis, L. M. Pfeiffer, and D. R. Hemenway, "Expansion of Interferon- γ – Producing Lung Lymphocytes in Mouse Silicosis," *Am J Respir Cell Mol Biol*, vol. 20, no. 4, pp. 813–824, Apr. 1999, doi: 10.1165/ajrcmb.20.4.3407.

[179] T. P. T. Ferreira *et al.*, “IL-13 Immunotoxin Accelerates Resolution of Lung Pathological Changes Triggered by Silica Particles in Mice,” *The Journal of Immunology*, vol. 191, no. 10, pp. 5220–5229, Nov. 2013, doi: 10.4049/jimmunol.1203551.

[180] C. Cohen, E. Fireman, E. Ganor, A. Man, J. Ribak, and Y. Lerman, “Accelerated Silicosis With Mixed-Dust Pneumoconiosis in a Hard-Metal Grinder,” *J Occup Environ Med*, vol. 41, no. 6, pp. 480–485, Jun. 1999, doi: 10.1097/00043764-199906000-00014.

[181] T. Hamza, J. B. Barnett, and B. Li, “Interleukin 12 a Key Immunoregulatory Cytokine in Infection Applications,” *Int J Mol Sci*, vol. 11, no. 3, pp. 789–806, Feb. 2010, doi: 10.3390/ijms11030789.

PERMISSONS

Figure 1 is Copyrighted by CDC and is available for free use (CDC policy: https://www.cdc.gov/other/agencymaterials.html). The use of this material, including any links to the material on the CDC website, does not constitute its endorsement or recommendation by the U.S. Government, Department of Health and Human Services, or Centers for Disease Control and Prevention. The material is otherwise available on the agency website for no charge (https://wwwn.cdc.gov/eWorld/Data/763).

All the information, results, and conclusions related to the geografic location analysis (in Chapter 1, Section 2.3, Chapter 3, Section 4.1, and Chapter 5) are based on large on the author's paper V. Salinas *et al.*, "Characterization and Toxicity Analysis of Lab-Created Respirable Coal Mine Dust from the Appalachians and Rocky Mountains Regions," *Minerals*, vol. 12, no. 7, p. 898, Jul. 2022, doi: 10.3390/min12070898.

The MDPI permissions section states the following: "No special permission is required to reuse all or part of article published by MDPI, including figures and tables. For articles published under an open access Creative Common CC BY license, any part of the article may be reused without permission provided that the original article is clearly cited. Reuse of an article does not imply endorsement by the authors or MDPI" (https://www.mdpi.com/openaccess#Permissions).

RESPIRABLE COAL MINE DUST RESEARCH: CHARACTERIZATION AND TOXICITY

by

Vanessa Paola Salinas Torres